

Ministère de l'enseignement Supérieur et de la recherche Scientifique  
وزارة التعليم العالي والبحث العلمي

Badji Mokhtar Annaba University  
Université Badji Mokhtar Annaba  
Faculté des Sciences de  
l'Ingénierat  
Département : d'électronique



جامعة باجي مختار – عنابة  
كلية علوم الهندسة  
قسم الإلكترونيك

**2021**

**Thèse**

Présentée pour obtenir le diplôme de

**Doctorat En-Sciences**

**Spécialité : automatique**

Par :

**ZINE Bachir**

Thème :

**Commande adaptative et gestion de l'énergie d'un véhicule électrique**

Thèse soutenue le : 01/12/2021, devant le jury composé de :

01	MIHOUB Mohamed Larbi	MCA	Université Badji Mokhtar -Annaba	Président
02	YAHMEDI SAID	Prof.	Université Badji Mokhtar -Annaba	Rapporteur
03	BECHERIF Mohamed	MCA	Fclab-UTBM, BELFORT-FRANCE	Co-rapporteur
04	BOUZID Aissa	Prof.	Université de Constantine	Examineur
05	BEKAKRA Youcef	MCA	Université d'Eloued	Examineur
06	KHERFANE Hamid	MCA	Université Badji Mokhtar -Annaba	Examineur
07	MAROUANI Khoudir	MCA	École Militaire polytechnique	Invité

## " التحكم التكيفي وإدارة الطاقة للسيارة الكهربائية "

**الملخص:** الهدف من هذا العمل هو تطوير مقدر شحن البطارية بناءً على سلسلة من اختبارات الشحن / التفريغ (التجريب) من أجل تطوير مقدر دقيق. لهذا السبب أجرينا دراسة نظرية وتجريبية لتقنية تقدير SOC على وجه الخصوص، عد كولوم متري. سيعتمد هذا التقدير على تقنية البطارية وخصائصها الكهربائية وكذلك درجة الحرارة المحيطة. وبالتالي، يتم استخدام هذه المعلومات حول حالة الشحن لإدارة الطاقة في السيارة الكهربائية، من أجل تكيف التحكم القوي في محول المحرك.  
**كلمات مفتاحية:** مقدر شحن، عد كولوم متري، إدارة الطاقة، السيارة الكهربائية، التحكم القوي.

### « Commande adaptative et gestion de l'énergie d'un véhicule électrique »

**Résumé :** L'objectif de ce travail est de développer un estimateur de charge de la batterie en se basant sur une campagne de tests de charge/décharge (expérimentation) afin de développer un estimateur précis. Pour cette raison nous avons fait une étude théorique et expérimentale de la technique d'estimation du SOC notamment, le comptage coulomb métrique. Cette estimation dépendra de la technologie de la batterie, de ses caractéristiques électriques mais également de la température ambiante. Ainsi, cette information sur l'état de charge est utilisée pour la gestion de l'énergie dans un véhicule électrique, afin d'adapter la commande robuste du convertisseur moteur.

**Mots clés :** SOC «état de charge», Comptage Coulomb métrique, Gestion de l'énergie, Véhicule Electrique, Commande Robuste.

### « Adaptive control and energy management of an electric vehicle »

**Abstract:** The objective of this work is to develop a battery charge estimator based on a series of charge / discharge tests (experimentation) in order to develop an accurate estimator. For this reason, we made a theoretical and experimental study of the SOC estimation technique which is a coulomb counting method. This estimate will depend on the battery technology, its electrical characteristics but also the ambient temperature. Thus, this information on the state of charge is used for energy management in an electric vehicle, in order to adapt the robust control of the motor converter.

**Key words:** SOC "state of charge", Coulomb Counting method, Energy Management, Electric Vehicle, Robust Control.

# Acknowledgment

I thank God the Almighty for giving me the power, the courage, the will. Patience, and wellbeing after all these years, and that, thanks to him this work could be completed.

The research presented in this thesis had been made as a collaboration with Laboratory of Control of electrical machines in Polytechnical Military School and Badji Mokhtar University. Foremost, I would like to express my sincere gratitude to my advisor **Pr. YAHMEDI SAID** my co-advisor **Dr. BECHERIF MOHAMED** and **Dr. MAROUANI KHOUDIR** for the continuous support of my thesis study and research, for their patience, motivation, enthusiasm, and immense knowledge. They guided me through my research.

I also would like to thank my thesis jury: **Dr. MIHOUB MOHAMED LARBI**, **Pr. BOUZID AISSA**, **Dr. BEKAKRA YUCEF**, **DR. KHERFANE HAMID** for accepted to judge this work and for their insightful comments and corrections.

My thanks also go to all the staff of the Badji Mokhtar-Annaba University, Faculty of Science of Engineering, Department of Electronics.

Finally, I would like to thank all those who have contributed to the realization of my work from near or far.

# Contents

## Table of Contents

No.	Contents	Page
	List of Abbreviations	i
	List of Symbols	iii
	List of Figures	vii
	List of Tables	viii
	General Introduction	1-2
	<b>Chapter I: State-of-the-Art of battery state-of-charge</b>	
I.1	Introduction	3
I.2	History of State-of-Charge indication	3
I.3	Battery Management Systems	6
I.4	A General State-of-Charge System	8
I.5	Definition of General Battery Parameters	9
I.6	State-of-the-Art of Battery State-of-Charge	10
I.6.1	Classification	11
I.6.1.1	The estimation method based on characteristic parameters	11
I.6.1.2	Ampere-hour integral estimation method	12
I.6.1.3	Model-based estimation method	13
I.6.1.4	Data-driven estimation method	15
I.7	Conclusion	17
	<b>Chapter II: Battery Modeling</b>	
II.1	Introduction	18
II.2	Electric Vehicle Battery Technologies	18
II.2.1	Overview	18
II.2.2	Basics of Lead Acid Battery	18
II.2.3	Basics of Lithium-ion Battery	19
II.3	Methods of Charging Electric Vehicle Battery	21
II.3.1	Methods of Charging Lead-Acid Batteries	21
II.3.2	Methods of Charging Lithium Batteries	22
II.3.3	Common Methods to Charge Batteries	25
II.4	Types of Battery Models	27
II.4.1	Lead Acid Battery Models	27
II.4.2	Lithium Battery Models	30
II.5	Comparing Lithium-ion and Lead Acid Batteries	36
II.6	Conclusion	40
	<b>Chapter III: Coulomb counting method estimation</b>	
III.1	Introduction	41
III.2	Coulomb Counting Method	41
III.3	Generic Battery Model	42
III.3.1	State of the Art	42
III.3.2	Charge/Discharge of this Model in MATLAB Simulink	44
III.3.3	The Assumptions of this model	45
III.3.4	The Limitations of this model	45

III.4	Application	45
III.5	Experimental method	46
III.5.1.	Battery specification	46
III.5.2.	Measurement System Setup	46
III.6.	Results and discussion	47
III.7	Conclusion	52
	<b>Chapter IV: Energy Management System Model</b>	
IV.1	Introduction	53
IV.2	State of the art of energy management strategies	53
IV.2.1	Rule-based strategies	53
IV.2.2	Strategy based on deterministic optimization methods	58
IV.2.3.	Strategy based on stochastic optimization methods	59
IV.2.4.	Summary of management strategies	60
IV.3	Architecture of electric vehicle	61
IV.4	Power supply system	66
IV.5	Model of supercapacitor	67
IV.5.1	Electrical equation of charge and discharge	68
IV.5.2	Equation Of state of charge	68
IV.6	Model of the batterie	68
IV.6.1	Electrical equation of charge and discharge	69
IV.6.2	Equation Of state of charge	69
IV.7	Model of DC-DC inverter (back-boost)	70
IV.8	Conclusion	71
	<b>Chapter V: description of control approaches</b>	
V.1	Introduction	72
V.2	Solving of the energy management problem	72
V.2.1	First order filter used for frequency separation	73
V.2. 2	Design of the control structure	74
V.2.3	Control of the supercapacitor and the battery current	75
V.2.4	Control of the DC bus voltage and the filters	77
V.3	Conclusion	80
	<b>Chapter VI: Simulation Results and Discussion</b>	
VI.1	Introduction	81
VI.2	Energy management simulation results	81
VI.3	Choosing the frequency of separation	88
VI.4	Conclusion	93
	General conclusion	94-95
	References	96-105
	Appendix	106-112

# **List of Abbreviations and Symbols**

## List of Abbreviations

Abbreviation	Definition
<i>ANN</i>	Artificial Neural Networks
<i>AR<sub>d</sub></i>	Actual Rate discharge current
<i>BMS</i>	Battery Management System
<i>cc</i>	Coulomb Counting
<i>CC</i>	Constant-Current
<i>CV</i>	Constant-Voltage
<i>Ch</i>	Charge
<i>EMF</i>	Electro-Motive Force
<i>EMF<sub>F</sub></i>	EMF fitting method
<i>EKF</i>	Extended Kalman Filters
<i>EMF<sub>m</sub></i>	Measured EMF data points
<i>ISP</i>	In-System Programming
<i>IF</i>	In-Functional
<i>IC</i>	Integrated Circuit
<i>Li – ion</i>	Lithium-ion
<i>LA</i>	Lead Acid
<i>Li – ion POL</i>	Lithium-ion Polymer
<i>Li</i>	Lithium
<i>NiCd</i>	Nickel-Cadmium
<i>NiMH</i>	Nickel-Metal Hybride

<i>NI</i>	National Instruments
<i>SOH</i>	State-of-Health
$n_m$	Overpotential model
<i>SOC</i>	State-of-Charge
<i>EMS</i>	Energy Management System
<i>OCV</i>	Open Circuit Voltage
<i>HEV</i>	Hybrid Electric Vehicle
<i>HEV<sub>s</sub></i>	Hybrid Electric Vehicles
<i>EV</i>	Electric Vehicle
<i>EV<sub>s</sub></i>	Electric Vehicles
<i>DC</i>	Direct Current
<i>Ah</i>	Ampere hour
<i>PV</i>	Photovoltaic
<i>AGM</i>	Absorbed Glass Matrix
<i>CC – CV</i>	Constant-Current-Constant-Voltage
<i>PSO</i>	Particle Swarm Optimization
<i>h</i>	hours
<i>AC</i>	Alternative Current
<i>R</i>	Resistance
<i>C</i>	Capacitance
<i>BATT</i>	Battery
<i>E<sub>OC</sub></i>	Charge of Open Circuit Voltage

$DOD$	Depth of discharge
$SOC_s$	State-of-Charge-Systems
$COV$	Cut-of-Voltage
$SOC_{est}$	State-of-Charge Estimated
$SOC_{bat}$	State-of-Charge battery
$SOC_0$	Initial State-of-Charge

## List of Symbols

Symbol	Definition	Unite
$DOD$	Depth-of-Discharge	[%]
$DOC$	Depth-of-Charge	[%]
$EMF$	Electro-Motive Force	[V]
$E_q^0$	Amount of the energy	[J]
$E_q^l$	Non-linear part of the amount of the energy	[J]
$E_{eq}^+$	Equilibrium potential of the positive electrode	[V]
$E_{eq}^-$	Equilibrium potential of the negative electrode	[V]
$E_0^+$	Standard redox potential of the positive electrode	[V]
$E_0^-$	Standard redox potential of the negative electrode	[V]
$E_0$	Parameter for the SOC-EMF	[V]
$EMF_P$	Predicted EMF voltage	[V]
$EMF_F$	Flited EMF	[V]
$F$	Faraday Constant	[C/mol]
$f$	Frequency	[Hz]

$I_S^{max}$	Constant maximum current	[A]
$I_S^{min}$	Predefined minimum current	[A]
$I_M$	Uncertainties from Maccor current measurement	[A]
$I_S$	Standby current	[A]
$I_d$	Measured discharge current	[A]
$n_0$	Parameter related to the magnitude of the diffusion overpotential	-
$n_1$	Parameter related to the magnitude of the diffusion overpotential	[1/T]
$OCV$	Open-Circuit-Voltage	[V]
$OCV_f$	Battery OCV for a fresh battery	[V]
$OCV_a$	Battery OCV for an aged battery	[V]
$Q_{in}$	Charge present in the battery at the time t	[Ah]
$Q_{max}$	Battery maximum capacity	[Ah]
$Q_d$	Discharge battery capacity	[Ah]
$Q_{max}^+$	Maximum capacity of the positive electrode	[1]
$Q_{max}^-$	Maximum capacity of the negative electrode	[1]
$Q_{ch}$	Amount of charge flowing into the battery during the charge state	[Ah]
$Q_d$	Discharge capacity	[A]
$R_S$	Sens resistor	[ $\Omega$ ]
$SOC$	State-of-Charge	[%]
$SOC_{(EMF)}$	SOC calculated based on the EMF voltage	[%]
$SOC_{(vp)}$	SOC Calculated based on the predicted voltage	[%]
$SOC_e$	SOC error	[%]

$SOC_{end}$	SOC indicated at the end	[%]
$SOC_{in}$	SOC in the initial state	[%]
$SOC_{ch}$	SOC in the charge state	[%]
$t$	Time	[s]
$T$	Temperature	[°C]
$T_{ref}$	Reference temperature	[°C]
$V_{bat}$	Battery terminal voltage	[V]
$V$	Battery voltage	[V]
$V_d$	Battery voltage after discharging	[V]
$V_{ch}$	Battery voltage after charging	[V]
$V_M$	Uncertainties from Maccor voltage measurement	[V]
$V_0$	Battery voltage at t=1min	[V]
$V_{ocf}$	Fully stabilized Open-Circuit-Voltage	[V]
$V_s^{max}$	Maximum charge voltage in CV	[V]
$V_{off}$	Voltage offset	[V]
$\gamma$	Rate-determining variable	-
$\delta$	Parameter in the voltage prediction model	-
$\Gamma$	Constant for voltage prediction	-
$\eta_{ch}$	Charge overpotential	[V]
$\eta_d$	Discharge overpotential	[V]
$\eta_f$	Overpotential model parameters for a fresh battery	[V]
$\eta_{ch}^a$	Measured charge overpotential for an aged battery	[V]

---

$\eta_{ch}^f$	Measured charge overpotential for a fresh battery	[V]
$\phi$	Phase angle	[rad]
$\tau$	Voltage relaxation time	[s]
$\tau_q$	Time constant associated with the increase in overpotential in almost empty battery	[s]
$\tau_d$	"Diffusion" time constant	[s]
$k_0$	Standard rate constant for heterogeneous reaction	-
$\alpha$	Transfer coefficient	-
$c$	Concentration at the surface of the electrode	-

# **List of Figures and Tables**

## List of Figures

No.	Figure	Page
Fig.I.1	Battery capacity indicator developed by Heyer (1938)	3
Fig.I.2	Astronauts exploring the Moon in Lunar Roving Vehicles in 1971–1972 relied only Curtis gauges	4
Fig.I.3	General architecture of a Battery Management System	7
Fig.I.4	General Practical Architecture of a State-of-Charge System	9
Fig.I.5	Classification of SOC estimation methods	11
Fig.I.6	Flowchart of the model-based estimation method	14
Fig I.7	Flowchart of the data-driven estimation method	15
Fig.II.1	Lithium-ion Reaction.	20
Fig.II.2	Five-step Charging Pattern	23
Fig.II.3	PSO Updating Concept	24
Fig.II.4	AC Impedance Model	27
Fig.II.5	Equivalent Circuit Model of Simple Model	28
Fig.II.6	Equivalent Circuit Model of Thevenin Model	28
Fig.II.7	Equivalent Circuit of Copetti Model	29
Fig.II.8	Circuit Structure of Rint Model	30
Fig.II.9	Circuit Structure of Thevenin Model	30
Fig.II.10	Circuit Structure of RC Model	31
Fig.II.11	Circuit Structure of PNGV Model	31
Fig.II.12	The Dispersion Effect in Electrochemical Impedance Spectroscopy	33
Fig.II.13	Lithium-ion Safety Mechanisms	38
Fig.III.1	Battery Charged Discharge Pattern	44
Fig.III.2	Test bench	47
Fig.III.3	The discharge voltage vs. time.	48
Fig.III.4	The state of charge (SOC) of the battery versus time	48
Fig.III.5	The charge voltage versus time (simulation and datasheet)	49
Fig.III.6	The charge voltage versus time (simulation and experimental)	50
Fig.III.7	The battery state of charge (simulation and data sheet) in charge	50
Fig.III.8	The battery state of charge (simulation and experimental) versus	51
Fig.IV.1	Existing energy management strategies	54
Fig.IV.2	Principle of the "All or Nothing" management strategy	55
Fig.IV.3	Principle of the "smoothed transition" management strategy	56
Fig.IV.4	Principle of the "power saturation" management strategy	56
Fig.IV.5	Principle of the "frequency sharing" management strategy	57
Fig.IV.6	A typical electric vehicle schematic diagram.	62
Fig.IV.7	Parallel architecture without converter	64

Fig.IV.8	Parallel architecture with converter on the supercapacitor side	64
Fig.IV.9	Architecture in parallel with two converters	64
Fig.IV.10	Model of a Supercapacitor .	67
Fig.IV.11	Simple electrical equivalent model of a battery .	69
Fig.IV.12	The topology of the power supply system	70
Fig. V.1	The architecture of the studied electric vehicle	72
Fig.V.2	Topology of the vehicle showing the interactions between its various subsystems	73
Fig.V.3	Global diagram of the energy management system, organized at two hierarchical levels with nested loops .	74
Fig.V.4	Low level control architecture	76
Fig.V.5	The linearized dynamics of the DC bus voltage	79
Fig.VI.1	Load Current	81
Fig.VI.2	IFF of Load current	82
Fig.VI.3	Current of the battery, supercapacitor and DC bus	82
Fig.VI.4	Zoom.1 of Figure. VI.3	83
Fig.VI.5	Zoom.2 of Figure. VI.3	83
Fig.VI.6	the DC bus voltage and its reference	84
Fig.VI.7	Zoom.1 of Figure. VI.6	84
Fig.VI.8	Zoom.2 of Figure. VI.6	85
Fig.VI.9	The current of the battery and its reference	86
Fig.VI.10	The current of the supercapacitor and its reference	86
Fig.VI.11	Voltage of the battery	87
Fig.VI.12	Voltage of the supercapacitor	87
Fig.VI.13	Battery duty cycle	88
Fig.VI.14	Supercapacitor duty cycle	88
Fig.VI.15	The current of the supercapacitor	89
Fig.VI.16	Zoom of Figure. VI.15	90
Fig.VI.17	The current of the battery	90
Fig.VI.18	Zoom of Figure. VI.17	91
Fig.VI.19	The voltage of the battery	91
Fig.VI.20	Zoom of Figure. VI.19	92
Fig.VI.21	The voltage of the supercapacitor	92
Fig.VI.22	Zoom of Figure. VI.21	93
Fig.A.B.1	battery photograph 6FM100EX 12V 100AH	106
Fig.A.B.2	the depth of discharge as a function of the number of cycles (a), V; I; SOC as a function of time (b)	107
Fig.A.B.3	the discharge voltage as a function of time (a), the self-discharge of the battery as a function of time (b)	107
Fig.A.B.4	effect of the temperature on discharge capacity with different rate of discharge current (datasheet).	107

Fig.A.B.5	the charge voltage margin as a function of temperature	109
Fig.A.C.1	Block diagram of the sensor LA 55-P	110
Fig.A.C.2	Block diagram of the sensor LV25-P	110
Fig.A.C.3	Sensor card (Current and voltage).	111

## List of Tables

No.	Table	Page
Table I.1	History of SOC development.	6
Table I.2	summarizes the advantages and disadvantages of four SOC estimation methods as well as their performances in accuracy and robustness	16
Table II.1	Lead Acid Charge States.	19
Table II.2	Lithium-ion Subcategory Comparison	21
Table II.3	Battery Technology Comparison	36
Table II.4	Advantages and Limitations of Lead Acid Batteries.	39
Table II.5	Advantages and Limitations of Li-ion Batteries.	40
Table III.1	Parameters of our Battery at 0.1C.	45
Table III.2	Lead Acid battery characteristics	46
Table IV.1	Comparison of deterministic rule-based strategies	57
Table IV.2	Evaluation of the different strategies	61
Table IV.3	Comparison of association architectures	65
Table VI.1	RMS value of the battery current corresponds to the different values of the separation frequency	89



# **General Introduction**

## General Introduction

The Electric vehicles and embedded applications typically require a power source on board, which mainly supply the propulsion and on-board organs. The electrochemical batteries are used mainly to ensure that role. However, these batteries are subject to more and more demanding performance in terms of mass and volume energy.

So, the autonomy of the Battery Electric Vehicle is a key point in the development and commercialization of this kind of vehicle. The requested autonomy is directly linked to the amount of the stored and remaining energy in the battery which is the State of Charge (SOC).

This thesis presents battery state of charge (SOC) estimation using coulomb counting method. So, the quantity of electric charge is calculated during the battery cycle of charge and discharge and compared to the estimated value based on the battery generic model. Also, experimental results are carried out in order to validate this study.

Energy management of energy sources in electric vehicles is a very important area of research today. The development of research concerns, among others, the integration of new energy storage sources and the implementation of advanced energy control and management techniques to optimize the performance (lifetime and cost) of the set [1,2].

The problem of the energy management of a hybrid system (or multi-sources system), is to find the best distribution of power between the different energy sources. This distribution must satisfy the power demands of the load and observe the operating constraints (e.g. the battery and the supercapacitor power).

Our goal is to improve the lifespan of hybrid systems. We have chosen the rule-based frequency sharing strategy offering a better degree of current smoothing on the battery side [3].

The final aim of this work is to develop a battery charge estimator based on a charge / discharge test campaign in order to develop an accurate estimator. This estimate will depend on the battery technology, its electrical characteristics but also the ambient temperature. Thus, this information on the state of charge is used for energy management in an electric vehicle, in order to adapt the robust control of the motor converter.

This thesis is divided into six chapters, in the first chapter, gives a state of the art on the state-of-charge indicator, some definitions of SOC and principles of some SOC estimation

techniques. The second section discusses a number of battery technologies, processes, modeling and charging methods. The third section describes the theoretical and experimental analysis of the SOC estimator using the Coulomb Counting technique. The fourth part concerns the model of the components of the energy management system in an electric vehicle. Chapter five presents the control and technological approaches of energy management system. In this last section, the results of the simulation are addressed in order to illustrate the robustness of the management technique to be studied.

## References

- [1] A. Devie, "Caractérisation de l'usage des batteries Lithium-ion dans les véhicules électriques et hybrides. Application à l'étude du vieillissement et de la fiabilité," 2012.
- [2] A. Lièvre, "Développement d'un système de gestion de batterie lithium-ion à destination de véhicules" mild hybrid": détermination des indicateurs d'état (SoC, SoH et SoF)," Université Claude Bernard-Lyon I, 2015.
- [3] A.-L. Allègre, A. Bouscayrol, and R. Trigui, "Flexible real-time control of a hybrid energy storage system for electric vehicles," *IET Electrical Systems in Transportation*, vol. 3, no. 3, pp. 79-85, 2013.



# **Chapter I:**

**State-of-the-Art of Battery**

**State-of-Charge**

## I.1. Introduction

The state of charge (SOC) is one of the essential factors to characterize the state of storage elements. Its knowledge is all the more critical for the Li-ion battery, as a poorly controlled charge for this technology can lead to the destruction of the accumulator [4].

In this chapter we will give the history of the SOC indicator, some definitions of SOC, battery management system, the principle of the different SOC techniques including estimation method based on characteristic parameters; Ampere-hour integral estimation method, Model-based estimation method and finally Data-driven estimation method.

## I.2. History of State-of-Charge indication

For almost as long as rechargeable batteries have existed, systems capable of indicating the amount of charge available inside a battery have been around. In 1938 Heyer introduced a single-meter device on which the value of a storage battery capacity is indicated [4]. The battery capacity is indicated on the basis of the measured battery voltage and a measured voltage drop across a sense resistor. When the battery is fully charged the device indicates 100% of the capacity (see Figure.I.1).

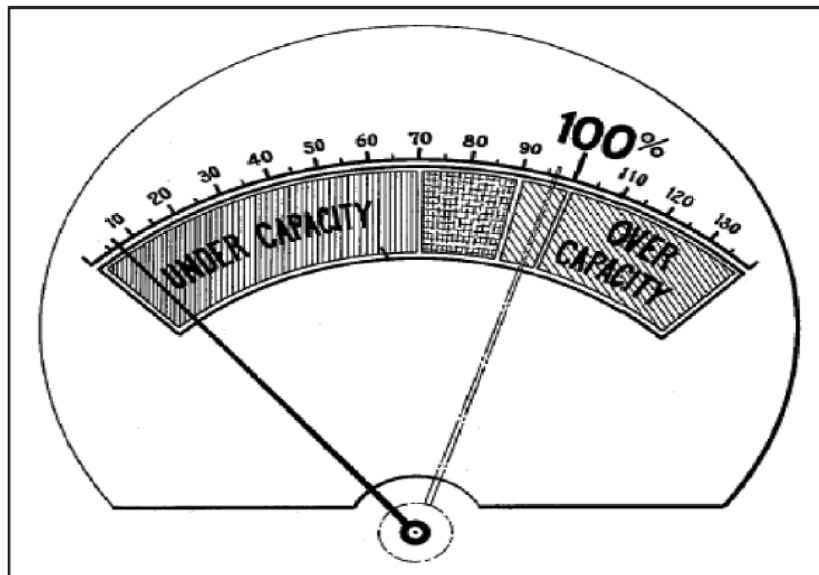


**Figure. I.1.** Battery capacity indicator developed by Heyer (1938) [4].

In 1963 Curtis Instruments pioneered gauges for monitoring the SOC, the ‘fuel’ level, of vehicle traction batteries. One of the methods used by Curtis involves predicting a battery’s remaining capacity by measuring the amount of time elapsed since the loaded voltage dropped below a

certain value. [5]. the Curtis fuel gauge was found to be the most sophisticated and accurate [6]. Curtis SoC gauges were even used on the Moon (see Figure. I. 2) [7].



**Figure. I.2.** Astronauts exploring the Moon in Lunar Roving Vehicles in 1971–1972 relied on early Curtis gauges [7].

In one of the Curtis patents filed by Finger *et al.* in 1975 the current flowing from the battery is sent to an integrator module, which registers the current depletion [8]. During charging, the current is integrated in the integrator module providing a continuous display of the SOC and information needed to regulate the charge rate. An account of the attempts made to develop an SoC indicator for a nickel–cadmium battery was given by Lerner in 1970 [9]. He concluded that the only reliable way of estimating the SOC is to use a current-sharing method. In this method, the current output of a battery having a known SOC is compared with that of a battery having an unknown SOC. The SOC of the unknown battery can be deduced from the outcome of this comparison.

In 1974 York *et al.* introduced an SOC indicator in which the value of the measured battery voltage is indicated with respect to two voltage levels stored in the system [10].

In 1974 Brandwein *et al.* developed a device for monitoring nickel–cadmium batteries [11]. In addition to voltage measurements, the current that flows into and out of the battery and the battery temperature are measured and used in order to provide SOC indication.

In 1975 Christianson *et al.* developed a method in which a battery's SoC is indicated on the basis of the open-circuit voltage (OCV) calculation [12]. The OCV is directly proportional to the battery SoC and can be calculated using the following equation:

$$\mathbf{OCV = V_{bat} + I.R} \quad \mathbf{(I.1)}$$

where  $\mathbf{V}_{bat}$  is the battery terminal voltage,  $\mathbf{I}$  the actual battery current – regarded as a positive value during discharge and a negative value during charge – and  $\mathbf{R}$  is the internal resistance. Note that  $\mathbf{OCV} = \mathbf{V}_{bat}$  when  $\mathbf{I} = 0$ , but after current interruption this takes a while due to several relaxation processes occurring inside a battery.

The first impedance measurements of batteries appear to have been made by Willihnganz in 1941 [13]. They involved excitation of the electrochemical cell by an ac voltage of small amplitude of about 5 mV and evaluation of the resistive and reactive components or other related parameters such as the modulus of impedance and phase angle.

In 1984 Peled developed a method for determining the SOC of lithium-ion batteries [14]. The presented method is based on predetermined voltage and temperature measurements that are used as input parameters for look-up tables. After a current step and a short resting period, a battery's OCV and temperature are measured. The measured value is compared with a corresponding predetermined value stored in a look-up table. The outcome of this comparison is used to indicate the SOC.

In 1981 Finger of Curtis Instruments patented a method according to which the SoC of Lead-Acid (LA) batteries is determined during a quiescent interval with no current flowing through the battery [8]. The battery terminal voltage is measured after a current step and the combination of these two measurements (battery voltage and time) is used for battery OCV recovery characteristics determination. This predictable time function of voltage recovery is substantially independent of the actual voltage level of the terminal voltage.

The methods presented in [15, 16] use Coulomb counting, *i.e.* battery current measurement and integration, as a basis. The method developed by Aylor (1992) holds for LA batteries [15]. The described technique is a combination of the previously described OCV method and coulometric measurements (Coulomb counting).

The methods presented in [17, 18] also use adaptive methods for determining a battery's SOC. In 1997 Gerard *et al.* developed a method in which a battery's 'state variables' are replaced with neural weights with the aim of providing portable equipment users with an accurate estimation of the remaining working time, *e.g.* how much time is left until the battery voltage reaches the end-of-discharge voltage defined in a portable device [17]. Two artificial neural networks are used to model the system's implementation, more precisely, to adapt the prediction of the current discharge curve to the general behaviour of the employed battery pack.

In 2000 Bergveld *et al.* developed a method for estimating the SOC of a rechargeable lithium-ion battery [4, 19]. The basis of the algorithm is current measurement during the charge or discharge state and voltage measurement during the equilibrium state (state in which no current is flowing into or out of the battery and all the conditions inside the battery are fully stabilized). In the charge and discharge states the determination of the SOC relies on calculating the charge withdrawn from or supplied to the battery by means of current integration and subtracting this charge from or adding it to the previously calculated SOC. So, in these states Coulomb counting is applied and the battery is viewed as a simple linear capacitor.

Table I.1. summarizes the most important points of the history of SOC development outlined above.

**Table.I.1.** History of SOC development. [4]

Year	Researcher/ Company	Method
1938	Heyer	Voltage measurements
1963	Curtis	Voltage measurements and threshold in voltage levels
1970	Lerner	Comparison between two batteries (one with a known SoC)
1974	Brandwein	Voltage, temperature and current measurements
1975	Christianson	OCV
1975	Dowgiallo	Impedance measurements
1975	Finger	Coulomb counting
1978	Eby	OCV and voltage under load
1980	Kikuoka	Book-keeping
1981	Finger	Voltage relaxation
1984	Peled	Look-up tables based on OCV and T measurements
1985	Muramatsu	Impedance spectroscopy
1986	Kopmann	Look-up tables based on V, I and T measurements
1988	Seyfang	Book-keeping and adaptive system
1992	Aylor	OCV, OCV prediction and coulometric measurements
1997	Gerard	Voltage and Current Measurements, Artificial Neural Networks
1999	Salkind	Coulomb counting, impedance spectroscopy, fuzzy logic
2000	Garche	Voltage and Current Measurements, Kalman filters
2000	Bergveld	Book-keeping, overpotential, EMF, maximum capacity learning algorithm

### I.3.Battery Management Systems

The design of a battery-powered device requires many battery-management features, including charge control, battery-capacity monitoring, remaining run-time information, charge-cycle

counting, *etc.* For it to be able to offer high precision, each part of the system must be near to perfection. The basic task of a BMS can be defined as follows [20]:

The basic task of a Battery Management System (BMS) is to ensure that optimum use is made of the energy inside the battery powering the portable product and that the risk of damage to the battery is prevented. This is achieved by monitoring and controlling the battery's charging and discharging process.

The DC/DC converter is used to efficiently condition the unregulated battery voltage (3-4.2 V in Li-ion chemistry) for compatibility with stringent load requirements. The basic task of the load is to convert the electrical energy supplied by a battery into an energy form that will fulfill the load's function, such as mechanical energy, light, sounds, heat, EM radiation, *etc.* The battery status can be indicated in one light-emitting diode (LED) or several such diodes connected in series or on a liquid-crystal display (LCD) that indicates the SOC and the battery's condition (*e.g.* the State-of-Health (SOH)) [20].

The processor is used to run the battery-management software, including the SOC algorithm. Communication between the BMS and other devices is another important task of the BMS. Depending on the application, various systems can be used for data exchange, such as an inter-integrated-circuit bus interface (I<sup>2</sup>C) or some other form of serial interface. The battery state is used as an input parameter for the portable device's electrical management and it is an important parameter for the user. The battery state can be used to estimate the battery's expected lifetime. It can be simply described by two parameters: SOC and SOH. Both parameters depend on each other and influence the battery performance [4].

A general block diagram of a BMS is shown in Figure.I.3.

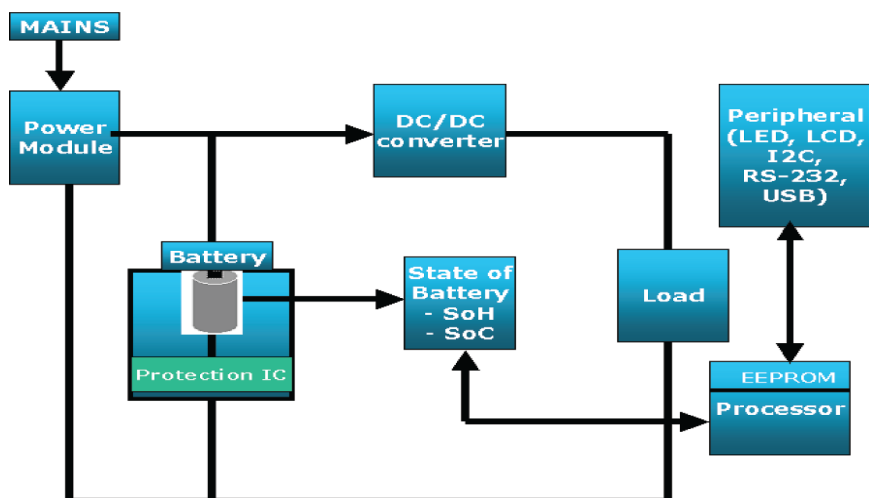


**Figure.I.3.** General architecture of a Battery Management System

### I.4.A General State-of-Charge System

In science, the quality unit want to communicate battery limit is Coulomb (named when the French scientist C. A. Coulomb, 1736–1806), that portrays the time a battery will produce a given current. The Coulomb is that the unit of electrical charge like one quantity unit (As).

In observe, however, cell or battery capability is a lot of usually expressed in ampere-hours (Ah) or milliampere-hours (mAh). Of nice importance for users is to understand a battery's SOC. In [21] SOC is defined as the percentage of the full capacity of a battery that is still available for further discharge. In [13] it is the ratio of a cell's available capacity and its maximum attainable capacity. For a correct understanding of what the term 'SOC' extremely implies a transparent definition is needed; SOC is the percentage of maximum possible charge that is present inside a rechargeable battery. The SOC measuring methodology and also the machine model supported the right SOC definition should be straightforward, convenient, sensible and reliable.

Figure. I.4. suggests an instance of a sensible SOC system. The battery may also encompass a plurality of battery cells related in sequence and/or parallel, every of the battery cells having at least two terminals. The SOC device may additionally include an analogue-to-digital converter (ADC) for converting a voltage drop between at least two feel resistor connection pins as a measure of the modern-day (I) into a digital sign and also for changing the measured analogue values of the battery voltage (V) and temperature (T) into digital signals.

A microprocessor/microcontroller (in which the SOC algorithm is stored) determines a battery system's SOC on the groundwork of the measured signals. Two sorts of reminiscence are needed. Basic battery data, such as the amount of self-discharge as a function of T and the discharging efficiency as a feature of I and T, are read from the read-only reminiscence (ROM).

When the SOC algorithm is primarily based on EMF measurements, the EMF–SOC relationship can be saved in ROM collectively with different battery-specific data. The random get right of entry to reminiscence (RAM) is used to save the history of use, such as the quantity of charge/discharge cycles, which can be used to replace the most battery capacity. Each part of this system (software algorithm or hardware device) will have an effect on the last accuracy of the SOC indication (e.g. inaccuracy in the V, T and I measurements will result in inaccuracy in the closing SOC). Also essential is the calibration of the SOC, because if the SOC algorithm is based on, say, present day size and integration, the error triggered via the cutting-edge measurement inaccuracy will accumulate over time.

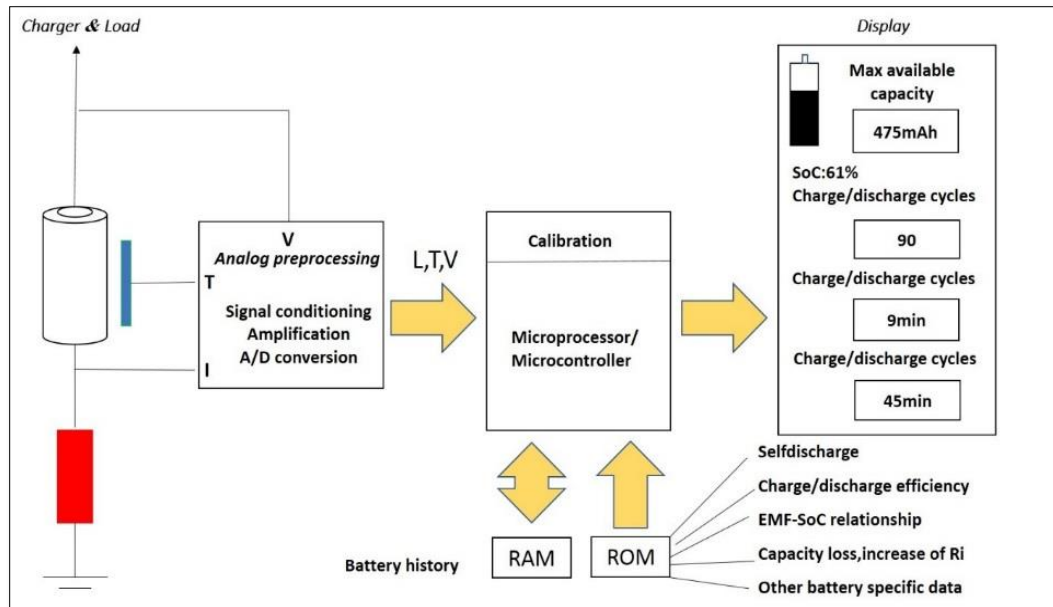


Figure I.4: General Practical Architecture of a State-of-Charge System [6].

### I.5. Definition of General Battery Parameters

For an environment friendly dialogue of SOC indication methods, some of the phrases frequently used in the battery SOC should be defined.

- ❖ **Ampere-hour.** A measure of electric powered charge described as the imperative product of present day (in Amperes) and time (in hours).
- ❖ **Cell.** The fundamental electrochemical unit used to generate electrical strength from saved chemical electricity or to save electrical electricity in the form of chemical energy. A cell consists of two electrodes in a container stuffed with an electrolyte.
- ❖ **Battery.** Two or extra cells related in a fantastic series/parallel arrangement to acquire the working voltage and capacity required for a certain load. The term is additionally often used for single cells.
- ❖ **Li-ion cells.** Cells containing a liquid organic or polymer electrolyte in which the anode and cathode are both made of intercalation compounds [22].
- ❖ **C-rate.** A charge or discharge contemporary = in Amperes to the rated potential in Ah. Multiples larger or smaller than the C-rate are used to categorical larger or smaller currents. For example, the C-rate is 1100 mA in the case of an 1100 mAh battery, while the C/2 and 2C-rates are 550 mA and 2.2 A, respectively.
- ❖ **Capacity.** A battery's electrical power content material expressed in ampere-hours.

- ❖ **Maximum capacity.** Maximum amount of ability that can be removed from a battery below defined discharge conditions.
- ❖ **Cycle life.** The number of cycles that a cell or battery can be charged and discharged under specific conditions before the available ability in Ah fails to meet particular performance criteria. This will normally be 80% of the rated capacity.
- ❖ **Cut-off voltage.** The lowest operating voltage at which a cell is considered depleted. Also often referred to as end-of-discharge voltage or final voltage [15].
- ❖ **Self-discharge.** The recoverable loss of a cell's beneficial ability on storage due to interior chemical action. This is normally expressed in a share of the rated capacity lost per month at a sure temperature because batteries' self-discharge prices are strongly temperature-dependent. The self-discharge mechanism is a local redox process caused by decomposition of the electrolyte [22]. Other vital sources for the self-discharge are micro-shorts and shuttle-molecules.
- ❖ **Spread.** Difference between characteristics of batteries of the same type.
- ❖ **State-of-Health (SOH).** A 'measurement' that reflects a battery's regular situation and its capability to supply the detailed overall performance in contrast with a fresh battery.
- ❖ **State-of-Charge (SOC).** The percentage of the maximum viable cost that is current inside a rechargeable battery.
- ❖ **Depth-of-Discharge (DoD).** The amount of ability withdrawn from a battery expressed as a share of its most capacity.
- ❖ **Depth-of-Charge (DOC).** The quantity of potential put into a battery expressed as a proportion of its maximum capacity.
- ❖ **Remaining run-time.** The estimated time that a battery can grant modern to a transportable machine under legitimate discharge conditions before it will end functioning.

### **I.6.State-of-the-Art of Battery State-of-Charge**

The battery SOC of new energy vehicle is equivalent to the oil meter of traditional fuel vehicle. As one of the significant factors in energy management, SOC plays a crucial role in optimizing vehicle energy management, improving battery capacity and energy utilization, preventing batteries from overcharging and over discharging, as well as ensuring the safety and long service lifetime of batteries.

### I.6.1. Classification

The electrochemical reaction process and stage of the battery are complex and difficult to determine, and the operating conditions are harsh and variable for vehicles. Therefore, it is quite difficult to obtain accurate SOC as it is a hidden state. The battery SOC estimation methods could be divided into four categories [23]: the estimation method based on characteristic parameters, the ampere-hour integral estimation method, the model-based estimation method, and the data-driven estimation method, as shown in Figure.I.5.

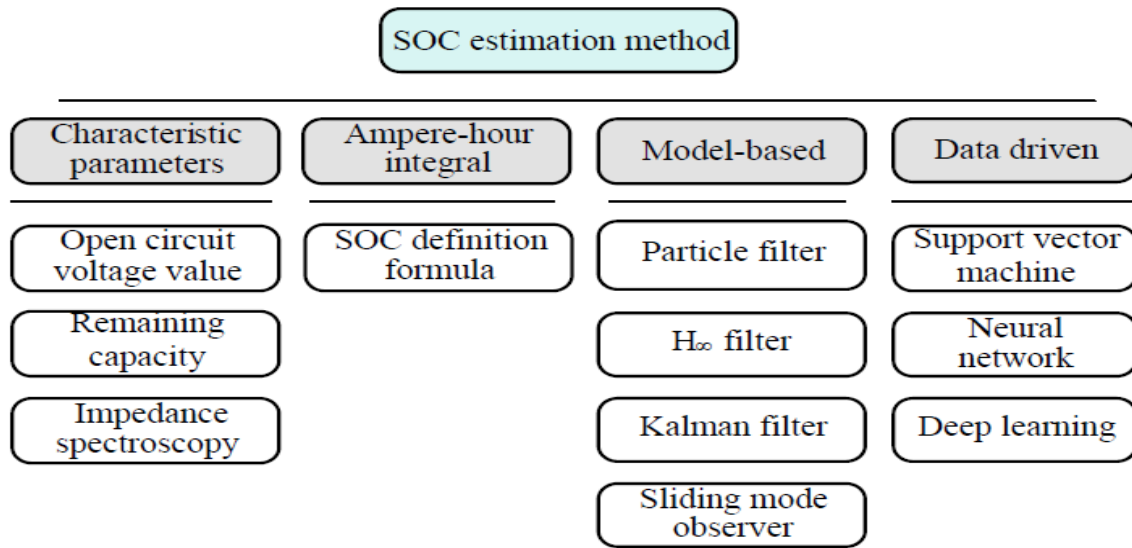


**Figure I.5.** Classification of SOC estimation methods

#### I.6.1.1. The estimation method based on characteristic parameters

The method is mainly divided into two steps:

- ✓ Establishing an offline relationship between the characteristic parameters and SOC.
- ✓ Calculating the parameter values in real time, and calibrating the SOC of battery.

The application of this method needs to meet two premises: the offline relationship between the established characteristic parameters and the SOC ought to be relatively stable, and the selected characteristic parameters should be easily available. Optional characteristic parameters include the remaining capacity, impedance spectrum, OCV, etc.

The available capacity can be obtained using the discharge experiment method, which is considered to be the most direct method for determining the battery SOC. However, it is difficult to determine the available capacity by constant current discharge for a long time during actual driving, which limits this method only applicable to some specific environments such as

laboratories. The method based on electrochemical impedance spectroscopy [24] needs the electrochemical workstation to attain the impedance under different SOC and establish the mapping relationship between SOC and parameters, then calibrate SOC by looking up tables. The stable OCV-SOC relationship [25] is often used in the industry to calibrate battery SOC, and a large number of BMS products also rely on this relationship to calibrate the initial battery SOC. However, the battery is required to rest for a long time so that the accurate OCV can be acquired. As a result, it often needs to be combined with online OCV identification methods in practical applications.

### I.6.1.2. Ampere-hour integral estimation method

This method is also known as the coulomb counting method [26], which is based on the definition of SOC, as shown in Equation (I.2).

$$Z(t) = Z(t_0) - \frac{\int_{t_0}^t \eta_i \times i_L(\tau) \times d\tau}{C_{max}} \quad (\text{I.2})$$

where  $\mathbf{z(t)}$  represents the estimated value of the battery SOC at time  $\mathbf{t}$ ,  $\mathbf{z(t_0)}$  indicates the initial value of the battery SOC.  $\boldsymbol{\eta_i}$  denotes the coulomb efficiency of the battery, which is determined by experiments. For lithium-ion batteries, the discharge efficiency is generally regarded as **1**, the charging efficiency ranges between **0.98** and **1** (within 3C charging current).  $\mathbf{i_L(\tau)}$  stands for the charging and discharging current at time  $\boldsymbol{\tau}$  and  $\mathbf{C_{max}}$  refers to the maximum available capacity of the battery under current conditions.

Despite the ampere-hour integral method is classical and widely used for SOC estimation, it has the following three major defects:

- ✚ The accurate value of the initial SOC is difficult to obtain.
- ✚ The method requires accurate current sensors. However, the accuracy of current sensors is usually affected by noise, temperature drift, and other unknown random disturbances in practical applications. In integral calculation, these random variables are easy to cause accumulated errors, and the rounding calculation carried out by the controller also has a certain impact.
- ✚ The deterioration of the battery static capacity affects the SOC estimation accuracy.

The three factors mentioned above mutually affect each other, which further reduce the reliability of this method. In order to eliminate the restriction imposed by the above factors and improve the estimation accuracy, complex and tedious periodic calibration is required.

For this reason, this method is often combined with other methods to develop a fusion method. For example, OCV is used to determine the initial SOC of the battery, and the SOC trajectory is calculated using the ampere-hour integral method.

### **I.6.1.3. Model-based estimation method**

The method uses the model and state estimation algorithm to complete the SOC estimation of the battery. Therefore, the method first needs to establish a reliable model. This section mainly introduces and illustrates the model-based SOC estimation method with the ECM. Based on the established ECM and its state-space equation, the filter and the observer algorithms are applied to build a model-based SOC estimation framework. The specific implementation processes (Figure.I.5) are summarized as following:

1. Based on the SOC of previous moment or the initial SOC and the measured current, the SOC estimation at the current time is calculated by using the ampere-hour integral method;
2. Calculate the model parameters based on the relation between parameter and SOC, such as the OCV-SOC relationship;
3. Calculate the terminal voltage based on the state-space equation;
4. Calculate the voltage error, that is, the innovation with the measured voltage;
5. Modify the estimated SOC with a certain gain of the innovation, so as to obtain the final SOC correction value and use it as the input of the next moment.

The form of the gain in Step (5) depends on the state estimation algorithm. Obviously, the model-based method is a closed-loop method, which makes the algorithm have certain robustness by continuously modifying the SOC results. In general, the estimation accuracy of the model-based method is determined by the prior estimation process and posteriori process. In case that the estimation result of the ampere-hour integral is reliable (the prior SOC estimation value is accurate), the gain can be appropriately reduced; otherwise, it will be increased. However, the excessive correction will make the SOC value vary significantly, the gain should be adjusted according to the actual situation.

The performance of the model-based estimation method relies on the model and estimation algorithm. Kalman filter (KF) algorithm [27] is the most widely used algorithm for battery SOC estimation. KF is an optimal estimation method with minimum variance proposed by American scholar Kalman in the early 1960s, which is convenient for real-time processing. It provides a solution to deal directly with random noise. The KF treats the parameter error as noise and treats

the parameters to be estimated as space state variables. The system noise and random noise are filtered out by recursive method to obtain the accurate state. However, the original KF is only applicable to linear systems, and the proposed extended Kalman filter (EKF) [27] extends it to the nonlinear systems. EKF linearizes the battery model with Taylor expansion. However, in the process of linearization, truncation error will arise, which will increase SOC estimation error, and even cause divergence under improper initial settings. Therefore, it is necessary to improve and optimize the battery model, or use the improved KF algorithm to guarantee the accuracy and robustness of the system. Although EKF considers the noise in the actual process as much as possible, it still encounters two problems.

1. It assumes that the noise remains unchanged, which obviously does not match with the actual. The noise covariance algorithm is proposed to address this problem. It updates adaptively the statistical characteristics of noise in the filtering algorithm as the change of estimated results, such as the adaptive extended Kalman filter (AEKF) [28].
2. It assumes the noise as white noise. When this assumption fails to meet, the  $H^\infty$  filter (HIF) [29] based on the principle of minimizing the maximum estimation error can be used to complete the SOC estimation of battery. It acknowledges that the statistical characteristics of noise are unknown in the actual process. Based on the principle of HIF, the optimal solution to the state estimation in the worst case is acquired.

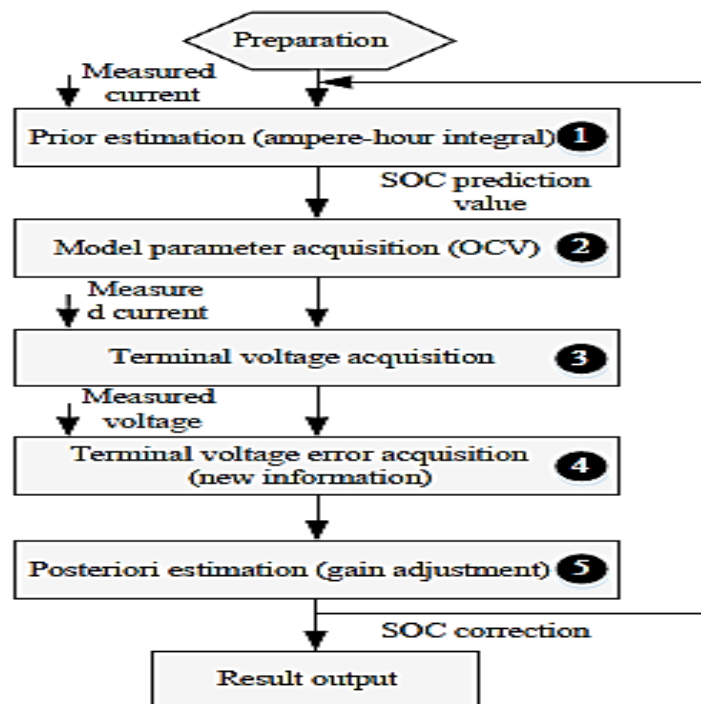


**Figure I.6.** Flowchart of the model-based estimation method

#### I.6.1.4. Data-driven estimation method

Based on a large amount of offline data, this method establishes and trains a mapping relationship model between the battery current, voltage, temperature and SOC [30].

The flowchart is shown in Figure.I.7, which is divided into three steps:

1. Preprocessing of the offline data. To obtain the format that meets the input and output requirements of the model, offline data needs to be preprocessed such as data cleaning, normalization, data segmentation. Data segmentation refers to dividing the normalized data into the training set, verification set, and test set according to a certain proportion.
2. Modeling and training. According to the size of the data, the structure of the model is preliminarily determined. Afterward, the training set is adopted to train the model, and the verification result of the verification set is used as the training cutoff criteria.
3. Model test. The test set is used to determine whether or not the accuracy meets the requirements. If so, the training is completed. Otherwise, it will return to Step (1) to design and plan again.

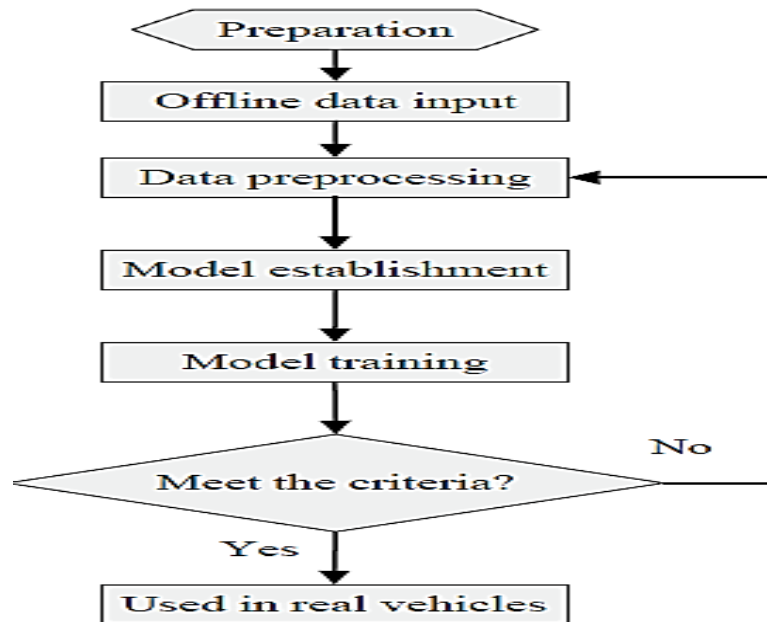


**Figure.I.7.** Flowchart of the data-driven estimation method

The data-driven method has special advantages in solving strongly nonlinear problems and has high estimation accuracy, but it often requires a large amount of experimental data as prior knowledge. In addition, the experimental data should fully reflect the characteristics of the battery; otherwise, it will easily lead to over-fitting of the model. Meanwhile, the complexity

of the model, the selected training function, and the training cutoff criteria also have a direct impact on the estimation accuracy and generalization ability of the model.

The typical representative of this method is the neural network model [31], which requires little consideration given to the internal chemical reaction details of the battery. Meanwhile, it displays a strong fitting ability, which makes it suitable for SOC estimation of any kind of batteries in theory. However, in recent years, it has been discovered that increasing the number of neurons in the neural network often contributes to a rapid increase in the parameters of the model, which further leads to the over-fitting of the model. Therefore, the study of neural networks has gradually shifted to the deep learning network [32] with stronger generalization ability. Meanwhile, the structure of the trained neural network model is more complex and the calculation cost is substantial, thus high-performance chips are often needed in vehicle applications. Therefore, a large number of chips used for neural network/deep learning are gradually launched in the market.

This table summarizes the advantages and disadvantages of four SOC estimation methods as well as their performances in accuracy and robustness.

**Table.I.2.** The advantages and disadvantages of four SOC estimation methods [33].

Methods	Advantages	Disadvantages	accuracy	robustness
Estimation method based on characteristic parameters	-easy to implement -low computing cost -good real-time performance	-easily affected by the uncertainty factors, such as temperature, working condition, and degree of aging  -regular calibration of OCV or EIS information is required	poor	good
Ampere-hour integral estimation method	-easy to implement -low computing cost -excellent real-time performance	-dependence on the accurate SOC initial value  -the open-loop calculation method needs periodic revision  -it is susceptible to current drift, noise, and aging	ordinary	poor
Model-based estimation method	-high estimation accuracy  -closed-loop	-it depends strongly on the accuracy of the model	excellent	excellent

	feedback control -good real-time performance -strong adaptability	-computing costs are relatively high -improper initial values diverge the estimated results		
Data-driven estimation method	-high estimation accuracy -good at dealing with nonlinear problems	-high algorithm complexity -high dependence on the training data	excellent	poor

## I.7.Conclusions

This chapter gives an overview of the state-of -the-art of state-of-charge indication of rechargeable batteries, including a historical SOC technology, battery management systems general state-of-charge system and SOC classification techniques. Where we see after this study that we will choose the coulomb counting method to study in the third chapter because it is the easiest and most effective method according to the approved references in this study.

**references**

- [4] V. Pop, H. J. Bergveld, D. Danilov, P. P. Regtien, and P. H. Notten, *Battery management systems: Accurate state-of-charge indication for battery-powered applications*. Springer Science & Business Media, 2008.
- [5] H. Dreer, "Curtis wheelchair battery fuel gauge Product Test Report Marketing Services Dept., Curtis Instruments," ed: Inc, 1984.
- [6] J. Kauzlarich, "Electric wheelchair fuel gauge tests," *Report N° UVA-REC-102-86. UVA Rehabilitation Engineering Center*, 1986.
- [7] J. S. Martinez, D. Hissel, M.-C. Péra, and M. Amiet, "Practical control structure and energy management of a testbed hybrid electric vehicle," *IEEE Transactions on Vehicular Technology*, vol. 60, no. 9, pp. 4139-4152, 2011.
- [8] E. P. Finger and E. A. Sands, "Method and apparatus for measuring the state of charge of a battery by monitoring reductions in voltage," ed: Google Patents, 1980.
- [9] S. Lerner, H. Lennon, and H. Seiger, "Development of an alkaline battery state of charge indicator," *Power Sources*, vol. 3, pp. 135-7, 1970.
- [10] V. Pop, H. J. Bergveld, D. Danilov, P. P. Regtien, and P. H. Notten, "State-of-the-art of battery state-of-charge determination," *Battery Management Systems: Accurate State-of-Charge Indication for Battery-Powered Applications*, pp. 11-45, 2008.
- [11] R. Brandwein and M. L. Gupta, "Nickel-cadmium battery monitor," ed: Google Patents, 1976.
- [12] C. C. Christianson and R. F. Bourke, "Battery state of charge gauge," ed: Google Patents, 1976.
- [13] S. Rodrigues, N. Munichandraiah, and A. Shukla, "A review of state-of-charge indication of batteries by means of ac impedance measurements," *Journal of power Sources*, vol. 87, no. 1-2, pp. 12-20, 2000.
- [14] E. Peled, H. Yamin, I. Reshef, D. Kelrich, and S. Rozen, "Method and apparatus for determining the state-of-charge of batteries particularly lithium batteries," ed: Google Patents, 1988.
- [15] J. H. Aylor, A. Thieme, and B. Johnso, "A battery state-of-charge indicator for electric wheelchairs," *IEEE transactions on industrial electronics*, vol. 39, no. 5, pp. 398-409, 1992.
- [16] G. Richter and E. Meissner, "Method for determining the state of charge of storage batteries," ed: Google Patents, 2002.
- [17] O. Gérard, J.-N. Patillon, and F. d'Alché-Buc, "Neural network adaptive modeling of battery discharge behavior," in *International Conference on Artificial Neural Networks*, 1997, pp. 1095-1100: Springer.
- [18] J. Garche and A. Jossen, "Battery management systems (BMS) for increasing battery life time," in *TELESCON 2000. Third International Telecommunications Energy Special Conference (IEEE Cat. No. 00EX424)*, 2000, pp. 81-88: IEEE.

- [19] H. Feil, H. J. Bergveld, and J. R. G. C. M. Van, "Method of predicting the state of charge as well as the use time left of a rechargeable battery," ed: Google Patents, 2003.
- [20] H. J. Bergveld, W. S. Kruijt, and P. H. Notten, "Battery management systems," in *Battery Management Systems*: Springer, 2002, pp. 9-30.
- [21] M. W. Verbrugge, E. D. Tate Jr, S. D. Sarbacker, and B. J. Koch, "Quasi-adaptive method for determining a battery's state of charge," ed: Google Patents, 2002.
- [22] B. A. Johnson and R. E. White, "Characterization of commercially available lithium-ion batteries," *Journal of power sources*, vol. 70, no. 1, pp. 48-54, 1998.
- [23] R. Xiong, J. Cao, Q. Yu, H. He, and F. Sun, "Critical review on the battery state of charge estimation methods for electric vehicles," *Ieee Access*, vol. 6, pp. 1832-1843, 2017.
- [24] D. Andre, M. Meiler, K. Steiner, H. Walz, T. Soczka-Guth, and D. Sauer, "Characterization of high-power lithium-ion batteries by electrochemical impedance spectroscopy. II: Modelling," *Journal of Power Sources*, vol. 196, no. 12, pp. 5349-5356, 2011.
- [25] H. He, R. Xiong, and H. Guo, "Online estimation of model parameters and state-of-charge of LiFePO<sub>4</sub> batteries in electric vehicles," *Applied Energy*, vol. 89, no. 1, pp. 413-420, 2012.
- [26] Y. Zhang, W. Song, S. Lin, and Z. Feng, "A novel model of the initial state of charge estimation for LiFePO<sub>4</sub> batteries," *Journal of Power Sources*, vol. 248, pp. 1028-1033, 2014.
- [27] G. L. Plett, "Sigma-point Kalman filtering for battery management systems of LiPB-based HEV battery packs: Part 1: Introduction and state estimation," *Journal of Power Sources*, vol. 161, no. 2, pp. 1356-1368, 2006.
- [28] R. Xiong, H. He, F. Sun, and K. Zhao, "Evaluation on state of charge estimation of batteries with adaptive extended Kalman filter by experiment approach," *IEEE Transactions on Vehicular Technology*, vol. 62, no. 1, pp. 108-117, 2012.
- [29] Y. Zhang, R. Xiong, H. He, and W. Shen, "Lithium-ion battery pack state of charge and state of energy estimation algorithms using a hardware-in-the-loop validation," *IEEE Transactions on Power Electronics*, vol. 32, no. 6, pp. 4421-4431, 2016.
- [30] L. Kang, X. Zhao, and J. Ma, "A new neural network model for the state-of-charge estimation in the battery degradation process," *Applied Energy*, vol. 121, pp. 20-27, 2014.
- [31] W. He, N. Williard, C. Chen, and M. Pecht, "State of charge estimation for Li-ion batteries using neural network modeling and unscented Kalman filter-based error cancellation," *International Journal of Electrical Power & Energy Systems*, vol. 62, pp. 783-791, 2014.
- [32] E. Chemali, P. J. Kollmeyer, M. Preindl, R. Ahmed, and A. Emadi, "Long short-term memory networks for accurate state-of-charge estimation of Li-ion batteries," *IEEE Transactions on Industrial Electronics*, vol. 65, no. 8, pp. 6730-6739, 2017.

- [33] C. Lin, H. Mu, R. Xiong, and W. Shen, "A novel multi-model probability battery state of charge estimation approach for electric vehicles using H-infinity algorithm," *Applied Energy*, vol. 166, pp. 76-83, 2016.

# **Chapter II: Battery Modeling**

## **II.1. Introduction**

In this chapter we will learn about how batteries are charged and their models. We'll discuss the various types of batteries and their benefits and disadvantages. And we're going to look at the best form of battery today for your EV conversion, where we're going to talk intensively about the lithium and lead acid batteries in this chapter and then we're going to do specific research on these two types.

## **II.2. Electric Vehicle Battery Technologies**

### **II.2.1. Overview**

EV's chassis included mechanical elements, and its electrical motors and controllers. Its batteries will take you into the chemical zone now. Although there are all sorts of battery innovations going on in the laboratories, the aim here is to give you a brief history to the battery and introduce the lead-acid and lithium batteries with which you will be working on your EV conversion.

EV battery pack-a collection of 16 to 24 6-volt (or 12-volt equivalent) individual lead-acid and lithium batteries represents the single largest replacement cost item, and quite possibly is also your largest initial expense item, it's worth spending some time learning about batteries so you can choose and use them wisely [19].

Batteries are the breath of your EV's life, and they should be familiar to any EV converter on three levels. To be battery graduate you need to:

- Comprehend what happens inside a battery
- Become familiar with the external properties of a battery
- Know the pros and cons of real-world batteries working

Knowledge in these three fields is a good investment in business and can save you time and money.

### **II.2.2. Basics of Lead Acid Battery**

Lead acid batteries have been around for more than a century. In the fully charged state, a 2V electric potential exists between the cathode and the anode [20]. Electrons are pushed through the load externally during discharge, while internal chemical reactions at the electrolyte interface and the electrodes work to balance the balance of charge. The chemical state of a fully charged and discharged lead acid battery is demonstrated in table II.1.

**Table II.1:** Lead Acid Charge States [22].

	<b>Anode</b>	<b>Electrolyte</b>	<b>Cathode</b>
Fully Charged	$Pb$	$H_2SO_4$	$PbO_2$
Fully Discharged	$PbSO_4$	$H_2SO_4$	$PbSO_4$

Lead acid batteries can be divided into two distinct categories: flooded and sealed/valve regulated (SLA or VRLA) [21]. The two types are similar in their internal chemistry (shown in Table II.1), and the device level design criteria are the most important variations between the two types. Flooded batteries with lead acid need three things VRLA doesn't:

1. Upright orientation against leakage of electrolytes.
2. Ventilated area, created during cycling to disperse the gasses.
3. Routine Electrolyte management.

Such variations include balancing the lower cost of flooded lead acid against the additional expense and secondary costs. There are two types of VRLA batteries: Gel and Absorbed Glass Mat (AGM). The different names represent different methods of electrolyte-containment. A thickening agent is inserted into Gel batteries to transform the electrolyte from liquid to gel. In AGM cells the liquid electrolyte is covered by a glass matrix.

“Deep cycle” and “shallow cycle” lead acid batteries can be found in both the VRLA and flooded classes. Shallow cycle VRLA batteries are commonly used for automotive start, light, ignition (“SLI”) batteries that must deliver high power pulses for short durations [22]. The stationary power market uses a deep loop, as the batteries often discharge at a low rate over multiple hours.

### II.2.3. Basics of Lithium-ion Battery

The concept of a lithium-ion battery was initially conceived in the 1970's and began to see widespread adoption by the 1990's [20]. The basic mechanism is that a charged lithium ion is shuttled back and forth between the cathode and the anode during charge and discharge. Figure II.1 shows a diagram of a  $LiCoO_2$  variation of the lithium-ion family.

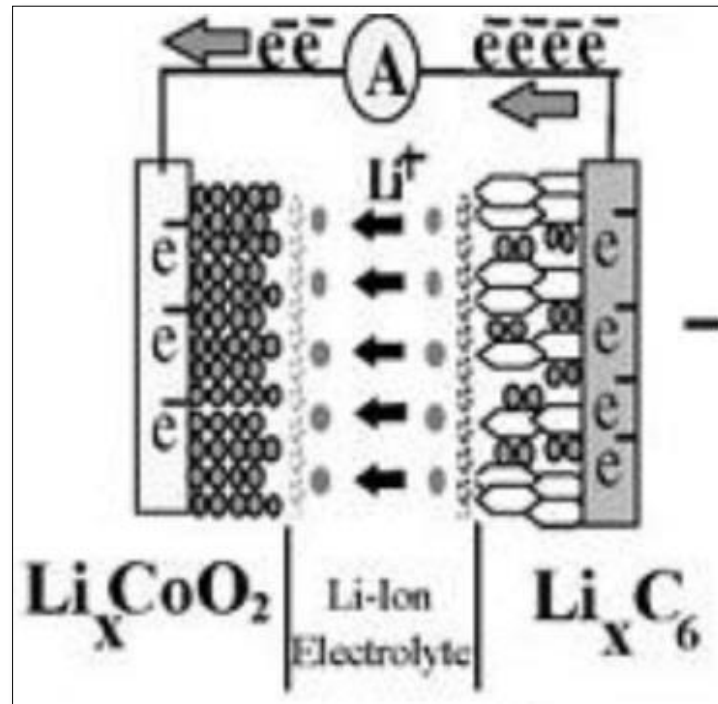


**Figure II.1:** *Lithium-ion Reaction* [23].

Chemical variations in the cathode, anode and electrolyte affect the efficiency of the cells, as do packaging geometry. The cathode chemistry is the factor most commonly altered from cell manufacturer to cell manufacturer with terms like LFP, NCM, NCA, Cobalt, and Manganese reflecting the cathode chemistry class [23]. Graphite constitutes over 90 percent of lithium-ion anodes; silicon and titanium-based materials are sometimes used to enhance life and efficiency, in return for substantially higher costs.

The electrolyte exists in liquid form, but for “lithium polymer” cells, the electrolyte is absorbed in a polymer membrane [24]. This allows cell manufacturers to use a pocket enclosure on the cell rather than the metal enclosure used when the liquid electrolyte in cylindrical and prismatic cells is present. Growing of those variations influences a lithium-ion cell's efficiency.

In spite of the various chemical variations, lithium-ion batteries can generally be separated into two groups: lithium iron phosphate (LFP,  $LiFePO_4$ ) and metal oxides (NCM, NCA, Cobalt, Manganese) [25]. Table II.2 outlines the variations on a cell-level between the two chemical groups. The table values represent the average values provided that there are differences in each class.

**Table II.2:** Lithium-ion Subcategory Comparison [26, 27].

	LFP	LiNCM
Voltage	3.3 V nominal (2-3.6 V/cell)	3.7 V nominal (2.7-4.2 V/cell)
Energy Density	300 Wh/L	735 Wh/L
Specific Energy	128 Wh/kg	256 Wh/kg
Power	1000 W/kg	512 W/kg
Cycle Life	2,000 @ 100% DoD 3,000 @ 80% DoD	750 @ 100% DoD 1,900 @ 80% DoD
Calendar Life	6 years	8 years
Max recommended temperature	40°C	55°C
Safety	High	Moderate
Commercial Suppliers	A123, Valence, BAK, BYD, K2, Lishen, many Chinese vendors	Sanyo, Panasonic, Samsung, DowKokam, Sony, LG Chem, Moli

Both lithium-ion cells are "deep cycle" which means they are capable of being both charged and discharged. The battery life would improve dramatically if increasing discharge depth is limited to 80 per cent of the rated capacity.

### II.3. Methods of Charging Electric Vehicle Battery

#### II.3.1. Methods of Charging Lead-Acid Batteries

##### a) Taper Charging Method

Taper charging is a variation of the modified constant-potential method, using less sophisticated controls to reduce equipment cost. This method does result in gassing at the critical point of recharge, and the cell temperature is increased [28].

The end of the charge is often controlled by a fixed voltage rather than a fixed current. Therefore, when a new battery has a high counter-EMF, this final charge rate is low and the battery often does not receive sufficient charge within the time period allotted to maintain the optimum charge state [28]. In the latter part of life when the counter-EMF is small, the charging rate is higher than the usual finishing rate and thus the battery receives excessive charging, which degrades life.

For photovoltaic battery systems and other systems designed for maximum life, circuits for charging and regulating will generate a voltage and current pattern equal to the best industrial circuits. Changed constant-potential charging methods are favored with starting constant current. Optimum control to maximize the life and energy output from the battery is best achieved when the depth of discharge and the time for recharge are predetermined and repetitive, a condition which is not always realized in solar photovoltaic applications [29].

#### b) **Float Charging Method**

Float charging is a low-rate, constant-potential charging and is often used to hold the battery fully charged. This method is primarily employed for stationary batteries that can be charged from a DC bus. The float voltage for a non-antimonial grid battery containing 1.210 specific gravity electrolytes and have an open-circuit voltage of 2.059 V per cell is 2.17 to 2.25 V per cell [29].

### **II.3.2. Methods of Charging Lithium Batteries**

#### a) **Five-step Charging Pattern**

As seen in the CC-CV method above, the CV stage prolongs the charging time and reduces the cycle life of the battery. For that reason, an alternative method is derived in order to reduce the charge time and give more life cycles for the cell. The five-step charging method consists of partitioning the charging time into 5 steps [30]. In each step, the battery is charged with a different and lower constant current for some duration shown in Fig. II.2 While charging, the battery voltage increases until it reaches a preset value, at this moment the charger switches to the next step. The charging current in each step is set to predetermined value; this value is found in different algorithms [31, 32]. In this step a Particle Swarm Optimization (PSO) based search method will be mentioned.

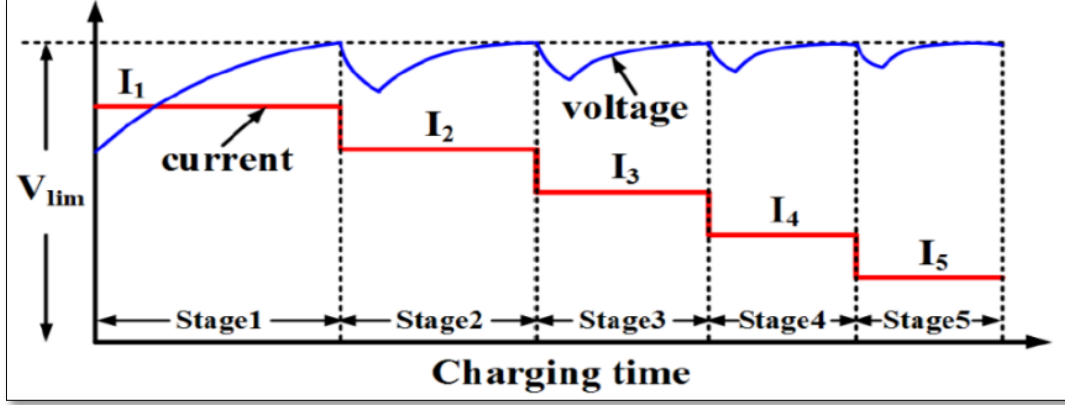


**Figure II.2:** Five-step Charging Pattern [31].

One way of achieving the optimum charging pattern is by using the PSO technique. The PSO is an evolutionary computational technique focused on the population and inspired by the social behavior of bird flocks. It has attracted many researchers for its simplicity in implementation where it has few parameters to tune and adjust, features the characteristic of fast convergence and less computational time, non-gradient derivative-free algorithm which can estimate several solutions in a single iteration, there is no relation between the solution obtained and the initial solution [31]. A PSO is composed of several particles, which form a swarm, moving in the feasible solution space in search of the optimal solution shown in Fig II.3. Each particle will exchange information with the rest of the swarm in order to find the global best solution ( $G_{best}$ ). In each iteration, every particle will update its flying direction based on its own best solution ( $P_{best}$ ) and ( $G_{best}$ ) according to the model equations as follows:

$$v_{id}^{k+1} = wv_{id}^k + C_1rand_1^k(P_{best}_{id}^k - x_{id}^k) + C_2rand_2^k(G_{best}_d^k - x_{id}^k) \quad (\text{II.1})$$

$$x_{id}^{k+1} = x_{id}^k + v_{id}^{k+1} \quad (\text{II.2})$$

where,  $v_{id}^k$  is the value of dimension  $d$  in the velocity vector of particle  $i$  at iteration  $k$ .  $x_{id}^k$  is the position of particle  $i$  along dimension  $d$  at iteration  $k$ .  $w$  is the selected inertia weight,  $C_1$  and  $C_2$  are the cognitive and social learning rates, respectively, which change the velocity of a particle towards  $P_{best}$  and  $G_{best}$ .

To find the optimum five-step charging speeds for C to satisfy the quick charging requirements and the best cost benefits for charging, the PSO algorithm is used to find the optimum charging pattern. The formulation of problems is defined as follows:

$$\text{Maximize} \quad f_{cost}^i(T_{ch}^i, C_{dis}^i) = \alpha T_{ch}^i(\vec{I}_j^i) + \beta C_{dis}^i(\vec{I}_j^i), \quad \vec{I}_j^i \in \mathbb{S} \quad (\text{II.3})$$



which batteries can be recharged with very high current for a limited period of time close to fully discharged. The detrimental effect of charging the battery with high current is taken into consideration so that the boost charge method does not introduce any negative degradation effects [33].

### **II.3.3. Common Methods to Charge the Batteries**

#### **a) Constant-Current Charging**

Constant-current recharging is not commonly used for lead-acid batteries but for lithium batteries at one or more current speeds. This is due to the need for current adjustment unless the charge current is kept at low during the charge (Ampere-hour rule), resulting in long charge times of 12 h or more. Typical charger and characteristics of the battery for continuous current charging, for single and two-stage charging. Some small lead-acid batteries use constant-current charging. Due to the ease of measuring Ampere-hour input and since constant-current charging can be achieved with easy, inexpensive equipment, constant-current charging is also sometimes used in the laboratory. In the field, constant-current charging at half the 20-h rate can be used to decrease sulfating in overloaded or underloaded batteries. This treatment, however, may diminish the battery life and should be only used with the advice of the battery manufacturer [29].

#### **b) Constant-Potential Charging**

The modified constant-potential charging methods (methods b and c) are used in typical industrial applications. Modified constant charging capacity is used for on - the-road vehicles and applications for electricity, telecommunications and uninterruptible power systems where the charging circuit is connected to the battery. The charging circuit has a current limit in this case, and that value is retained until a fixed voltage is reached. The voltage is then kept constant until the battery is asked to discharge. Decisions on the current limit and the constant-voltage value must be made. This is determined by the time period when the battery is at constant voltage at a charge state of 100 per cent. A low charge current is desirable to reduce overload, grid corrosion associated with overload, water loss due to electrolysis of the electrolyte, and maintenance to substitute this water for this "float"-type operation with the battery still on load. Achieving a full recharge with a low constant potential requires the proper selection of the starting current, which is based on the manufacturer's specifications [34].

The adjusted constant-potential charge, with constant start and finish levels, is normal for deep-cycling batteries typically discharged at a depth of 80 percent at the 6-h rate; recharging is usually completed in an 8-h cycle. The charger is set for the constant potential of 2.39 V per cell (the gassing voltage), and the starting current is limited to 16 to 20A per 100 Ah of the maximum 6-h Ampere-hour range by means of a series of charger circuit resistors. This initial current remains constant until the battery's average cell voltage exceeds 2.39 V. At constant voltage, the current decays to the finishing rate of 4.5 to 5A per 100 Ah, which is then sustained until the end of the charge. A Timer monitors the total charge time. The time of charge is selected to ensure a recharge input capacity of a predetermined percent of the Ampere-hour output of the previous discharge, normally 110 to 120%, or 10 to 20% overcharge. The 8-h charging time can be reduced by increasing the initial current limit rate [29].

### c) Pulse Charging

This method aims at obtaining an even distribution of ions in the battery electrolyte, speeding up the charging process, and slowing battery polarization and increasing life cycles.

The charging frequency is critical in this form of loading process. It relates to the time and efficiency of charging. Different techniques are being carried out to determine the optimal charging frequency instead of the outdated techniques of trial and error. It has suggested the varied duty pulse charge, it can detect the best pulse charging duty cycle to get the best charging speed and output. The AC impedance technique is suggested to find the optimal pulse charging frequency related to the minimum AC impedance frequency [35, 36].

The duty varied pulse charge strategy consists of changing the duty cycle. It is based on the fact that a smaller duty cycle,  $D$ , means better current density exchange  $i_0$  which results with better efficiency and with larger rest period the charging time will be long. Therefore, it is important to compromise between high charging efficiency and faster battery charge. Thus, the pulse charge factor is defined as:

$$\eta = D \cdot i_0 \quad (\text{II.4})$$

Given that, the exchange current density  $i_0$  is given by:

$$i_0 = Fk_0(1 - \theta)^{1-\alpha}\theta^\alpha c^{1-\alpha} \quad (\text{II.5})$$

The pulse charge factor will be as follow:

$$\eta = D \cdot F \cdot k_0(1 - \theta)^{1-\alpha}\theta^\alpha c^{1-\alpha} \quad (\text{II.6})$$

It is necessary to note that  $\alpha$  and  $c$  are not proportional to  $(1-D)$ , so the service cycle  $D$  is not set at 50 per cent for better efficiency and quick charge time. Thus, a search method is implemented into the controller to find the best load duty cycle that results in the best pulse charge factor.

Concerning the optimal pulse charge frequency, the AC impedance technique is widely used [37, 38]. The AC impedance model of the Li-ion battery given in Fig. II.4 is formed by, ohmic resistance,  $R_0$ , charging transfer resistance,  $R_{ct}$ , Warburg impedance,  $Z_w$ , a capacitance,  $C_d$ , and an electrode inductance,  $L_d$ . Different charging frequency can charge the AC impedance of the battery, therefore, to obtain the minimum loss in the battery impedance and maximum charging energy the pulse charging frequency is set to be equal to the minimum AC impedance frequency  $f_{z_{min}}$ .

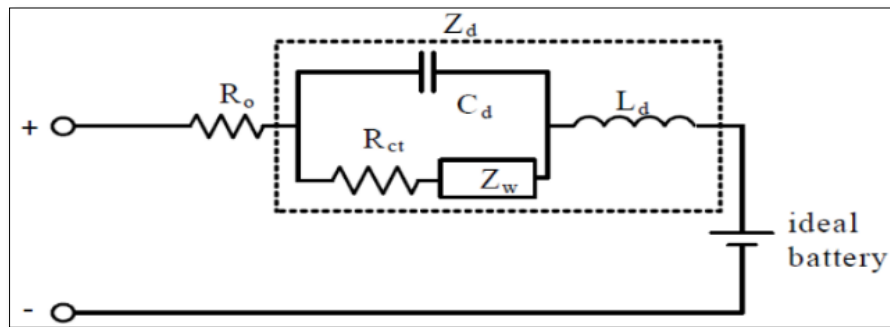


**Figure II.4:** AC Impedance Model [7].

## II.4. Types of Battery Models

### II.4.1 Lead Acid Battery Models

Modeling of the lead acid batteries can be done in numerous ways depending on the system requirement and accuracy [39]. These include Electrochemical Models, Models of Computational Fluid Dynamics, Models of Finite Elements and Models of Electric Equivalents. Such models involve experimentation to determine battery characteristics and plot response curves, measuring voltage and currents during charging and discharging phase. Electrochemical Models, Computational Fluid Dynamics Models, Finite Element Models are effective in acquiring battery technological knowledge but not very useful in actual simulation and device behavior analysis. But the electrical equivalent circuit model describes the various parameters and characteristics of the battery via the electrical equation, which is useful for the purpose of simulation which device behavior analysis.

Studying the various models goes from a very basic battery model to a complicated battery model. The research is conducted to obtain in-depth knowledge of the battery's electrical behavior. Thus, various models of electrical batteries are listed below:

**a) Simple Battery Model**

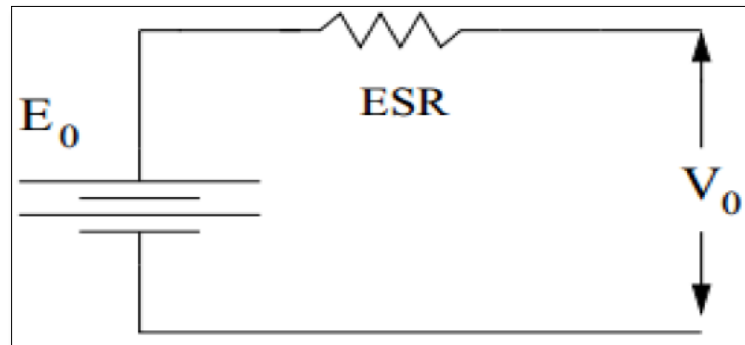


**Figure II.5:** Equivalent Circuit of Simple Model [41].

If battery was linear then it acts as an electric bipolar. A simple ideal model consists of  $E_0$  as the electromotive force of the battery and a constant equivalent resistor ESR connected in series as an internal resistance.  $V_0$  is the terminal voltage of the battery [40].  $V_0$  can be obtained by measuring the open circuit voltage and ESR can be obtained from both open circuit measurement and with load connected when the battery is fully charged

**b) Thevenin Battery Model**

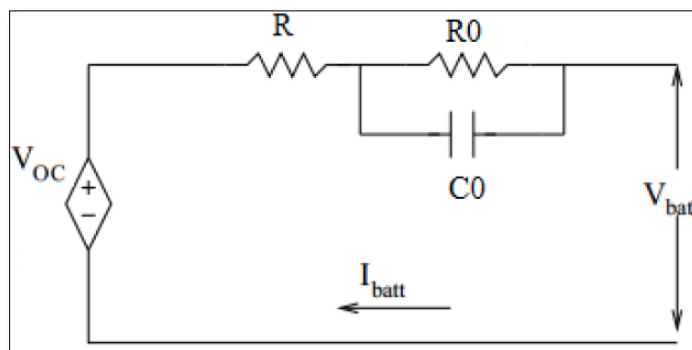


**Figure II.6:** Equivalent Circuit of Thevenin Model [42].

Thevenin battery model is one of the most commonly used battery models. The model consists of ideal no-load battery voltage  $V_{OC}$ , internal resistance ( $R$ ), Capacitance ( $C_0$ ) and over voltage resistance ( $R_0$ ). Capacitance between electrolyte and electrodes is given by ( $C_0$ )

whereas  $R_0$  represents the battery overvoltage due to the contact resistance of plate to electrolyte [41].

$$V_{batt} = V_{oc} - (I_{batt}R - V_0) \quad (\text{II.7})$$

$$V_0 = \left( \frac{1}{R_0} + \frac{1}{C_0} \right) I_{batt} \quad (\text{II.8})$$

### c) Copetti Model

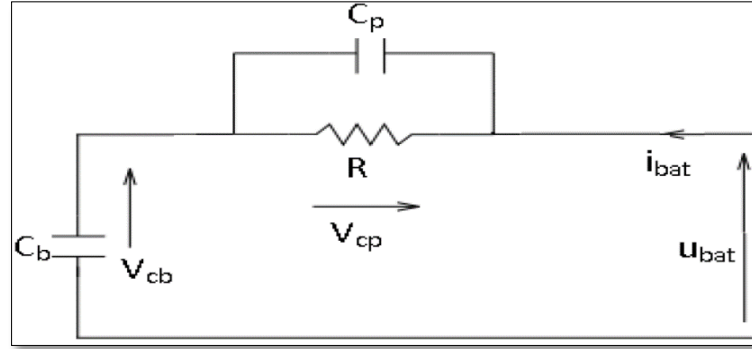


**Figure II.7:** Equivalent Circuit of Copetti Model [42].

The model is a generic battery model that has constant parameters and is valid for any battery size. This model is simple, since it does not require the experimental identification of empirical parameters. The model is defined according to the following equation:

If  $u_{batt} < nV_g$

$$u_{batt} = n(V_{cb}(t) + V_{cp}(t)) \quad (\text{II.9})$$

$$\frac{dV_{cb}}{dt} = \frac{i_{bat}(t)}{C_b(t)} \quad (\text{II.10})$$

$$\frac{dV_{cp}}{dt} = -\frac{1}{R(t)C_p} V_{cp} + \frac{i_{bat}(t)}{C_p} \quad (\text{II.11})$$

If  $u_{batt} > nV_g$

$$u_{batt}(t) = n(V_{cb}(t) + R(t)i_{bat}(t)) \quad (\text{II.12})$$

$$SOC(t) = 1$$

## II.4.2. Lithium Battery Models

### a) Equivalent Circuit Model

The analogous circuit model can be used for simulating the battery's complex properties. It's composed of circuit elements such as resistors, condensers, a source of constant voltage, ... It can be used for the different battery working conditions, and the model's state-space equations can be deduced to enable study and application. This model is also commonly used in modelling simulations and battery management systems for different types of electric vehicles.

The Rint model in Figure II.8, designed by the Idaho National Laboratory, uses an ideal voltage source to describe the open-circuit voltage of the battery. The battery's internal resistance  $R$  and the open-circuit voltage are functions of the SOC and temperature, and the internal resistance value changes when charging under the same SOC [43].

In Figure II.9, the Thevenin model, which is the most typical circuit model, considers the characteristics of the battery as capacitive and resistive. The model uses an ideal voltage source  $U_{ocv}$  to describe the open-circuit voltage of the battery, and the resistance  $R_{\Omega}$  is the ohmic resistance of the battery, while the capacitor and resistor are connected in parallel in order to describe the battery's over-potential [44].

The RC model in Figure II.9, which consists of two capacitances and three resistances, is designed by the famous battery manufacturer SAFT. The large capacitance  $C_B$  describes the energy storage capacity; the small capacitance  $C_C$  describes surface effects of the battery electrodes; the resistance  $R_T$  is referred to as the terminal resistance;

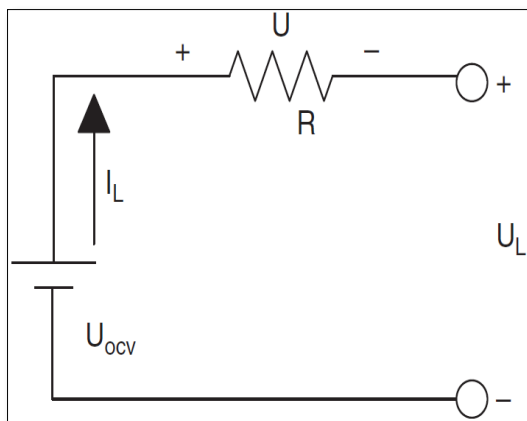


**Figure II.8:** Circuit Structure of Rint Model [44].

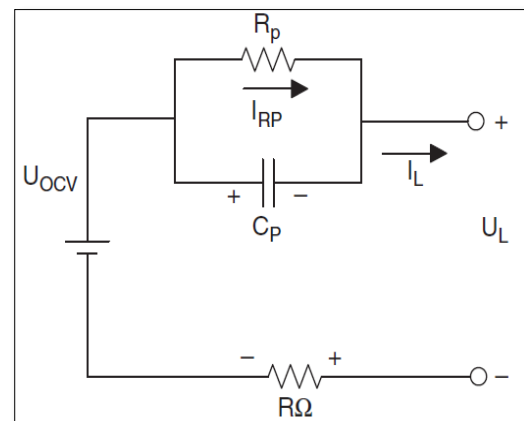


**Figure II.9:** Circuit Structure of Thevenin Model [45].

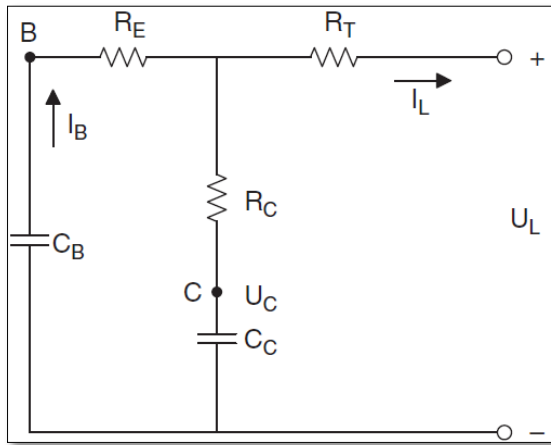


**Figure II.10:** Circuit Structure of RC Model [46].

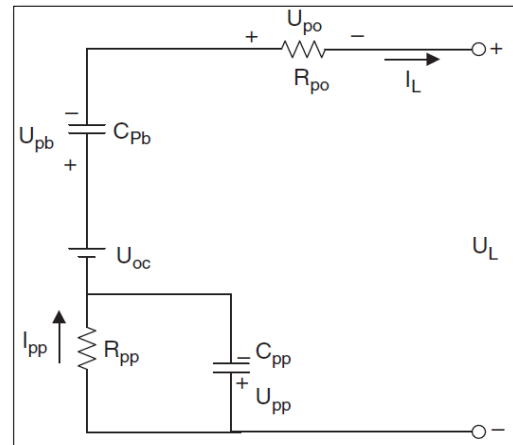


**Figure II.11:** Circuit Structure of PNGV Model [46].

as the cut-off resistance; and the resistance  $R_C$  is referred to as the capacitive resistance. In this model, the cathode of the battery is defined as the zero-potential point.

The PNGV model in Figure II.10 is the standard battery model in the “PNGV Battery Test Manual” in 2001, and extended into the standard battery model in “Freedom CAR Battery Test Manual” in 2003. In this model,  $U_{OC}$  is an ideal voltage resource, indicating open-circuit voltage of a battery,  $R_{PO}$  is the ohmic internal resistance,  $R_{PP}$  the polarization internal resistance,  $C_{PP}$  the polarization capacitance,  $I_{PP}$  the current with respect to polarization resistance; the capacitance  $C_{Pb}$  describes the cumulative open-circuit voltage change with respect to loading time [45].

### b) Electrochemical Model

The electrochemical model uses mathematical methods to describe the internal reaction process of a battery, based on electrochemical theory [23]. The Peukert formula is the most typical battery model, seen in Equation II.13, which expresses that the available charging of a battery decreases with increasing discharging current.

$$I^n T_i = \text{Constant} \quad (\text{II.13})$$

where  $I$  is the discharging current,  $n$  the constant of a battery, and  $T_i$  is the discharging time under current  $I$ .

The Shepherd model was proposed in 1965 and is expressed as Equation II.13. Electrochemical activities are described by the voltage and current of a battery [23].

$$E_t = E_O - R_i - K_i \left( \frac{1}{1-f} \right) \quad (\text{II.14})$$

where  $E_t$  is the terminal voltage of a battery,  $E_O$  the open-circuit voltage of a fully charged battery,  $R_i$  the ohmic internal resistance,  $K_i$  the polarization resistance,  $I$  the transient current and  $f$  the net discharging capacity calculated according to the Ah integration method. The Shepherd model is commonly used to analyze hybrid cars, and to calculate battery voltage and SOC together with the Peukert equation under different powers.

The Shepherd model applies to a small constant current battery and is able to find the turning point where the terminal voltage begins to rapidly decrease. Such a critical state happens occasionally during an electric car battery's actual operating cycle. In Equations II.14–II.16, Unnewehr and Nasar simplified the Shepherd model;

$$E_t = E_O - R_i - K_i f \quad (\text{II.15})$$

$$E_{OC} = E_O - K_i f \quad (\text{II.16})$$

$$R = R_O - K_R f \quad (\text{II.17})$$

where  $E_{OC}$  is the open-circuit voltage,  $R_O$  the total internal resistance of a fully charged battery,  $K_R$  the experimental constant, and  $R$  the battery equivalent resistance.

It is developed into the Nerst model and the Nerst expanded model based on the Unnewehr model, respectively expressed in Equations II.16 and II.18.

$$E_t = E_i - R_i I - K_i \ln(f) \quad (\text{II.18})$$

$$E_t = E_O - R_i I - K_i \ln(f) + K_j \ln(1-f) \quad (\text{II.19})$$

Based on the Shepherd model, the Unnewehr model and the Nerst expanded model, Dr. Gregory L. Plett from Colorado University developed a group formulation of the above three electrochemical models, seen in Equation II.19.

$$U_L = K_0 - R I_L - \frac{K_1}{SOC} - K_2 SOC + K_3 \ln(SOC) + K_4 \ln(1 - SOC) \quad (\text{II.20})$$

where  $U_L$  is the battery loading voltage,  $I_L$  the current,  $R$  the battery internal resistance, and  $K_0$ ,  $K_1$ ,  $K_2$ ,  $K_3$ , and  $K_4$  are the mean model coefficients, respectively.

### c) The Fractional-Order Model

Figure II.12 demonstrates the electrochemical impedance spectroscopy (EIS) test results for the battery 1-cell 2 [46]. There is a semicircle in the middle-frequency spectrum

whose center is under the horizontal axis. In general, this phenomenon is known to be connected to the double layer at the electrode-electrolyte interface.

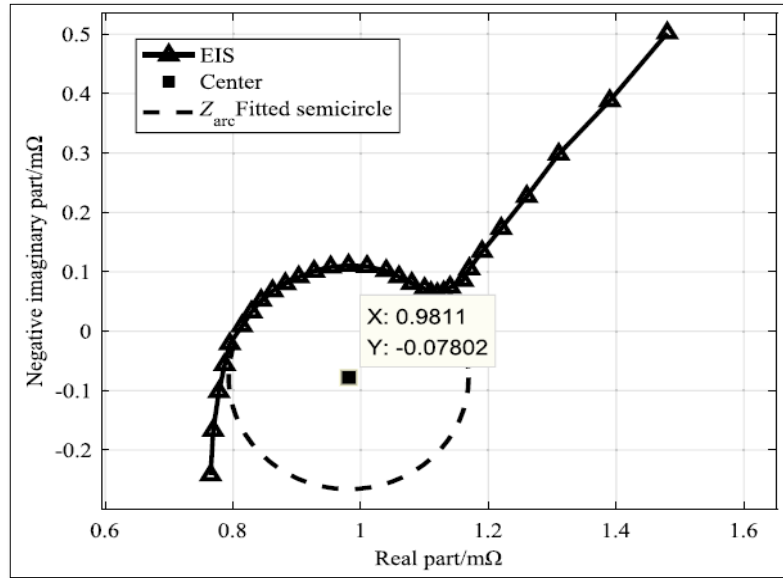


**Figure II.12:** *The Dispersion Effect in Electrochemical Impedance Spectroscopy [46].*

The researchers discovered when fitting impedance spectra that the ECM frequently failed to achieve the desired fitting precision using ideal capacitances. The phenomenon that the double layer's calculated frequency response characteristics are incoherent with the pure capacitance is called the dispersion impact. This deviation from the pure capacitance can be fitted by a *constant phase element (CPE)*. Its impedance expression is as follows [47]:

$$Z'_{CPE}(\omega) = \frac{\omega^{-\alpha}}{Y} \cos\left(\frac{\alpha\pi}{2}\right), Z''_{CPE}(\omega) = \frac{\omega^{-\alpha}}{Y} \sin\left(\frac{\alpha\pi}{2}\right), 0 < \alpha < 1 \quad (\text{II.21})$$

where  $\omega$  indicates the angular frequency. The CPE has two parameters. The first parameter is  $Y$ , with its unit being  $s^n \Omega^{-1}$ . The second parameter,  $\alpha$ , is a dimensionless exponent which is used to measure how far the CPE deviates from the pure capacitor element. If  $\alpha = 0$ , the CPE is a pure resistance element. If  $\alpha = 1$ , it converts into a pure capacitance element.

It can be seen from Eq. (II.22) that the phase angle of the CPE satisfies

$$\tan \phi = \tan\left(\frac{\alpha\pi}{2}\right), \phi = \frac{\alpha\pi}{2} \quad (\text{II.22})$$

Therefore, the phase angle of the element is independent of frequency, for which it is known as the constant phase angle element.

In the impedance spectra fitting, the CPE is often used in parallel with a pure resistance, and its impedance is recorded as  $Z_{arc}$ . It is expressed as:

$$Z_{arc}^0(\omega) = \frac{\frac{1}{R} + Y\omega^\alpha \cos\left(\frac{\alpha\pi}{2}\right) - jY\omega^\alpha \sin\left(\frac{\alpha\pi}{2}\right)}{\left(\frac{1}{R}\right)^2 + \left(\frac{2}{R}\right)Y\omega^\alpha \cos\left(\frac{\alpha\pi}{2}\right) + (Y\omega^\alpha)^2} \quad (\text{II.23})$$

$$Z'_{arc}(\omega) = \frac{\frac{1}{R} + Y\omega^\alpha \cos\left(\frac{\alpha\pi}{2}\right)}{\left(\frac{1}{R}\right)^2 + \left(\frac{2}{R}\right)Y\omega^\alpha \cos\left(\frac{\alpha\pi}{2}\right) + (Y\omega^\alpha)^2} \quad (\text{II.24})$$

$$Z''_{arc}(\omega) = \frac{-jY\omega^\alpha \sin\left(\frac{\alpha\pi}{2}\right)}{\left(\frac{1}{R}\right)^2 + \left(\frac{2}{R}\right)Y\omega^\alpha \cos\left(\frac{\alpha\pi}{2}\right) + (Y\omega^\alpha)^2} \quad (\text{II.25})$$

By eliminating  $Y$ , we get:

$$\left(Z'_{arc}(\omega) - \frac{R}{2}\right)^2 + \left[Z''_{arc}(\omega) - \frac{R \cot\left(\frac{\alpha\pi}{2}\right)}{2}\right]^2 = \left[\frac{R}{2\sin\left(\frac{\alpha\pi}{2}\right)}\right]^2 \quad (\text{II.26})$$

It is indicated that the arc of the intermediate frequency in Fig. II.12 can be fitted by the Eq. (II.25). The larger the parameter  $\alpha$  is, the greater distance from the center of the arc to the real axis, which also proves that the pure capacitor ( $\alpha = 1$ ) is incapable to fit the dispersion effect [48, 49].

However, the CPE is difficult to handle in the time domain and needs to be processed by fractional calculus theory. There are the following three commonly used definitions of fractional calculus [50]:

- ☒ The definition of Gruenwald–Letnikov (G-L) The G-L definition is derived from the traditional integer calculus and is defined as:

$${}^0D_t^\alpha f(t) = \lim_{h \rightarrow 0} h^{-\alpha} \sum_{j=0}^{[(t-a)/h]} (-1)^j \binom{\alpha}{j} f(t - jh) \quad (\text{II.27})$$

The above formula is a unified expression of fractional differential and integral, where  ${}^0D_t^\alpha$  indicates a fractional calculus operator. The positive and negative of  $\alpha$  represent the fractional differential and integral, respectively.  $a$  and  $t$  denote the lower and upper limits of

calculus.  $h$  is defined as the step size.  $[(t - a)/h]$  presents the rounding up of  $(t - a)/h$ .  $\binom{\alpha}{j}$  indicates the binomial coefficient:

$$\binom{\alpha}{j} = \begin{cases} 1 & j = 0 \\ \frac{\alpha(\alpha - 1) \dots (\alpha - (j - 1))}{j!} & j > 0 \end{cases} \quad (\text{II.28})$$

☒ The definition of Riemann–Liouville (R-L)

R-L integral definition:

$${}^0D_t^{-\alpha} f(t) = \frac{1}{\Gamma(-\alpha)} \int_a^t (t - \tau)^{-\alpha-1} f(\tau) d\tau \quad (\text{II.29})$$

R-L differential definition:

$${}^0D_t^\beta f(t) = \frac{1}{\Gamma(n - \beta)} \frac{d^n}{dt^n} \left[ \int_a^t (t - \tau)^{n-\beta-1} f(\tau) d\tau \right] \quad (\text{II.30})$$

where  $0 < \alpha \leq 1$ ,  $n - 1 < \beta \leq n$ ,  $n \in \mathbb{N}$ .

☒ The definition of Caputo

Caputo integral definition:

$${}^0D_t^{-\alpha} f(t) = \frac{1}{\Gamma(-\alpha)} \int_a^t (t - \tau)^{-\alpha-1} f(\tau) d\tau \quad (\alpha > 0) \quad (\text{II.31})$$

Caputo differential definition:

$${}^0D_t^\beta f(t) = \frac{1}{\Gamma(n - \beta)} \int_a^t (t - \tau)^{n-\beta-1} f^{(n)}(\tau) d\tau \quad (\text{II.32})$$

where  $n - 1 < \beta < n$ ,  $n \in \mathbb{N}$ .

It can be verified that G-L and R-L meanings are entirely identical to most functions. R-L concepts are used the most often in the theoretical research. Caputo definition is best suited to define and address initial value problems of fractional differential equations, while G-L definition offers the most direct form and method for approximating discretization.

## II.5. Comparing Lithium-ion and Lead Acid Batteries

Table II.3 presents a brief analysis of lithium-ion lead acid (LiNCM) at pack point. It should be remembered that there is a wide variety of parameter values in both chemistries, so this table is just a simplified representation of a very complex comparison.

**Table II.3:** Battery Technology Comparison [28, 51, 52] .

	Flooded lead acid	VRLA lead acid	Lithium-ion (LiNCM)
Energy Density (Wh/L)	80	100	250
Specific Energy (Wh/kg)	30	40	150
Regular Maintenance	Yes	No	No
Initial Cost (\$/kWh)	65	120	600
Cycle Life	1,200 @ 50%	1,000 @ 50% DoD	1,900 @ 80% DoD
Typical state of charge window	50%	50%	80%
Temperature sensitivity	Degrades significantly above 25°C	Degrades significantly above 25°C	Degrades significantly above 45°C
Efficiency	100% @20-hr rate 80% @4-hr rate 60% @1-hr rate	100% @20-hr rate 80% @4-hr rate 60% @1-hr rate	100% @20-hr rate 99% @4-hr rate 92% @1-hr rate

A significant observation of this table is that various standard charging windows have various chemistries. The consequence of this is that in order to have the same amount of energy available a lead acid battery will have a greater nameplate energy efficiency than the lithium-ion battery.

Given the major variations in the technological and economic characteristics of the types of batteries, it is fair that the "best" solution for which battery type is to be used is unique to application. Following is a closer look at some of the issues dealt with in Table II.3.

a) **Cycle Life Comparaison**

Lithium-ion has significantly higher cycle life than lead acid in deep discharge applications. The disparity is further increased as ambient temperatures increase. The cycle life of each chemistry can be increased by limiting the depth of discharge (DoD), discharge rate, and temperature, but lead acid is generally much more sensitive to each of these factors [53].

In hot climates where the average temperature is 92°F, the disparity between lithium-ion and lead acid is further exacerbated. The cycle life for lead acid (flooded and VRLA) drops to 50% of its moderate climate rating while lithium-ion will remain stable until temperatures routinely exceed 120°F [53].

b) **Rate Performance**

One important factor for lead acid is how long the device would take to discharge when deciding what battery capacity to use with a device. The shorter the discharge period, the less capacity is available from the lead acid battery. This condition makes lithium-ion very well suited for applications where full discharge occurs in less than eight hours [54].

c) **Cold Weather Performance**

Both lead acid and lithium-ion lose capacity in cold weather environments, but lithium-ion loses significantly less capacity as the temperature drops into the -20°C range [54]. The rate of discharge affects the output of lead acid, so two different values for the VRLA battery have been seen.

d) **Environmental Impact**

Concerning environmental friendliness, the lead acid batteries compete badly with the lithium-ion. In order to achieve the same energy storage, lead acid batteries need several times rawer material than lithium-ion, making a much greater effect on the environment during the mining process. The lead manufacturing industry is also extremely energy-intensive, resulting in significant quantities of contamination. While lead is highly hazardous to human health, the manufacturing methods and packaging of batteries make the risk to humans negligible. On the

plus side, over 97% of lead acid batteries in the United States are recycled, which makes a huge impact on the environmental equation [55].

Lithium is not without its own environmental problems [55]. Lithium carbonate, copper, aluminum, and iron ore are essential components of a lithium-ion battery. Furthermore, lithium mining is resource-intensive because lithium is only a small portion of the battery cell by mass, so the environmental effects of aluminum and copper are much greater. Right now, the lithium-ion recycling industry is still in its infancy, but the cell materials have demonstrated a high recovery and recyclability potential, and lithium-ion recycling levels are expected to exceed lead acid.

#### e) **Safety**

Lead acid and lithium-ion cells are capable of undergoing "thermal runaway" where the cell heats up rapidly and can release electrolyte, flames and toxic fumes. For lithium-ion, the probability and effects of an occurrence are greater, since it has a larger amount of energy in a smaller volume. Multiple cell and pack safety precautions shown in Figure II.13 are taken to prevent trigger events, such as short circuits and overheating, but incidents still occur[56] .

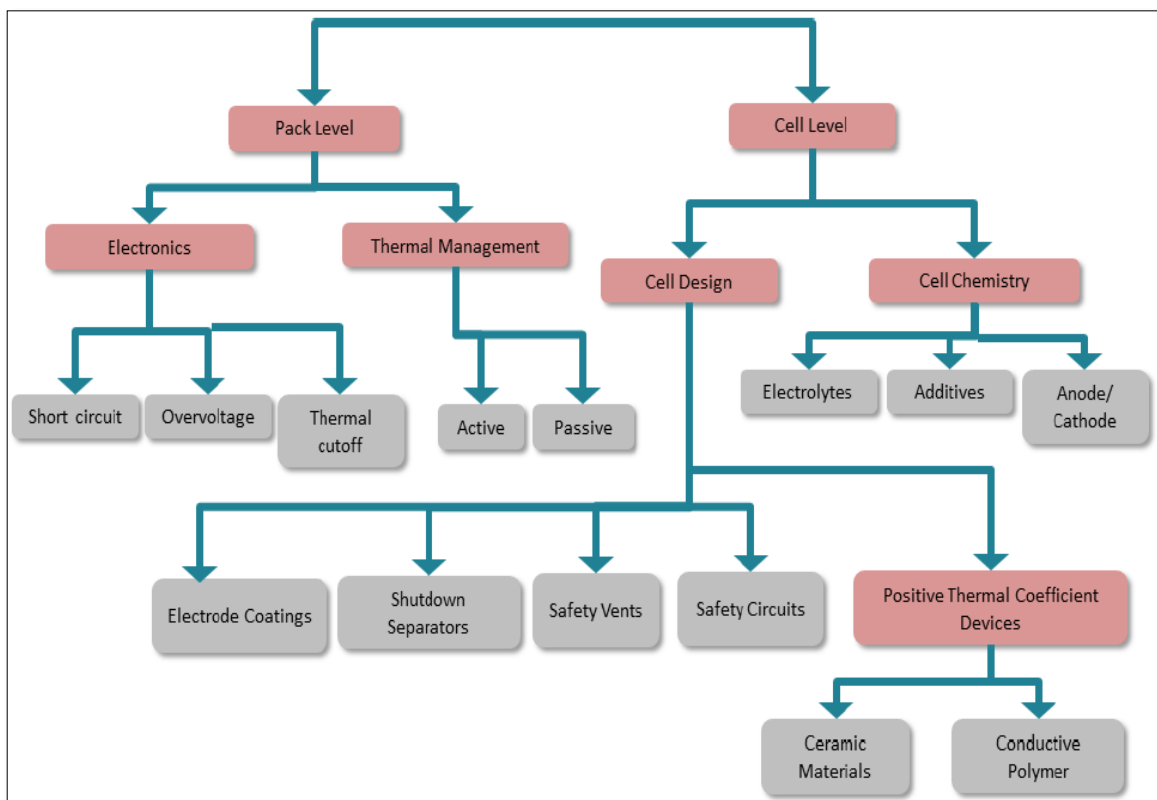


**Figure II.13:** *Lithium-ion Safety Mechanisms* [57].

### f) Voltage Comparaison

The most important factor when determining whether lithium-ion and lead acid can be interchanged within a given electrical device is the voltage range of each chemistry.

The lithium-ion has good agreement with lead acid systems for a majority of the voltage range, but any electrical system would have to be able to accommodate the higher charging voltage of lithium-ion to get optimal performance [57]. Many battery charging controllers and discharge inverters with renewable energy are able to switch between lead acid and lithium-ion. Manufacturers of Charge Controllers and Inverters and lithium-ion companies may help to ensure compliance with the device.

### g) Additional Comparaison Table

**Table II.4:** Advantages and Limitations of Lead Acid Batteries [59,60].

Advantages and Limitations of Lead Acid Batteries	
Advantages	<p>Inexpensive and simple to manufacture — in terms of cost per watt hours, the SLA is the least expensive.</p> <p>Mature, reliable and well-understood technology — when used correctly, the SLA is durable and provides dependable service.</p> <p>Low self-discharge — the self-discharge rate is among the lowest in rechargeable battery systems.</p> <p>Low maintenance requirements — no memory; no electrolyte to fill.</p>
Limitations	<p>Cannot be stored in a discharged condition.</p> <p>Low energy density — poor weight-to-energy density limits use to stationary and wheeled applications.</p> <p>Allows only a limited number of full discharge cycles — well suited for standby applications that require only occasional deep discharges.</p> <p>Environmentally unfriendly — the electrolyte and the lead content can cause environmental damage.</p> <p>Transportation restrictions on flooded lead acid — there are environmental concerns regarding spillage in case of an accident.</p>

**Table II.5:** Advantages and Limitations of Li-ion Batteries [59,60].

Advantages and Limitations of Li-ion Batteries	
Advantages	<p>High energy density — potential for yet higher capacities.</p> <p>Relatively low self-discharge — self-discharge is less than half that of NiCd and NIMIHE</p> <p>Low Maintenance — no periodic discharge in needed; no memory.</p>
Limitations	<p>Requires protection circuit — protection circuit limits voltage and current. Battery is safe if not provoked.</p> <p>Subject to aging, even if not in use — storing the battery in a cool place and at 40 percent state-of-charge reduces the aging effect.</p> <p>Moderate discharge current.</p> <p>Subject to transportation regulations — shipment of larger quantities of Li-ion batteries may be subject to regulatory control. This restriction does not apply to personal carry-on batteries.</p> <p>Expensive to manufacture — about 40 percent higher in cost than NiCd. Better manufacturing techniques and replacement of rare metals with lower cost alternatives will likely reduce the price.</p> <p>Not fully mature — changes in metal and chemical combinations affect battery test results, especially with some quick test methods.</p>

## II.6. Conclusion

In this chapter, we learned about how to charge batteries and their models.

Where we discussed the different types of batteries, and we talked in depth about lithium batteries and lead acid batteries, because they are the most used and we noticed that they are the most efficient. But we will discuss in the next chapter the lead acid battery, because it is available in our Country. We will also choose the generic battery model; it is detailed in the next chapter.

## I.1. Reference

- [19] S. Boschert, *Plug-in hybrids: The cars that will recharge America*. New Society Publishers, 2006.
- [20] S. Al-Hallaj and J. R. Selman, "Thermal modeling of secondary lithium batteries for electric vehicle/hybrid electric vehicle applications," *Journal of power sources*, vol. 110, no. 2, pp. 341-348, 2002.
- [21] D. H. Doughty, P. C. Butler, A. A. Akhil, N. H. Clark, and J. D. Boyes, "Batteries for large-scale stationary electrical energy storage," *The Electrochemical Society Interface*, vol. 19, no. 3, pp. 49-53, 2010.
- [22] Y. Onoda, "Development of a large-sized, long-life, valve-regulated lead-acid battery," *Journal of power sources*, vol. 88, no. 1, pp. 101-107, 2000.
- [23] J. Jiang and C. Zhang, *Fundamentals and applications of lithium-ion batteries in electric drive vehicles*. John Wiley & Sons, 2015.
- [24] C. Glaize and S. Genies, *Lithium batteries and other electrochemical storage systems*. Wiley Online Library, 2013.
- [25] R. Korthauer, "Areas of activity on the fringe of lithium-ion battery development, production, and recycling," in *Lithium-Ion Batteries: Basics and Applications*: Springer, 2018, pp. 249-251.
- [26] M. E. Spahr *et al.*, "Purely hexagonal graphite and the influence of surface modifications on its electrochemical lithium insertion properties," *Journal of The Electrochemical Society*, vol. 149, no. 8, pp. A960-A966, 2002.
- [27] J. Garche, C. K. Dyer, P. T. Moseley, Z. Ogumi, D. A. Rand, and B. Scrosati, *Encyclopedia of electrochemical power sources*. Newnes, 2013.
- [28] D. Pavlov, *Lead-acid batteries: science and technology*. Elsevier, 2011.
- [29] D. Linden, "Reddy TB handbook of batteries," ed: The McGraw-Hill Companies, Inc., New York, 2002.
- [30] T. Ikeya *et al.*, "Multi-step constant-current charging method for an electric vehicle nickel/metal hydride battery with high-energy efficiency and long cycle life," *Journal of power sources*, vol. 105, no. 1, pp. 6-12, 2002.
- [31] C.-L. Liu, S.-C. Wang, Y.-H. Liu, and M.-C. Tsai, "An optimum fast charging pattern search for Li-ion batteries using particle swarm optimization," in *The 6th International Conference on Soft Computing and Intelligent Systems, and The 13th International Symposium on Advanced Intelligence Systems*, 2012, pp. 727-732: IEEE.
- [32] Y.-H. Liu, C.-H. Hsieh, and Y.-F. Luo, "Search for an optimal five-step charging pattern for Li-ion batteries using consecutive orthogonal arrays," *IEEE Transactions on Energy Conversion*, vol. 26, no. 2, pp. 654-661, 2011.
- [33] P. H. Notten, J. O. het Veld, and J. Van Beek, "Boostcharging Li-ion batteries: A challenging new charging concept," *Journal of Power Sources*, vol. 145, no. 1, pp. 89-94, 2005.
- [34] C.-H. Lin *et al.*, "Fast charging technique for Li-Ion battery charger," in *2008 15th IEEE International Conference on Electronics, Circuits and Systems*, 2008, pp. 618-621: IEEE.

- [35] L.-R. Chen, "Design of duty-varied voltage pulse charger for improving Li-ion battery-charging response," *IEEE Transactions on Industrial Electronics*, vol. 56, no. 2, pp. 480-487, 2008.
- [36] T. T. Vo, X. Chen, W. Shen, and A. Kapoor, "New charging strategy for lithium-ion batteries based on the integration of Taguchi method and state of charge estimation," *Journal of Power Sources*, vol. 273, pp. 413-422, 2015.
- [37] L.-R. Chen, S.-L. Wu, T.-R. Chen, W.-R. Yang, C.-S. Wang, and P.-C. Chen, "Detecting of optimal Li-ion battery charging frequency by using AC impedance technique," in *2009 4th IEEE Conference on Industrial Electronics and Applications*, 2009, pp. 3378-3381: IEEE.
- [38] L.-R. Chen, S.-L. Wu, D.-T. Shieh, and T.-R. Chen, "Sinusoidal-ripple-current charging strategy and optimal charging frequency study for Li-ion batteries," *IEEE Transactions on Industrial Electronics*, vol. 60, no. 1, pp. 88-97, 2012.
- [39] Q. Gong, "Modeling study of a vehicle traction battery model," *Chinese LABAT Man*, vol. 42, no. 2, p. 76, 2005.
- [40] M. Ceraolo, "New dynamical models of lead-acid batteries," *IEEE transactions on Power Systems*, vol. 15, no. 4, pp. 1184-1190, 2000.
- [41] F. M. González-Longatt, "Circuit based battery models: A review," in *Congreso Iberoamericano de estudiantes De Ingenieria Electrica. Cibelec*, 2006.
- [42] H. Fakham, D. Lu, and B. Francois, "Power control design of a battery charger in a hybrid active PV generator for load-following applications," *IEEE Transactions on Industrial Electronics*, vol. 58, no. 1, pp. 85-94, 2010.
- [43] V. Johnson, "Battery performance models in ADVISOR," *Journal of power sources*, vol. 110, no. 2, pp. 321-329, 2002.
- [44] B. A. Manual, "Gates Energy Products," *Inc., Gainesville, FL*, 1989.
- [45] J. P. Christophersen *et al.*, "DOE Advanced technology development program for lithium-ion batteries: INEEL Interim report for Gen 2 cycle-life testing," 9: *INEEL/EXT-02-01055*, 2002.
- [46] S. Wu, R. Xiong, H. Li, V. Nian, and S. Ma, "The state of the art on preheating lithium-ion batteries in cold weather," *Journal of Energy Storage*, vol. 27, p. 101059, 2020.
- [47] J. Huang, Z. Li, B. Y. Liaw, and J. Zhang, "Graphical analysis of electrochemical impedance spectroscopy data in Bode and Nyquist representations," *Journal of Power Sources*, vol. 309, pp. 82-98, 2016.
- [48] B. Wang, Z. Liu, S. E. Li, S. J. Moura, and H. Peng, "State-of-charge estimation for lithium-ion batteries based on a nonlinear fractional model," *IEEE Transactions on Control Systems Technology*, vol. 25, no. 1, pp. 3-11, 2016.
- [49] R. Yang, R. Xiong, H. He, and Z. Chen, "A fractional-order model-based battery external short circuit fault diagnosis approach for all-climate electric vehicles application," *Journal of cleaner production*, vol. 187, pp. 950-959, 2018.
- [50] I. Petráš, *Fractional-order nonlinear systems: modeling, analysis and simulation*. Springer Science & Business Media, 2011.

- [51] G. R. Dahlin and K. E. Strøm, *Lithium batteries: research, technology, and applications*. Nova Science Publishers, 2010.
- [52] M. Faizan, "Synthesis and Characterization of Lead based Anodic Electrode for Lead Acid Batteries," Department of Physics, COMSATS University Islamabad, Lahore campus, 2019.
- [53] D. Doerffel and S. A. Sharkh, "A critical review of using the Peukert equation for determining the remaining capacity of lead-acid and lithium-ion batteries," *Journal of power sources*, vol. 155, no. 2, pp. 395-400, 2006.
- [54] G. Albright, J. Edie, and S. Al-Hallaj, "A comparison of lead acid to lithium-ion in stationary storage applications," *Published by AllCell Technologies LLC*, 2012.
- [55] H. Chang and H. Wu, "Graphene-based nanocomposites: preparation, functionalization, and energy and environmental applications," *Energy & Environmental Science*, vol. 6, no. 12, pp. 3483-3507, 2013.
- [56] H. Keshan, J. Thornburg, and T. S. Ustun, "Comparison of lead-acid and lithium ion batteries for stationary storage in off-grid energy systems," 2016.
- [57] E. M. Krieger, J. Cannarella, and C. B. Arnold, "A comparison of lead-acid and lithium-based battery behavior and capacity fade in off-grid renewable charging applications," *Energy*, vol. 60, pp. 492-500, 2013.

# **Chapter III: Coulomb Counting Method Estimation**

### III.1. Introduction

The aim of this chapter is to estimate the SOC of Lead-Acid battery using coulomb counting method through experimental measurements of battery voltage and current. Also, the objective is to demonstrate the effectiveness of this method, and compare the theoretical SOC estimation and experimental measurement based on the generic battery model.

### III.2. Coulomb Counting Method

The Coulomb Counting method, also called the method of current integration, is based on calculating the number of ampere hours in and out of a battery, [Alzieu et. al, 1997]. The accuracy of this method depends mainly on the resolution of the current sensor. This counting should reflect the coulombic efficiency depending on the charge or discharge rate. However, these methods allow the determination of relative changes of charge's state only without taking into account the self-discharge [73].

The determination of the charge's state, therefore, requires knowledge of the initial state of charge [74,75]. The charge's state of the battery estimation based on this method is as following [76]:

$$SOC = SOC_0 - \frac{100}{C_n} \int_{t_0}^t \eta \cdot I(\tau) d\tau \quad (III.1)$$

If the initial value of the state of charge  $SOC_0$  is specified, the coulomb counting method becomes very precise and particularly easy to determine the SOC. But if the  $SOC_0$  is not known, this method is less accurate.

In addition, the coulombic efficiency, which depends on the operating conditions (SOC, temperature, current and so on) [1, 39], is difficult to obtain. As the current sensor may introduce an offset that increases the imprecision of this estimation. With time, all these factors contribute to the increasing of the SOC error, especially in the reserve batteries (Back-up) and in packs for hybrid electric vehicle (HEV). However, the method of coulomb counting is widely used in practice because of its simplicity [76].

N. K. Soon et al [77] proposed an intelligent estimation approach based on the coulomb counting method from the characteristics of charge and discharge of Lithium-Ion batteries. Their proposed method has proven its efficiency and accuracy, and this through several experiments conducted over lithium-ion batteries.

F. Feng et al [78] used a method of estimation of the SOC combining the improved method of Ampere-hour (Ah) counting and the method of Open Circuit Voltage (OCV). However, the improved method of Ah counting may affect the available capacity and the coulombic efficiency, and thus, depending on the temperature during the calculation of SOC. In addition, the SOCs of the battery with different temperatures can be mutually converted according to the loss of capacity. The method of open circuit voltage (OCV) is used to offset accumulation error in Ah counting caused by the low accuracy of current sensors and the lack of specific initial SOC for calibration and as a supplement as well.

### III.3. Generic Battery Model

#### III.3.1. State of the Art

P.Vyroubal et al [79] are used the existing model of MATLAB/ Simulink and compared the simulation, results datasheet and the actual measurements of the lithium-ion battery in the discharge phase with two discharge currents rates 0.2C and 0.5 C. They found that this model represents correctly the lithium-ion battery discharge characteristic.

The model proposed by [80] is the same model available in MATLAB/ Simulink-R2013. The discharge model is similar to the model of Shepherd but it can accurately represent the dynamics when power varies and consider the open circuit voltage (OCV) based on the SOC. A term concerning the voltage polarization is added to better represent the behavior of the OCV and the term concerning the resistance polarization is slightly modified. The battery voltage is given by the following equation [77]:

$$V_{batt} = E_0 - K \frac{Q}{Q-it} \cdot it - R \cdot I + A \cdot \exp(-B \cdot it) K \frac{Q}{Q-it} \cdot i^* \quad (III.2)$$

The special feature of this model is the use of filtered current ( $i^*$ ) through the polarization resistance. This filtered current solves the problem of the algebraic loop due to the simulation of power systems in Simulink. Finally, the OCV varies nonlinearly with the SOC. This phenomenon is modeled by the term of the polarization voltage [80].

In [81], Olivier Tremblay and Louis-A. present an improved and easy-to-use battery dynamic model. The charge and the discharge dynamics of the battery model are validated experimentally with four batteries types. An interesting feature of this model is the simplicity to extract the dynamic model parameters from batteries datasheets. Only three points on the manufacturer's discharge curve in steady state are required to obtain the parameters. Finally,

the battery model is included in the Sim Power Systems simulation software and used in a detailed simulation of an electric vehicle based on a hybrid fuel cell-battery power source. The results show that the model can accurately represent the dynamic behaviour of the battery.

S.M. Wijewardena in [82], presents mathematical modelling and dynamic simulation of battery storage systems can be challenging and demanding due to nonlinear nature. Simulation in time domain could be time consuming as battery storage (BS) systems do not behave according to readily available mathematical functions. Economic advantages, partial sustainability and the portability of these units pose promising substitutes for backup power systems in hybrid vehicles, hybrid electricity power generation systems, telecommunication exchanges and computer networks. Though, there have been many research papers published in this area with complex mathematical models and simulation systems, each system has its own constraints and specific applications. The aim of this research is to present a suitable convenient and dynamic battery model that can be used to model a general BS system. The proposed new dynamic battery model has the capability to analyse the effect of temperature, cyclic charging/discharging, and voltage stabilization effects. Simulink has been used to study the characteristics of the system and the proposed system has produced very good successful results.

In [83], Essam M. Allam. Presents battery model applied to dynamic simulation software. Simulation using nickel hydrogen battery model thus makes it possible to analyse very complex phenomena. The model was realized in MATLAB / Simulink software packages. The battery block implements a generic dynamic model parameterized to represent most popular types of rechargeable batteries. In this case, the battery's model parameters are not exactly the same as those of the electric vehicle battery but it is nevertheless possible to study, with good precision, phenomena caused by the battery. Moreover, this model helps to develop the energy management system (EMS) which controls the flow of energy between the solar panels and battery. Finally, it is possible to control the charge and the discharge of the battery with precision. The results obtained show that the use of this battery model makes it possible to properly represent the transient states. It is thus possible to analyse them in order to fine-tune the various control devices and they show accurately the general behavior of the battery. The battery monitoring system developed is used to prevent people from being stranded. This device makes sure that no matter what, a car will be able to start and that a person will not be left with a dead battery.

In this work the battery of Lead Acid is used, this choice corresponds to the batteries that are available in our control laboratory.

### III.3.2. Charge / Discharge of this Model in MATLAB Simulink 2013

The battery block implements the parameterized dynamic model which represents different types of rechargeable batteries:

- Lead Acid Model
- Lithium-ion Model
- Nickel-Cadium Model
- Nickel-Metal-Hybrid Model

Fig. III.3 shows the equivalent electrical circuit of the battery in MATLAB Simulink.

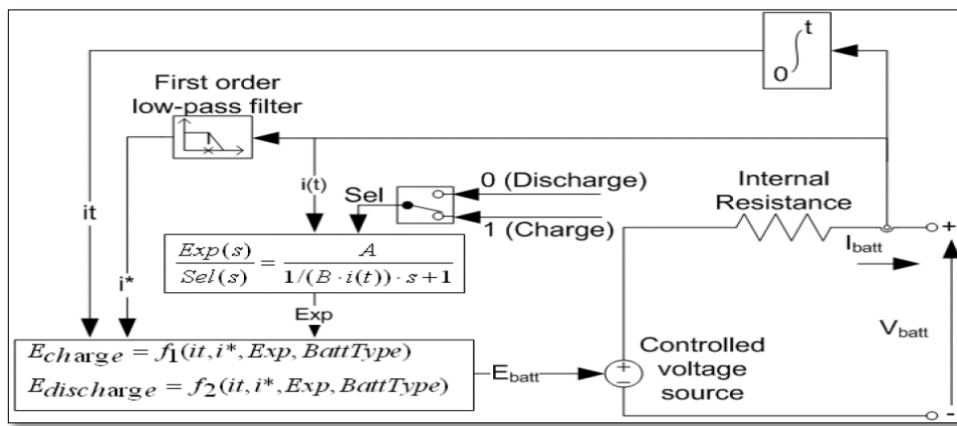


**Figure III.1: Battery Charge / Discharge Pattern.**

In this research, we studied the lead acid model because it is the available in our country, Algeria.

The general charge and discharge model are:

✓ *Discharge Model* ( $i^* > 0$ )

$$f_1(it, i^*, i, Exp) = E_0 - K \cdot \frac{Q}{Q - it} \cdot i^* - K \cdot \frac{Q}{Q - it} \cdot it + Laplace^{-1} \left( \frac{Exp(s)}{Sel(s)} \cdot 0 \right)$$

Where:  $Q$ : The battery capacity (Ah),  $K$ : constant polarization,  $E_0$ : The constant battery voltage (V)  $Exp(s)$ : The exponential voltage (V),  $Sel(s)$ : The exponential capacity (Ah) -1,  $it = \int Idt$ : Actual battery charge (Ah),  $i^*$ : The filtered current (A)

✓ **Charge Model ( $i^* < 0$ )**

$$f_2(it, i^*, i, Exp) = E_0 - K \cdot \frac{Q}{it + 0.1 \cdot Q} \cdot i^* - K \cdot \frac{Q}{Q - it} \cdot it + Laplace^{-1} \left( \frac{Exp(s)}{Sel(s)} \cdot \frac{1}{s} \right)$$

This model is based on assumptions and limitations.

### III.3.3. The Assumptions of this model

- The parameters of the model are deduced from the characteristics of the discharge and assumed the same for the charge.
- The capacity of the battery does not change with the amplitude of the current.
- No effect of temperature in the behavior of the model.
- Self-discharge of the battery is not shown.

### III.3.4. The Limitations of this model

- The minimum voltage of the battery without load is 0 V and the maximum of this is  $2 \cdot E_0$ .
- The minimum capacity of the battery is 0 Ah and the maximum capacity is Q.

## III.4. Application

The parameters in tables III.1 is extracted from the data sheet.

**Table III.1:** Parameters of our Battery at 0.1C.

<b>Nominal Voltage (V)</b>	12
<b>Rated Capacity (Ah)</b>	100
<b>Initial State of Charge (%)</b>	100
<b>Maximum Capacity (Ah)</b>	110
<b>Fully Charged Voltage (V)</b>	12.72
<b>Nominal Discharge Current (A)</b>	10
<b>Internal Resistance (ohms)</b>	0.0057
<b>Capacity (Ah) @ Nominal Voltage</b>	59.37
<b>Exponential Zone [Voltage(V), Capacity (Ah)]</b>	[12.48, 10]

### III.5. Experimental method

#### III.5.1. Battery specification

The Battery used in this work was AGM Lead Acid battery with nominal voltage of 12V and capacity of 100Ah. This battery type is chosen because it is available in our laboratory. While charged with standby usage, recommended voltage for individual cell is 2.28 V (6 cells in series). In addition, for cycle usage that requires fast charge, maximum voltage is 2.45 V. Another characteristic of these battery is shown in Table.III.1. See Appendix B.

**Table III.2.** Lead Acid battery characteristics

Parameter	Value
<b>Manufacturer</b>	VISION
<b>Model</b>	6FM100E-X
<b>Nominal capacity</b>	100Ah
<b>Nominal voltage</b>	12V
<b>Charging/discharging</b>	Cut-off-voltage (13.8/10.8V)
<b>Recommend charging current (0.25C)</b>	25A
<b>Maximum discharge current</b>	(short time<5s) 900A
<b>Design life</b>	10 years
<b>Operating temperature (charge/discharge)</b>	-10C°-60C°/-20C°-60C°
<b>Shell material</b>	ABS
<b>weight</b>	29Kg

#### III.5.2. Measurement System Setup

##### a) The test of the Charge process

The battery is charged by a stabilized power supply. Before connecting the battery, the value of the voltage is regulated to 14 V, and the value of the current is limited to 5.5 A. Then, the battery is connected to the stabilized power supply. The voltage and the current are measured respectively (by using a Multimeter and a hall sensor) every 10 min, until the battery is filled. At this point, the value of the voltage and the current respectively are equal to  $V_{end} = 13.92$  V,  $I_{min} = 0.89$ A. Also, the value of the current given by the manufacturer is equal to 0.85 A, in this value the battery is disconnected with the stabilized power supply. This test was carried out for 05 days, it is equal to  $T_{ch} = 1518$ min or  $T_{ch} = 25.3$ h.

### b) The test of the Discharge process

The variable resistor is connected with the battery as load (before, the discharge process the value of the resistor is regulated in the value of the current of 10A. The value of this resistor it is not varied all the discharge process), then the voltage and the current are measured every 5 min during the discharge process. After 10h and 17 minutes, the value of the cut off voltage is achieved to 10.8 V. In this value, the variable resistor is disconnected. In this test the value of the ambient temperature is equal to  $T = 22^{\circ}\text{C}$ . See Appendix. C



**Figure.III.2.** Test bench

1. Supply table
2. Lead Acid battery
3. Stabilized power supply
4. Multimeter
5. Current sensor
6. Variable resistor as load

### III.6. Results and discussion

Fig.3 shows that the discharge voltage of the battery datasheet and simulation are slightly different. This difference is due to the imprecision when extracting the parameters of the battery model (Table.2) from the curve of the discharge voltage given by the manufacturer. The discharge voltage decreases to 10.8 V for 10 hours which is called the cut-off voltage. The value of 10.8 V does not correspond to the full discharge of the battery (SOC = 0%) but is suitable to minimum SOC value which is equal to nearly 20%. [77, 84].

Experimental discharge voltage is fitted to that of the simulation except that the value of the end of discharge voltage (10.8 V) is reached after a period of  $T = 10\text{h}$  and 17 min. this difference indicates that the battery's capacity varies according to the parameters of exploitation (charge mode, the ambient temperature, the discharge current, the battery history ....). Moreover, the voltage given by the manufacturer is related to ideal conditions ( $T = 25\text{C}^\circ$ ,  $I_{\text{disch}} = 10\text{A}$ , the battery State Of Health (SOH = 0%)). The three curves (datasheet, simulation and experimental) are superposed which indicate that the adopted model of the battery represents the actual behavior of the battery discharge phase with high accuracy.

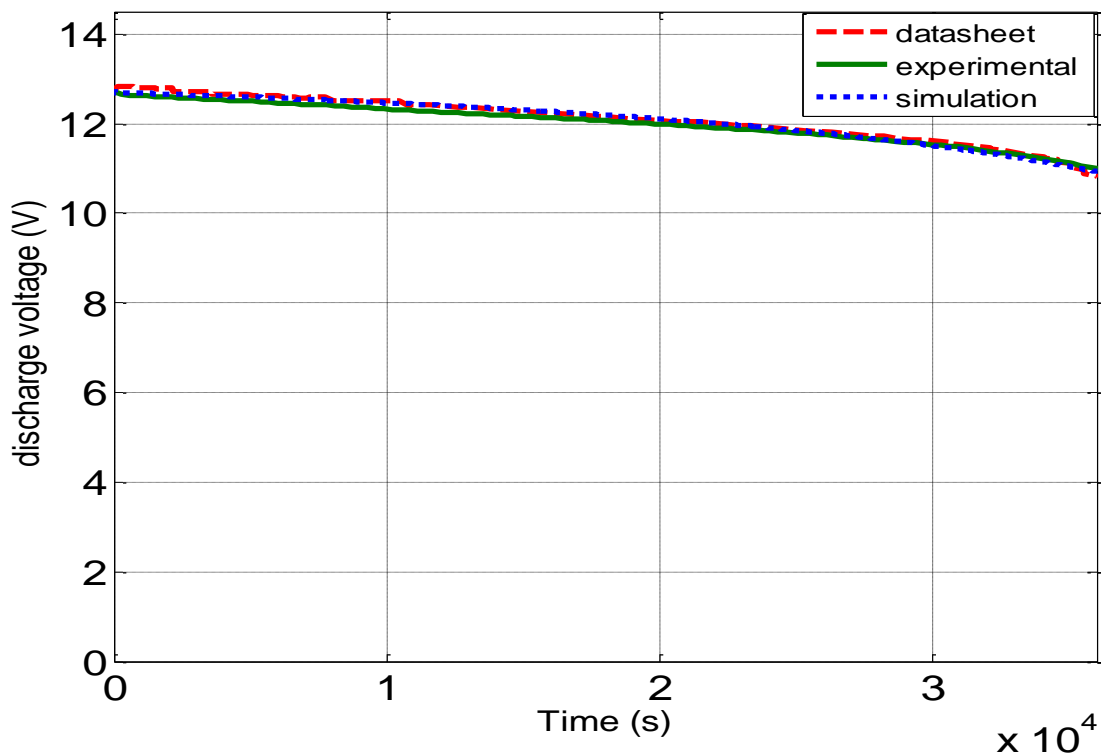


**Figure.III.3.** The discharge voltage vs. time.

According to Fig.4, note that the battery is initially full ( $\text{SOC}_0 = 100\%$ ) and after 10 hours the state of charge of the battery decreases to the minimum value ( $\text{SOC} = 20\%$ ). This value corresponds to the actual value of the Lead Acid battery ( $\text{SOC}_{\text{min}} = 20\%$ ) [77,84,85].

Furthermore, this value must not be exceeded in the aim to prevent the damage of the battery. The curve of the SOC estimated by the estimator of Coulomb Counting shows that the discharge of the battery is under a constant discharge current ( $I_{\text{disch}} = 10\text{A}$ ). Although, this technique follows the state of charge of the battery throughout the discharge time (10h).  $\text{SOC}_{\text{exp}}$  and  $\text{SOC}_{\text{th}}$  are fitted which show that this technique is very precise and robust.

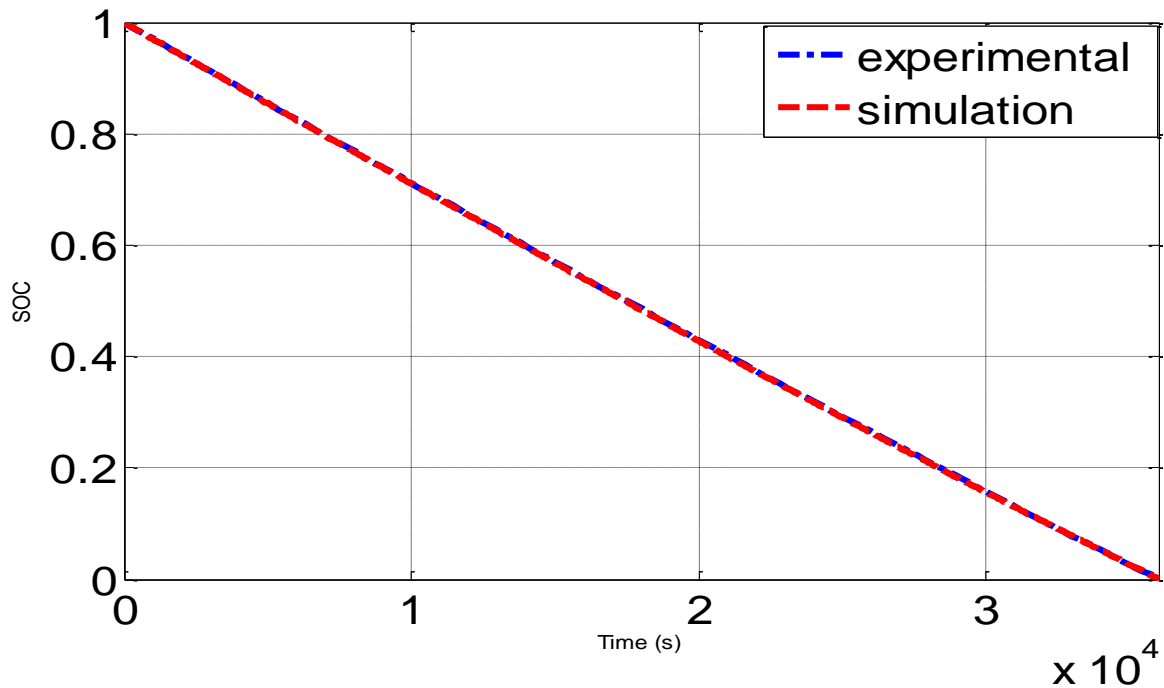


**Figure.III.4.** The state of charge (SOC) of the battery versus time

The Fig.5 shows that the initial value of the charging voltage of the battery in the two curves (simulation and datasheets) is equal to 12.6 V. This is explained by the initial state of charge or the amount of charge remaining in the battery, (here  $SOC_0 = 20\%$ ). [77, 84]. Note that the charging voltage increases rapidly to 13.8V and stabilizes at this value. In fact, there are two intervals: the first is [0-3] h in the datasheet curve and [0-0.69] h in the simulation curve, corresponding for the charging mode with a constant current (CC) [77]. The second interval is [3-20] h corresponds to the charging mode by a constant voltage (CV). [77].

In fact, the charge phase depends on several factors (charging mode,  $SOC_0$ , ambient temperature, charging current, charging voltage). To avoid overcharging the battery, cut off the supply voltage of the charger when the end of charge current is equal to 0.85 A. This corresponds to a value of the charging time is equal to 20h.

The Fig.6 shows that the simulation parameters are extracted by the experimental data; this is not the same as in Fig.5 (the parameters are extracted by the manufacturer's data). Note that the difference between Fig.6 and Fig.5 is obtained in the interval of the charging process by the constant current, which the during of this interval in Fig.6.is larger than to in Fig.5. Also, this difference is explained by value of the charge current is equal to 25 A in the Fig.5 but, is equal to 5.5 A in the Fig.6. Moreover, the duration of this interval is increased with the increase of the charging current.

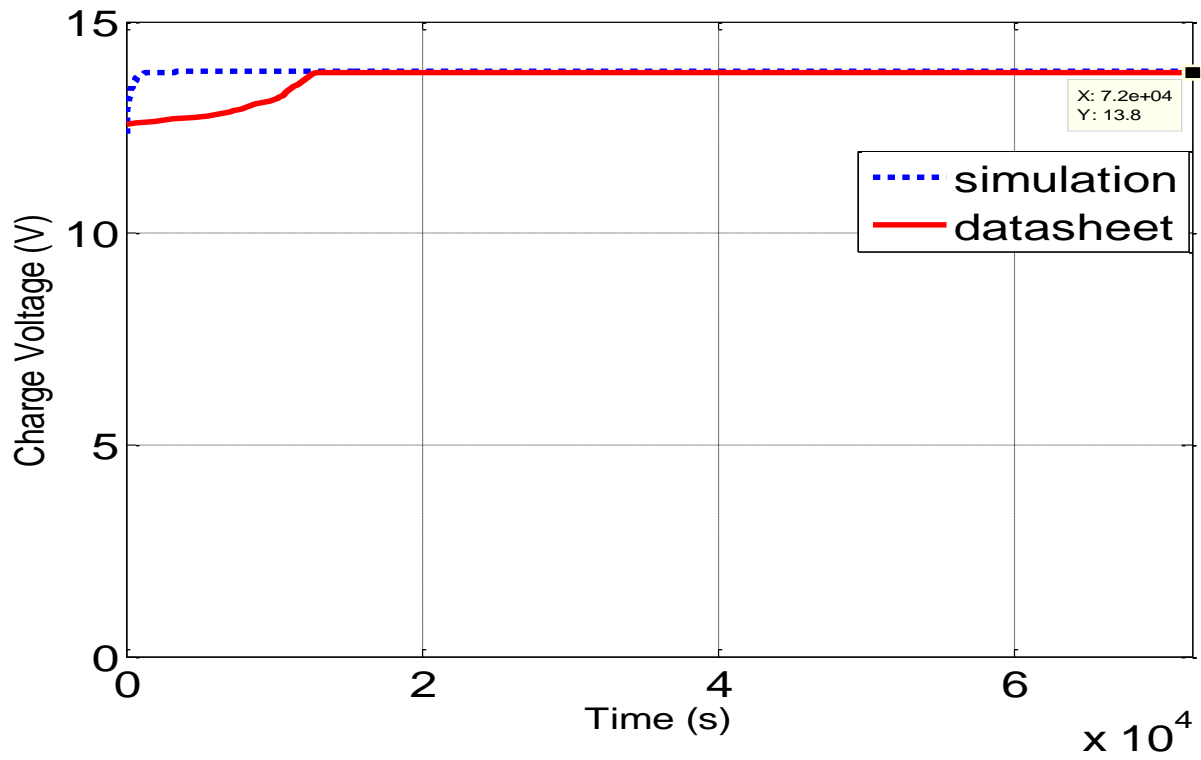


Figure.III.5. The charge voltage versus time (simulation and datasheet)

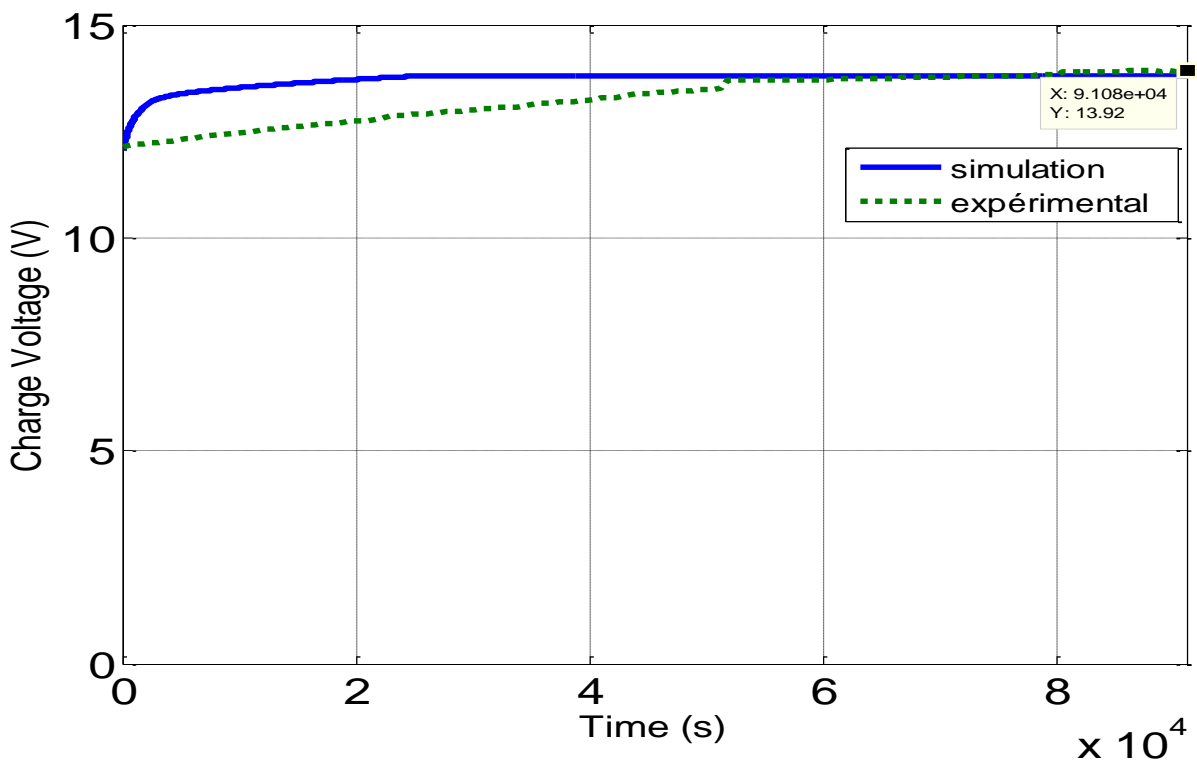
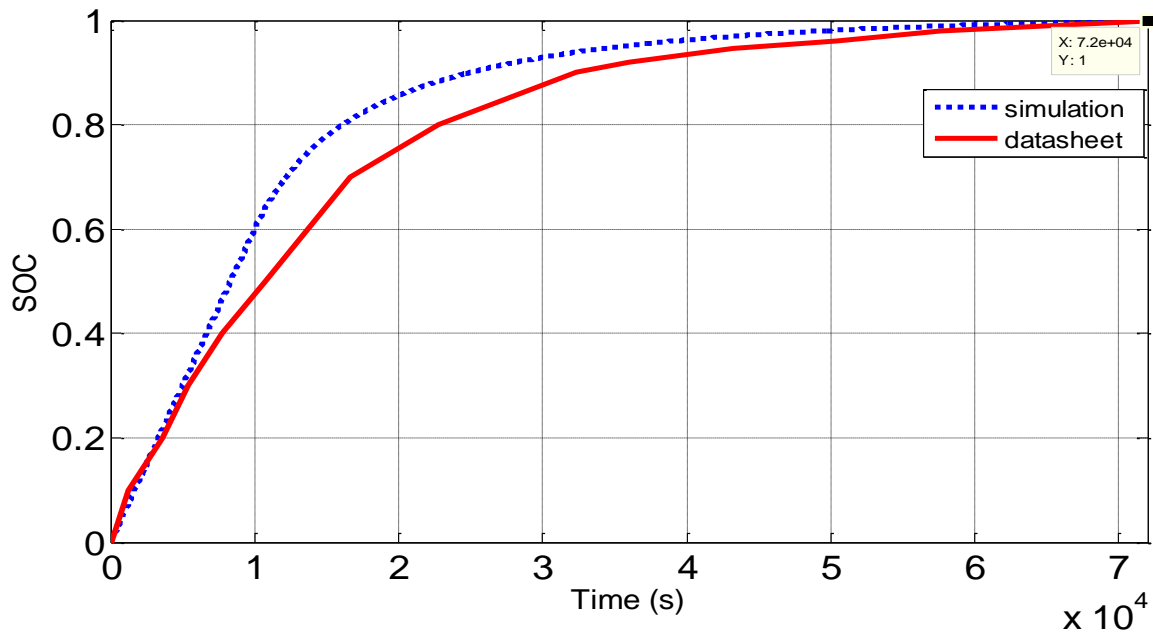


Figure.III.6. The charge voltage versus time (simulation and experimental)

According to Fig.7, we note that the value of the initial state of charge is equal to  $SOC_0=20\%$  then, it is increased with the time until the final value is equal to  $SOC=100\%$  that means that the battery is fully charged. There are two intervals in the curve, the first is [0-3] h corresponding to the charging process by the constant current, which is a linear form. Also, this interval is characterized by the rapid increase in the state of charge with time [86], for example, the value of state of charge of datasheet and simulation curves at 3h respectively are equal to  $SOC(\text{datasheet}) = 50\%$ ,  $SOC(\text{simulation}) = 70\%$ .

Although, the second interval is a curved line form, it corresponds to the charging process by the constant voltage. Also, this interval is characterized by the slow increase in the state of charge. So, the charge capacity of the battery is depended on the charging mode, it is faster in the charging process by constant current and slower in the charging process by the constant voltage. As well as recent chargers are faster to save time especially in the Lead Acid batteries.



**Fig.7.** The battery state of charge (simulation and data sheet) in charge mode with time.

The Fig.8, shows that the SOC curve (experimental and simulation) is slightly different; this difference is caused by the inaccuracy of the battery model in the charging process. In addition, the generic model of the battery is more accurate by using the experimental data than by using the manufacturer data. [87]. Also, in this figure we are noted that the Coulomb Counting method is followed although the SOC during the charging process, that is mean this method does not depend of the model and the battery technology. See Appendix a.

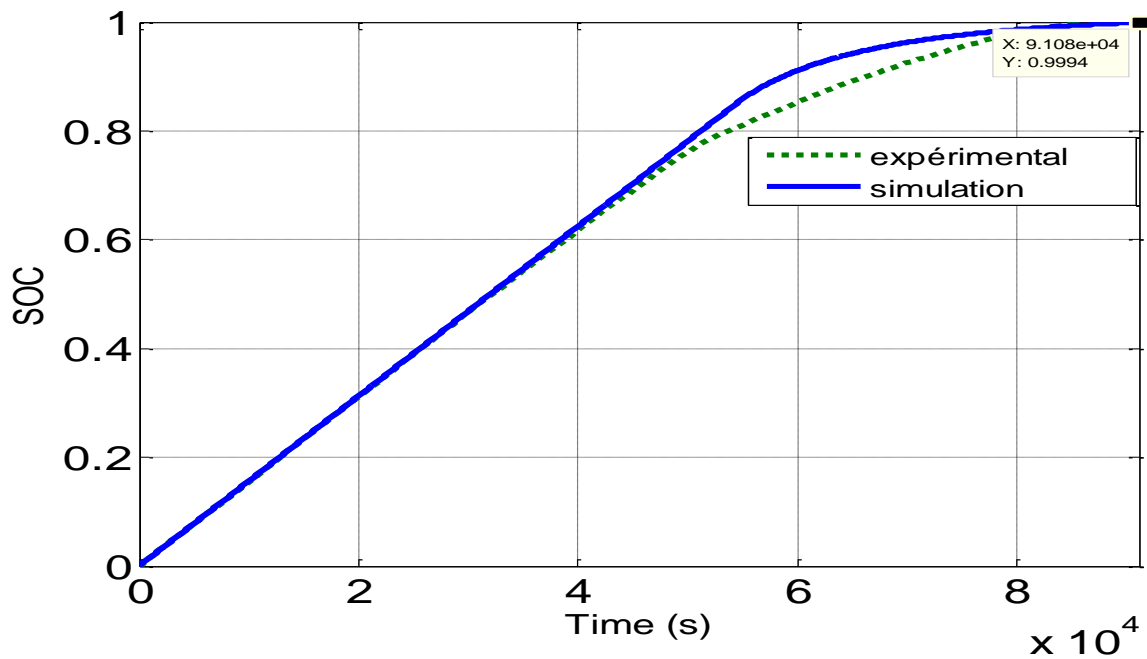


**Fig.8.**The battery state of charge (simulation and experimental) versus time.

### Conclusions

The estimator of the state of charge of the battery by Coulomb Counting method is very accurate and is widely used in practice especially in embedded applications type hybrid / electric vehicles; or renewable energy applications in the case of photovoltaic systems for example.

The disadvantage of this technique is an inaccuracy and difficulty to finding the initial SOC. Also, it requires high-precision measuring instruments (voltage, current, and temperature sensor), i.e. it has to calibrate these devices every time otherwise, gives less accurate results.

## REFERENCES

- [73] B. Zine, K. Marouani, M. Becherif, and S. Yahmedi, "Estimation of battery SOC for hybrid electric vehicle using coulomb counting method," *International Journal of Emerging Electric Power Systems*, vol. 19, no. 2, 2018.
- [74] D. DinhVinh, "Lithium-Ion batteries diagnosis in embedded applications," *ThesisforobtainingthedegreeofdoctorofCompiègneUniversityof TechnologyinInformationTechnologyandSystems*, 2010.
- [75] X. Hu, F. Sun, and Y. Zou, "Estimation of state of charge of a lithium-ion battery pack for electric vehicles using an adaptive Luenberger observer," *Energies*, vol. 3, no. 9, pp. 1586-1603, 2010.
- [76] D. Lindner and F. Niedermayr, "Report for work package 6," ed: FRAUNHOFER-ITALIA, 2014.
- [77] K. S. Ng, C.-S. Moo, Y.-P. Chen, and Y.-C. Hsieh, "Enhanced coulomb counting method for estimating state-of-charge and state-of-health of lithium-ion batteries," *Applied energy*, vol. 86, no. 9, pp. 1506-1511, 2009.
- [78] F. Feng, R. Lu, and C. Zhu, "A combined state of charge estimation method for lithium-ion batteries used in a wide ambient temperature range," *Energies*, vol. 7, no. 5, pp. 3004-3032, 2014.
- [79] P. Vyroubal, J. Maxa, and T. Kazda, "Simulation of the behavior of the lithium ion battery," *Advances in Military Technology*, vol. 9, no. 1, pp. 107-115.2014 ,
- [80] V. Pop, H. J. Bergveld, D. Danilov, P. P. Regtien, and P. H. Notten, *Battery management systems: Accurate state-of-charge indication for battery-powered applications*. Springer Science & Business Media, 2008.
- [81] O. Tremblay and L.-A. Dessaint, "Experimental validation of a battery dynamic model for EV applications," *World electric vehicle journal*, vol. 3, no. 2, pp. 289-298, 2009.

- [82] S. Wijewardana, "New Dynamic Battery Model for Hybrid Vehicles and Dynamic Model Analysis Using Simulink ", *Engineer: Journal of the Institution of Engineers, Sri Lanka*, vol. 47, no. 4, 2014.
- [83] E. M. Allam, "Study vehicle battery simulation and monitoring system," *American Journal of Modeling and Optimization*, vol. 3, no. 2, pp. 40-49, 2015.
- [84] H. Alloui ,M. Becherif, and K. Marouani, "Modelling and frequency separation energy management of fuel cell-battery hybrid sources system for hybrid electric vehicle," in *21st Mediterranean Conference on Control and Automation*, 2013, pp. 646-651: IEEE.
- [85] M. Becherif, F. Claude, T. Hervier, and L. Boulon, "Multi-stack fuel cells powering a vehicle," *Energy procedia*, vol. 74, pp. 308-319, 2015.
- [86] M. Becherif, M. Ayad, D. Hissel, and R. Mkahl, "Design and sizing of a stand-alone recharging point for battery electrical vehicles using photovoltaic energy," in *2011 IEEE Vehicle Power and Propulsion Conference*, 2011, pp. 1-6: IEEE.
- [87] S. Melentjev and D. Lebedev, "Overview of simplified mathematical models of batteries," in *13th International Symposium" Topical problems of education in the field of electrical and power engineering".-Doctoral school of energy and geotechnology: Parnu, Estonia*, 2013, pp. 231-235.

# **Chapter IV: Energy Management System Model**

## IV.1. Introduction

In this chapter, we introduced and described the State of the art of energy management strategies, Architecture of electric vehicle. While, the tractive performance of an EV power-train system was described at each architecture. The Power supply system, Model of the supercapacitor, the battery and the DC/DC converters are also studied.

## IV.2. State of the art of energy management strategies

Energy management defines the way in which power flows are distributed across the various components of the hybrid system. Many studies have contributed to the definition of how to manage energy between batteries and supercapacitors in order to make the most of the complementarity between these two sources.

These strategies may be based on three concepts [100,101] (see Figure. IV.1).

1. Rule-based strategies: these strategies are defined in advance on the basis of expertise or knowledge of the particularities of the system components. These strategies are simple at the level of implementation, but they do not guarantee the best possible solution.
2. Strategies based on deterministic optimization methods: these strategies make the system evolve in order to minimize (or maximize) the performance criterion. Several optimization techniques are based on this principle, such as optimum control, dynamic programming and linear programming. Two categories are possible: offline optimization and real-time optimization.
3. Strategies based on stochastic optimization methods such as the learning machine: The learning machine offers the ability to learn in order to achieve an objective (maximization / minimization of a criterion) without being explicitly programmed with cycles training.

### IV.2.1. Rule-based strategies

The few management rules that can be cited for hybrid sources in the automotive industry are fuzzy rules, neural networks and deterministic rules.

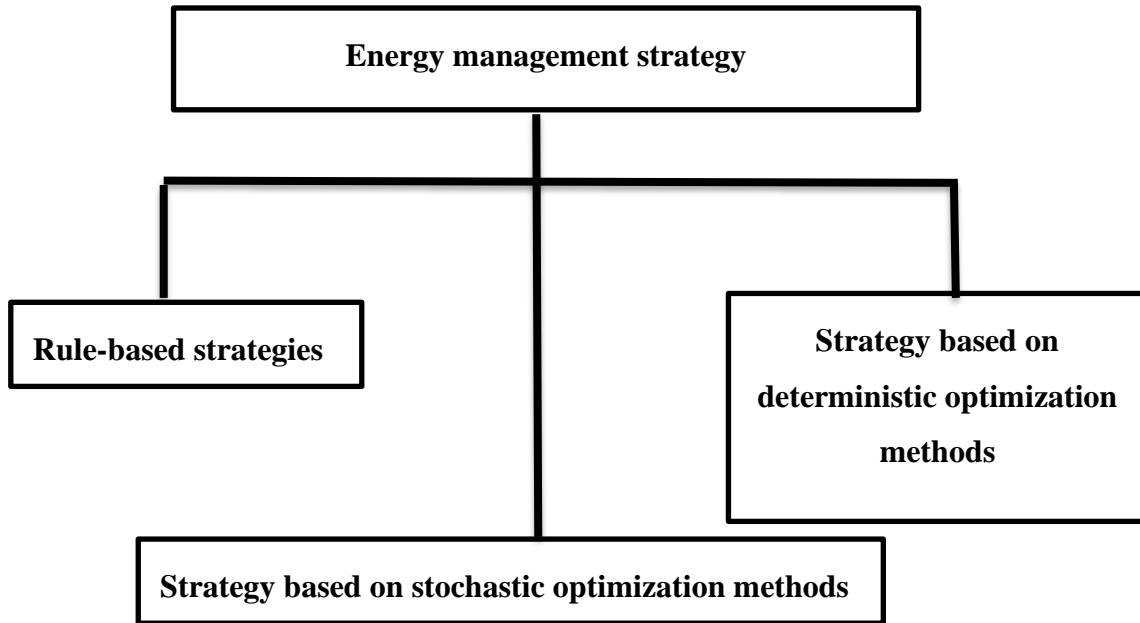


**Figure IV.1.** Existing energy management strategies

#### **A. Fuzzy rules**

The fuzzy rules are very practical in cases where the analytical modeling of the system is complex. Fuzzy Logic Controllers (FLCs) are the most widely used because of their independence from the mathematical model of the system to be controlled.

Researchers such as Gao, Caux and Erdinc have applied a fuzzy logic approach to fuel cell hybrid systems [102,103]. Eren [104] integrated the control of the internal dynamics of the fuel cell into an energy management approach based on fuzzy logic. However, the implementation of fuzzy rules has a negative impact due to the dependence on a certain level of expertise built into the strategy. This means that certain strong assumptions that depend on the designer's knowledge of the problem must be made [101,105].

#### **B. Neural networks**

Neural Network Models are computer models designed to emulate human processing capabilities (memorization and reasoning). Some studies using the approach to energy management of neural networks can be found in the literature. Ates [106] provided a neural network-based supervisory controller using the Adaptive Linear Neural Network (ADALINE) method to define the power delivered by a fuel cell system in a hybrid vehicle.

Askarzadeh [107] and Prokhorov [108] also used the same type of neural network, but combined with fuzzy logic there were more possibilities. The disadvantage of this approach is, on the one hand, that the formation of the knowledge process requires a large experimental database and, on the other, a lack of proof of stability [100,101,105].

### C. Deterministic rules

Deterministic rules define the power sharing techniques between the energy sources of the hybrid system. In this context, we shall cite various techniques used in multi-source vehicles.

- **Strategy for « All or Nothing »**

These are on/off thermostat strategies. Their principle is to distribute the power flows between the two sources in such a way as to ensure that each source operates around its best overall performance. Power sharing is done by assigning an active (On) or deactivated (Off) state to each power source (all or nothing switching). As shown in Figure IV.2, it is either the battery that takes the entire required profile or the supercapacitors that delivers the required power with a sudden switch between the two states [3].

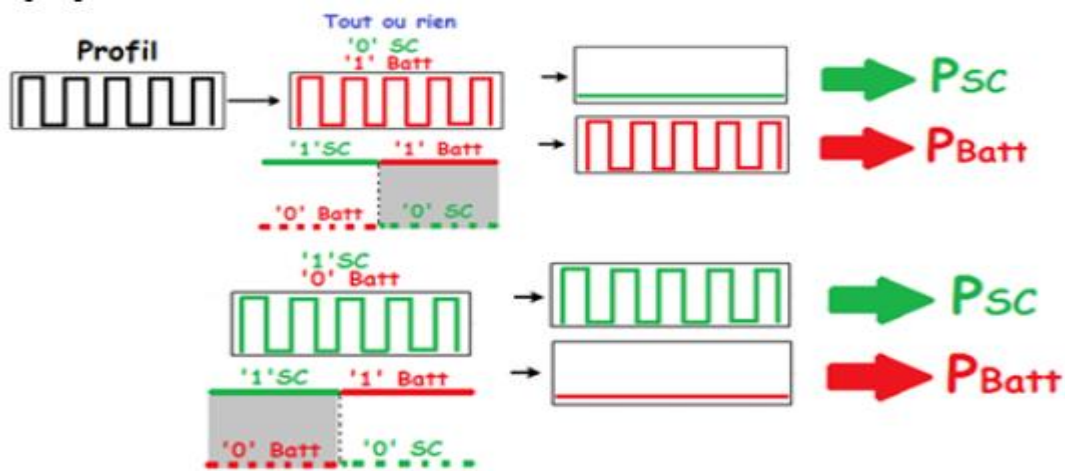


**Figure IV.2.** Principle of the "All or Nothing" management strategy

Where:  $P_{batt}$ : power of the battery,  $P_{sc}$ : power of the supercapacitor, SC: supercapacitor, Batt: battery.

The "smooth transition" between storage systems is an improved version of this strategy. As shown in Figure IV.3, switching between the supercapacitors and the battery takes place at a

linear transition stage in order to avoid additional current requirements during sudden switching [108].

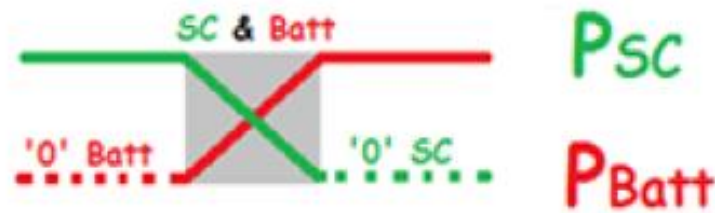


**Figure IV.3.** Principle of the "smoothed transition" management strategy

- **Strategy for « Power saturation »**

This technique is based on limiting the power of the battery over the entire required power profile. The power threshold for the battery is defined in advance. As a result, the supercapacitors take care of the difference between the power of the profile and the threshold defined (see Figure IV.4) [101,109]. This strategy makes it possible to limit current variations within a well-defined range of power. The choice of the power threshold is generally based on the peculiarities and characteristics of the storage systems used.

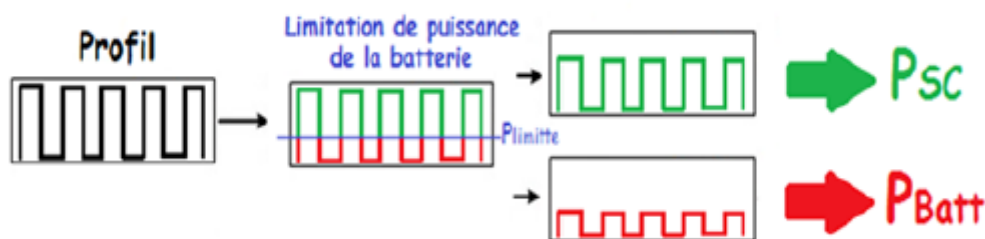


**Figure IV.4.** Principle of the "power saturation" management strategy

- **Strategy for « Adaptive power saturation »**

This strategy is an evolved version of the strategy presented above. The concept of distribution of the flow is the same. However, it offers more flexibility as the power limit on the battery side varies depending on the amount of energy in the supercapacitors. This strategy offers more freedom in the manipulation of power flows and therefore better performance [101].

- Strategy for “Frequency sharing”

The power frequency sharing strategy is based on the high/low frequency decomposition of the requested profile (see Figure IV.5). It makes it possible to take advantage of the inherent characteristics of the storage sources used. This type of sharing requires the supercapacitors to take charge of the power peaks and to assign the low-frequency components to the batteries [110].

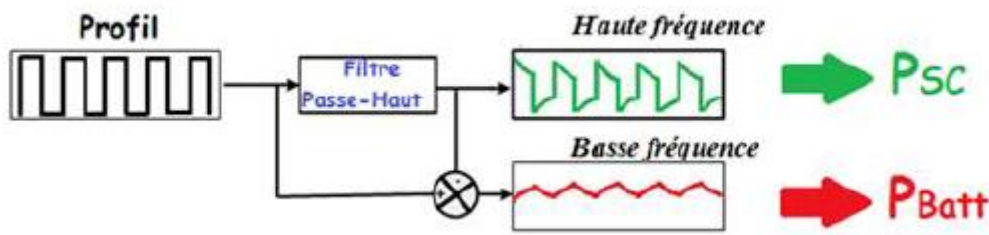


**Figure IV.5.** Principle of the “frequency sharing” management strategy

Table IV.1 evaluates the different rule-based strategies presented in terms of ease of implementation and performance.

**Table. IV.1.** Comparison of deterministic rule-based strategies

strategies	simplicity of implementation	performances
all or nothing	+ + +	-
power saturation	+ -	+ - -
adaptive power saturation	+ -	+ +
frequency sharing	-	+ + +

+ advantage - disadvantage

### IV.2.2. Strategy based on deterministic optimization methods

The aim of these optimization methods is to find an optimal control of the power flows of a multi-source system. The classification of these optimization strategies varies depending on the resolution methods. In this context, we define two types of resolution both offline and online (real time).

#### D. Offline optimization strategy

Offline optimization strategies require knowledge of the driving cycle. The optimum distribution of power is determined according to the target objectives and is carried out beforehand. The implementation of this type of optimization strategy in real-time systems is therefore impractical. However, these types of offline optimization are useful in the following cases of use:

- ✓ to use it as a reference for the evaluation of other real-time strategies [111];
- ✓ Aid for the dimensioning of multi-source systems [112],
- ✓ Adjusting other rule-based management strategies upstream [113].

According to the literature, many researchers have used dynamic programming techniques to solve optimization problems in order to find an optimal distribution of power in a hybrid storage system combining a battery and a supercapacitor with an "objective" function. Based on minimizing the RMS current of the battery [114,115].

#### E. Online optimization strategy

In contrast to offline optimization techniques, online control strategies achieve optimum distribution of power flows in real time. This method does not require prior knowledge of the driving profile. The challenge of the success of this approach therefore concerns two key points:

- ❖ on the one hand, the time of calculation that must be limited in order to make the solution workable in real time;
- ❖ on the other hand, it is necessary to decouple the optimal solution from the knowledge of driving conditions in order to make the implementation possible.

It is therefore possible to obtain the best solution irrespective of the driving conditions of the vehicle. Several real-time optimization techniques have been used to solve the problem of energy management in multi-source systems, namely predictive control and optimal control based on equivalent consumption minimization (ECMS) [116].

### **Predictive control**

The predictive control “Model-Predictive control” MPC-type is based on the estimation of the future driving conditions of the vehicle. This is done using a predefined template of the system [117]. A comparative study has made it possible to position the MPC command in relation to the rule-based strategies. The result of this study confirms that the MPC command is less efficient in terms of convergence time and solution efficiency than the rule-based strategy. This predictive control is quite efficient in systems with multiple inputs and outputs [118].

### **Optimal control**

The optimal control strategy based on the "Maximum Pontriaguine Principle" (PMP) is an offline method of resolution. However, this approach has been adapted for the case of real-time use. The versions of the strategies resulting from the PMP offer an instantaneous optimal distribution of power flows in a multi-source system [116,119], for example by using the "Equivalent Consumption Minimization" (ECMS) method derived from the PMP. The principle of this latter method is to minimize the weighted sum of powers [120]. The ECMS has been used in several works on multi-source vehicles [121]. The  $\lambda$ -control method makes it possible to adjust the parameter characterizing the resolution method by integrating the control loop [100].

#### **IV.2.3. Strategy based on stochastic optimization methods (Machine Learning)**

Machine learning (ML) is a sub-field of artificial intelligence. It refers to adaptive changes in the system [122]. Adaptive changes mean changes that allow the system to perform the same tasks or tasks for the same population but more efficiently in the future. It is a computer algorithm discipline that learns to perform "intelligent" tasks based on data observation and experience. More precisely, this method teaches how to do better in the future on the basis of what has been observed or experienced in the past [123]. For example, apps from popular websites such as "Amazon" "Facebook" and "Google" use machine learning. For example, the recommendation for movies in the “Netflix” app is based on one of these methods. Machine learning intersects with physics, statistics, theoretical computer science, and so on. It is widely used to solve problems related to optical character recognition, face detection, spoken language comprehension, weather forecasting and robotics [124].

The efficiency of the techniques (ML) has also been demonstrated in the algorithms applied to the energy management of battery-based storage systems. In his job, M. Triki [125] used the

dynamic power management algorithm "Dynamic Power Management" to extend the battery life of a mobile phone. In vehicle applications, this control technique (ML) can optimize the distribution of power flow while learning how to make optimal decisions in real time from historical driving cycles [126,127]. Work as it were [128] confirms that the machine learning technique can reduce the fuel consumption of a hybrid vehicle. In other works, it has been shown that a control strategy based on this algorithm (ML) offers a compromise between the simplicity of real-time implementation, the computation time and the optimality of the solution [129].

#### **IV.2.4. Summary of management strategies**

##### **A. Evaluation of deterministic optimization strategies**

In order to solve the problem of energy management in a hybrid source, optimization-based strategies make it possible to converge towards a well-defined objective [118]. They are based on minimizing (or maximizing) the performance criterion. However, the real-time implementation of these strategies remains a major problem, since even the most efficient online resolution algorithms require significant processing times [101,119]. In addition, methods that offer the best degree of optimality require prior knowledge of the power profile [130,100].

##### **B. Evaluation of strategies based on deterministic rules**

The advantage of management strategies based on deterministic rules is that they are simple to implement, making them easy to implement on a real-time computer. Moreover, these strategies do not require a prior knowledge of the vehicle's path [108]. However, the degree of performance of these methods depends on the knowledge of the expert who sets the rules according to the inherent potential of the multi-source system. A radical change in the driving conditions under which the system has been configured can affect the optimality of the solution [101].

##### **C. Hybridization of strategies**

Hybridization of strategies is another alternative to multi-source energy management. Hybridization of strategies enables the use of the strengths of each type of strategy (Table IV.2).

**Table. IV.2.** Evaluation of the different strategies

strategies	real-time implementation	optimal solution	calculation time	A prior knowledge of driving conditions
Strategy based on deterministic optimization methods	+ -	+	- +	-
Rule-based strategies	+	-	+	+
Strategy based on stochastic optimization methods	+ -	+ -	+ -	+

**+ advantage   - disadvantage**

The use of hybrid strategies combining rule-based strategies with optimization strategies is becoming increasingly frequent. Several works have introduced additional intelligence to existing deterministic rules through the use of offline optimization results [131,118,121].

In these approaches, the definition of rule-based strategies is based on the results of offline optimization algorithms. For instance, A.L. Allègre [132] has developed a rule-based strategy with a coefficient that characterizes the distribution of power between two sources. This coefficient is then generated by an offline resolution that minimizes losses in the primary storage source (battery). In the work of J.P.F. Trovão [133,134], an offline “particle swarm optimization” (PSO) algorithm based on power saturation was used to limit the search interval for the optimal solution. Hybridization (rule-based and optimization-based strategies) improves the degree of solution optimization of rule-based approaches. At the same time, optimization approaches see their computation time reduced due to the predefined application of the rules.

### IV.3. Architecture of electric vehicle

The block diagram of a typical electric vehicle is shown in Figure IV.6. In this case, batteries that are recharged using a recharging device and also recover energy during braking are the only source of energy aboard.

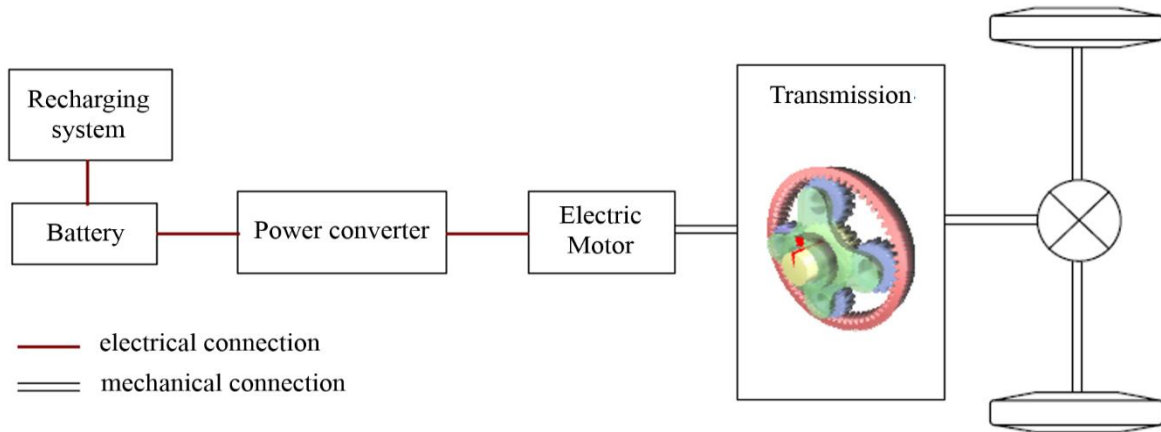


**Figure IV.6:** A typical electric vehicle schematic diagram.

The key source of energy is the weak point of this type of vehicle (the batteries). The main component of electric cars is the electric battery. It has a direct effect on the performance of the electric propulsion car and in particular, on its autonomy. In fact, their density of power expressed in  $W / kg$  is limited and their lifetime is directly related to the stresses applied to them. Therefore, their current of charge and discharge must be limited to ensure a lifetime compatible with a hybrid vehicle.

As far as battery charging is concerned, the alternative is to use a low current for a long time, such as charging the car at night, for example. A limitation of the discharge current, which is a driving cycle feature, is associated with a decrease in the vehicle's dynamic output.

For an electric vehicle with a single energy source, this is not feasible. Therefore, the current drawn during acceleration (high power constraint) from the batteries remains high. In certain cases, the batteries in the transport sector must be dimensioned primarily according to the power criterion (linked to service life, then according to an energy criterion).

Theoretically, in an EV, braking energy can be recovered. In this case, the electric motor acts as a generator and feeds the vehicle's kinetic energy back into the batteries, converted into electrical energy. The maximum charge current for regular model batteries is lower than the maximum discharge current. The braking power that can be recovered is directly related to the electrical energy storage element's maximum recharging current; as a result, not all braking energy can be recovered. Friction braking, of course, is still present.

In contrast to what we have presented above the key benefit of pure electric propulsion is that the EV does not release polluting gases during its use and that the energy on board the vehicle is contained in batteries. At the end user level, the electric vehicle is "clean" that is to

say, it does not locally emit polluting gases. On the other hand, it is important to take into account the recycling of used batteries and the output of energy for recharging. In the worst-case scenario, fossil fuels that release CO<sub>2</sub> into the atmosphere generate electrical energy.

In order to qualify as 'clean' in an electric vehicle, the energy needed for charging must be provided by renewable energy sources (solar, wind, hydraulic, etc.). In addition to the question of electrical supply for charging batteries, the major disadvantages of this type of vehicle using batteries are as follows:

- The battery life is limited especially if the instantaneous power limitations applied to them are important.
- The range that with traditional batteries can be achieved is limited;
- The maximum battery charging current is low, charging usually takes several hours, and only partial recovery of braking energy is possible.

Using auxiliary power sources such as super capacitors is one of the other solutions today to limit the difference in discharge and charge current in batteries.

Various association architectures have been considered in the literature. The choice between these architectures is based on a compromise between complexity, design costs and performance [102]. Generally, lower cost architecture is of interest to manufacturers, although some more flexible and complex architectures offer higher performance. For all the architectures that we are going to present, we note the presence of a DC/AC converter that allows the DC bus voltage to be adapted to the AC electrical machine of the vehicle. According to the literature [136,137] the parallel association architecture offers more advantages than the serial link in terms of the efficiency and reliability of the overall system. In this context, our study will focus on this parallel topology, for which the two energy sources (battery and supercapacitors) are simultaneously connected to the DC bus, allowing for more tolerance in the event of faults.

There are several parallel configurations. For the parallel, non-converter architecture (see Figure IV.7), we link the supercapacitors with the battery directly to the DC bus. The simplicity of this configuration makes it possible to have a low design cost, while offering rather limited performance due to the absence of flexibility. In fact, the DC bus voltage is stabilized by the battery due to the absence of a voltage matching converter, which prevents direct control of currents in storage systems for example, in the event of high-power demand or load short circuit [136].

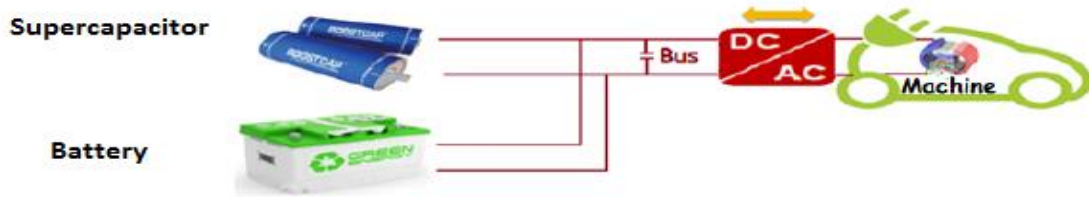


**Figure IV.7.** Parallel architecture without converter

In Figure IV.8, the parallel combination of the supercapacitors and the battery is done by a DC/DC converter. The role of this is to control the power flow on the side of the supercapacitors, which allows for more flexibility and therefore more performance. However, the design costs are quite high compared to the converter less architecture and the simplicity of implementation is lower [137].

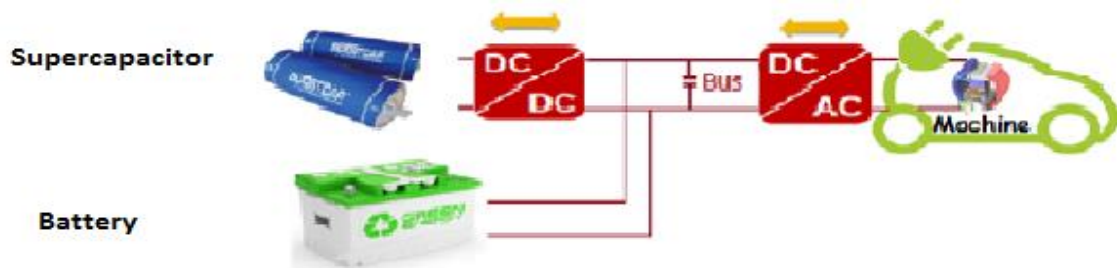


**Figure IV.8.** Parallel architecture with converter on the supercapacitor side

The two-converter architecture shown in Figure IV.9 contains two DC/DC converters linked to each source. This configuration gives the overall system the maximum degree of freedom to control the flow of power. Flexibility of this architecture can lead to significant performance, but it is complex at implementation level and has a high design cost [138].

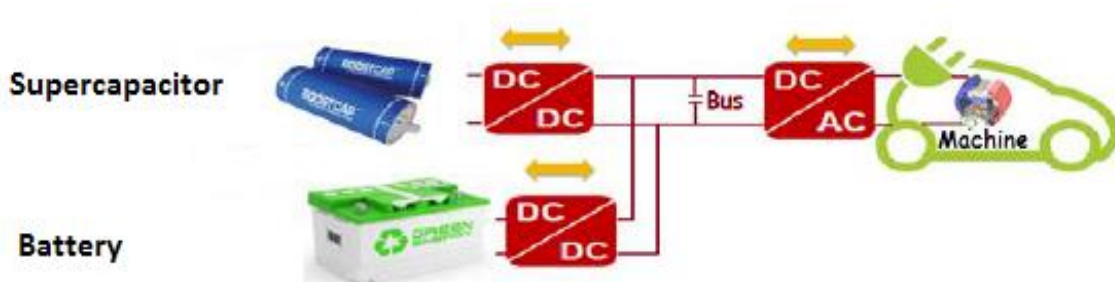


**Figure IV.9.** Architecture in parallel with two converters

Table IV.3 below summarizes the advantages and disadvantages of each architecture.

**Table IV.3.** Comparison of association architectures

architectures	simplicity of implementation	performances	flexibility	cost
architecture without converter	+ +	-	-	+ +
architecture with a single converter	+ -	+ -	+ -	+ -
architecture with two converters	-	+ +	+ +	-

**+ advantage   - disadvantage**

As part of this thesis, despite its cost and complexity drawbacks, we opted for the architecture with two converters because the objective is to make the best use of the flexibility and performance offered by this configuration in order to compensate for the inconvenience caused by improving the cost over the "life cycle" of the assembly.

#### IV.4. Power supply system

After the vehicle components have been modelled, the models of the power supply system are considered black boxes with inputs and outputs.

The battery considered has as input the current  $i_{bat}$  and at output the voltage  $v_{bat}$  which is in turn input for the Buck-boost converter block.

The supercapacitor considered has as input the current  $i_{sc}$  and in output the voltage  $v_{sc}$ , itself input for the second Buck-boost converter. The two output currents of the Buck-boost converters ( $i_1$  and  $i_2$ ) are chosen using the averaged models of the battery and of the supercapacitor including their power converters.

The power converter models are powered by the outputs of the energy sources ( $i_{sc}$  and  $i_{bat}$ ), by the values of the duty cycles ( $\alpha_{bat}$  and  $\alpha_{sc}$ ) calculated by the energy management strategy addressed and by the voltage of the DC bus,  $v_{DC}$ .

Finally, the DC bus has as inputs the two currents  $i_1$ ,  $i_2$  and the charging current  $i_L$  which is the image of the driving cycle.

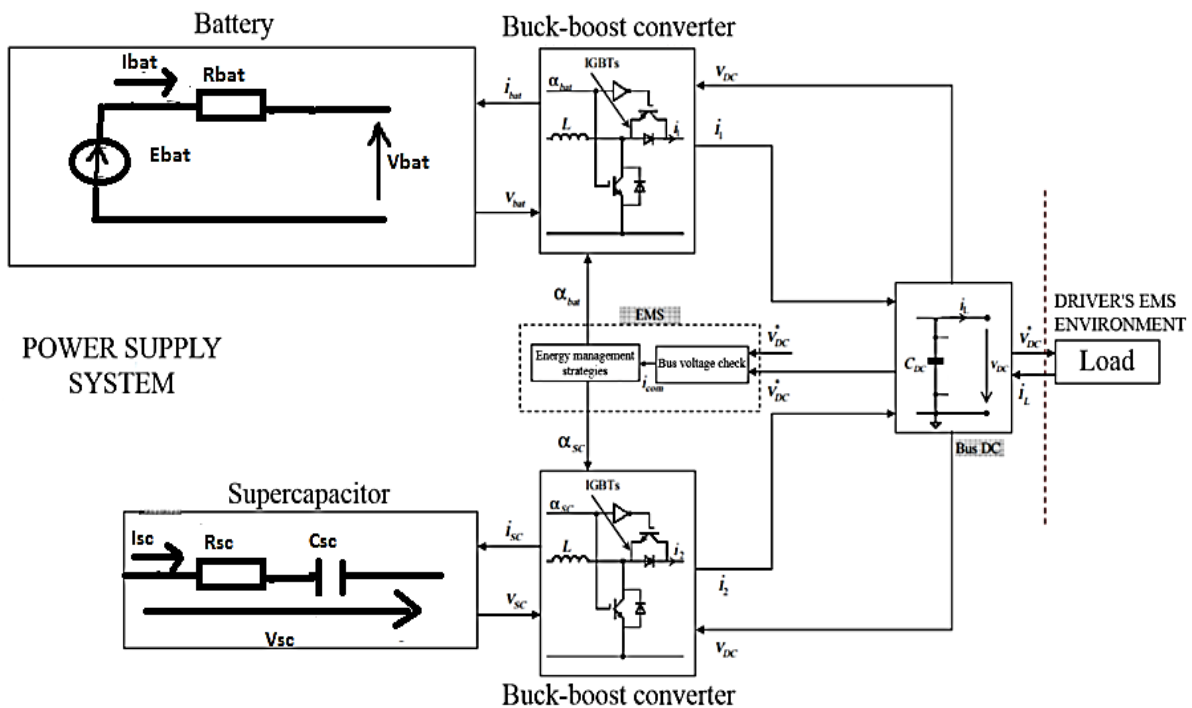


Figure IV.10: The topology of the power supply system [88].

### IV.5. Model of supercapacitor

Supercapacitors constitute a new specific energy storage technology that is superior to that of conventional capacitors, and of a specific power greater than that of electrochemical accumulators.

Electric double-layer supercapacitors, curiously called electrochemical capacitors, in fact operate similar to that of conventional electrostatic capacitors. The said ones typically consist of two metal electrodes separated by a dielectric material. The energy is stored in the form of an electric charge induced in the vicinity of the electrode-dielectric interface, by the application of a potential difference between these two electrodes. The ratio of stored charge to applied voltage is known as capacitance, or capacitance, and is representative of the device's ability to store energy. The basic relations are written, for a linear capacity [88]:

$$c_1 = \frac{Q}{V_1} = \varepsilon \frac{A}{d} \quad (\text{IV.1})$$

$$w = \frac{1}{2} c_1 V_1^2 \quad (\text{IV.2})$$

Thus, the objective is to establish a knowledge model of energy storage by supercapacitors, sufficiently precise and accessible. The equivalent model of a supercapacitor element is a capacitor  $C_{sc}$  in series with a resistor ( $R_{sc}$ ) [89] Figure IV.11. Resistance describes the ohmic losses of the component while capacitance designates the behaviour of the supercapacitor during charge and discharge [98].

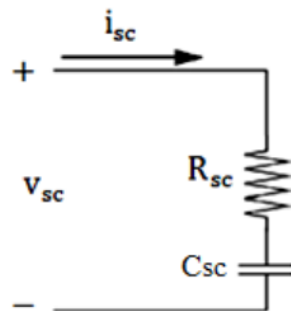


**Figure IV.11:** Model of a Supercapacitor [98].

### IV.5.1. Electrical equation of charge and discharge

To analyse the circuit of the previous model, we assume that the current of the supercapacitor  $i_{sc}$  is positive during the discharge phase and it is negative during the charge phase. The voltage across the super capacitors can be presented by:

$$V_{sc} = V_{csc} + R_{sc} \cdot i_{sc} \quad (IV.3)$$

### IV.5.2. Equation of state of charge

The state of charge, called  $SOC_{sc}$ , characterizes the amount of energy present in the supercapacitors. It is 100% when fully charged and 0% when charged to its minimum value. Equation (IV.4) presents the model adopted in this work [91].

$$SOC_{sc} = \frac{V_{sc}^2}{V_{scmax}^2} \quad (IV.4)$$

The SC's stored energy,  $E_{SC}$ , is expressed as [88]

$$E_{SC} = \frac{1}{2} CV_{SC}^2 \quad (IV.5)$$

where  $C$  is the capacitance in Faraday. The parameters of the supercapacitor are presented in Appendix. D.

## IV.6. Model of the battery

Currently, the most widely used technology for electric vehicles applications is Lithium-ion technology, but we use the Lead-acid technology for more simplicity in the complex system, disponible in our country and has a cheap price. We present here the model of this accumulator.

The battery model adopted is that which makes it possible to predict the autonomy of the electric vehicle system, that is to say to allow at any moment to estimate the remaining energy (state of charge  $SOC_{bat}$  or depth of discharge DoD) in the battery [91]. The model chosen is, therefore, an electrical equivalent model (Figure IV.12) composed of a voltage source in series with a resistance (internal resistance) [92, 93].

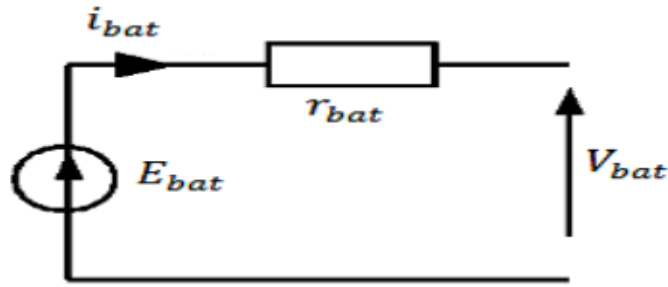


**Figure IV.12:** Simple electrical equivalent model of a battery [93].

#### IV.6.1. Electrical equation of charge and discharge

The on-load voltage is deduced directly from the no-load voltage and the voltage drop due to the series internal resistance [93]:

$$V_{bat} = E_{bat} - r_{bat} \cdot i_{bat} \quad (IV.6)$$

The open circuit voltage  $E_{bat}$  is approximately proportional to the state of charge of the battery [95]. Considering the DoD variable as a parameter varying between 0 and 1, depending on whether the battery is fully charged or fully discharged, equation (IV.8) presents a valid model for the electrical equation.

$$E_{bat} = \eta(2.15 - DOD \cdot (2.15 - 2.00)) \quad (IV.7)$$

$$DOD = 1 - SOC_{bat} \quad (IV.8)$$

#### IV.6.2. Equation of state of charge

The state of charge of the battery is an estimated parameter while the battery is traversed by an electric current. The  $SOC_{bat}$  is given by the ratio between the current capacity available and the total effective capacity available at the time preceding use [96].

$$SOC_{bat} = \frac{C_{actuelle}}{C_{totale}} = SOC_{b\ int} + \frac{100}{C_N} \times \int i(t) dt \quad (IV.9)$$

Where :  $SOC_{b\ int}$  : initial state of charge,  $C_N$  : nominal capacity;  $i(t)$  : battery current

The parameters of the battery are presented in Appendix. D.

### IV.7. Model of DC-DC inverter (back-boost) associate to the battery and the supercapacitor

The simplified diagram of the power supply system in Figure IV.10, showing its main components, is shown in more detail in Figure IV.13. This circuit supplies the DC bus voltage inverter,  $V_{DC}$ . In response, the electromechanical device draws the charging current,  $i_L$ . Both control inputs (duty cycles) are modulated widths pulse (PWM), allowing both power sources to deliver chopped output currents,  $i_1$  and  $i_2$ , which blend into the DC bus.

It is conventionally necessary for DC bus voltage to remain constant at the imposed value,  $V_{DC}^*$ , as in [135]. This regulatory action not only ensures the safety of the  $C_{DC}$  capacitor, but also ensures the transfer of electrical power to the load. So, the total current in the DC bus must match the current of the load to ensure the balance of the voltage (power balance).

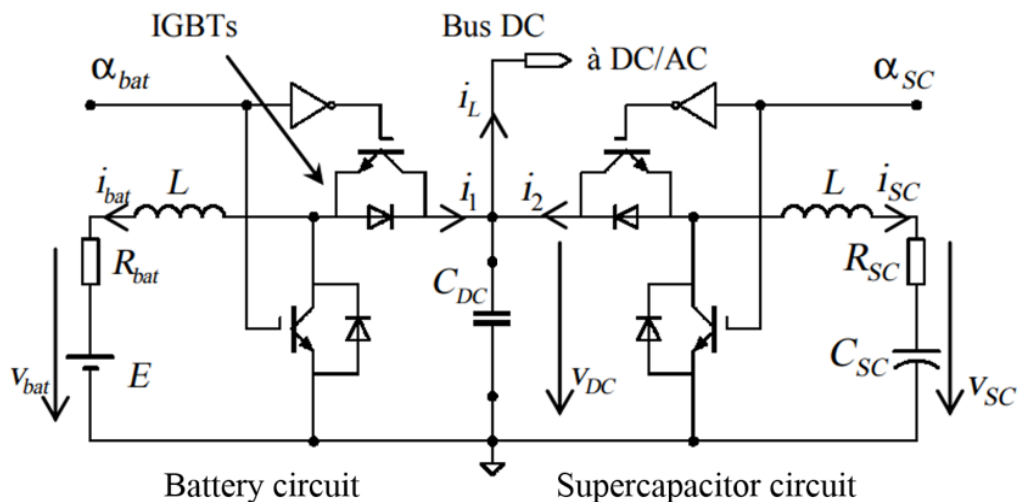


**Figure IV.13.** The topology of the power supply system

In many cases, we have an interest in transforming the original system into a continuous system which macroscopically best represents the dynamic and static behaviors of the circuit. For this purpose, the average behavior is quite suitable. The associated so-called "average" model finds a wide field of applications whether in control, simulation or even mode analysis [84]. The average model makes it possible to meet three essential requirements:

- Ease of implementation and use.
- Sufficient precision in its domain of validity.
- The possibility of use in a closed loop: possibility of switching to transfer function.

The average model of the circuit from the diagram provided in Figure **IV.13** is given by the following system of equations while respecting the assumptions we have mentioned:

$$\begin{cases} L \cdot \frac{di_{bat}}{dt} = v_{bat} - v_{DC} \cdot \alpha_{bat} - R_{bat} \cdot i_{bat} \\ L \cdot \frac{di_{SC}}{dt} = v_{SC} - v_{DC} \cdot \alpha_{SC} - R_{SC} \cdot i_{SC} \\ C_{DC} \cdot \frac{dv_{DC}}{dt} = i_{bat} \cdot \alpha_{bat} + i_{SC} \cdot \alpha_{SC} - i_L \end{cases} \quad (IV.10)$$

## IV.8. Conclusion

At present, multiple electric and hybrid vehicle architectures are feasible and have varied performance and functionality. The description of the elements of electrical energy storage shows that the optimization of the electrical source requires the combination of various battery and supercapacitor solutions. A very encouraging approach seems to be the use of supercapacitors as auxiliary power sources connected with main energy sources. This allows the peaks of the power supplied by the main energy source (the battery or the energy source considered) to be reduced, their over-sizing prevented and their lifetime extended. For this aim, we choose the architecture in parallel with two converters (Figure IV.9), a topology with more degrees of freedom that can ensure the adjustment of the DC bus voltage to a constant reference value, is the preferred architecture for the following chapters.

#### IV.10. References

- [88] J. Labbé, "L'Hydrogène électrolytique comme moyen de stockage d'électricité pour systèmes photovoltaïques isolés," 2006.
- [89] P. Thounthong, "Conception d'une source hybride utilisant une pile à combustible et des supercondensateurs," 2005.
- [90] H. Maker, "Optimisation et gestion d'énergie pour un système hybride: association Pile à Combustible et Supercondensateurs," Besançon, 2008.
- [91] D. Paire, M. G. Simoes, J. Lagorse, and A. Miraoui, "A real-time sharing reference voltage for hybrid generation power system," in *2010 IEEE Industry Applications Society Annual Meeting*, 2010, pp. 1-8: IEEE.
- [92] Y. Riffonneau, "Gestion des flux énergétique dans un système photovoltaïque avec stockage connecter au réseau—Application à l'habitat," 2009.
- [93] O. Gergaud, "Modélisation énergétique et optimisation économique d'un système de production éolien et photovoltaïque couplé au réseau et associé à un accumulateur," 2002.
- [94] A. O. M. Yahya, A. O. Mahmoud, and I. Youm, "Modélisation d'un système de stockage intégré dans un système hybride (PV/Eolien/Diesel)," *Revue des énergies renouvelables*, vol. 10, no. 2, pp. 205-214, 2007.

- [95] H. A. Dang, C. Guyon, B. Delinchant, P. Béguery, and F. Wurtz, "Gestion de l'énergie électrique dans l'habitat, cas du stockage électrochimique," *rapport de Schneider Electric*, 2012.
- [96] R. Sadoun, "Intérêt d'une Source d'Energie Electrique Hybride pour véhicule électrique urbain—dimensionnement et tests de cyclage," 2020.
- [97] A. Merdassi, "Outil d'aide à la modélisation moyenne de convertisseurs statiques pour la simulation de systèmes mécatroniques," 2009.
- [98] M. Ayad, M. Becherif, D. Paire, A. Djerdir, and A. Miraoui, "Passivity-based control of hybrid power sources using fuel cell, supercapacitors, and batteries on the dc link for energy traction system," in *2007 IEEE International Electric Machines & Drives Conference*, 2007, vol. 1, pp. 453-458: IEEE.
- [99] K. Agbli, M. Péra, D. Hissel, O. Rallières, C. Turpin, and I. Dombia, "Multiphysics simulation of a PEM electrolyser: Energetic Macroscopic Representation approach," *International journal of hydrogen energy*, vol. 36, no. 2, pp. 1382-1398, 2011.
- [100] A. Castaings, W. Lhomme, R. Trigui, and A. Bouscayrol, "Comparison of energy management strategies of a battery/supercapacitors system for electric vehicle under real-time constraints," *Applied Energy*, vol. 163, pp. 190-200, 2016.
- [101] T. Mesbahi, "Influence des stratégies de gestion d'une source hybride de véhicule électrique sur son dimensionnement et sa durée de vie par intégration d'un modèle multi-physique," Ecole centrale de Lille, 2016.
- [102] D. Gao, Z. Jin, and Q. Lu, "Energy management strategy based on fuzzy logic for a fuel cell hybrid bus," *Journal of Power Sources*, vol. 185, no. 1, pp. 311-317, 2008.
- [103] O. Erdinc, B. Vural, and M. Uzunoglu, "A wavelet-fuzzy logic based energy management strategy for a fuel cell/battery/ultra-capacitor hybrid vehicular power system," *Journal of Power sources*, vol. 194, no. 1, pp. 369-380, 2009.
- [104] Y. Eren, O. Erdinc, H. Gorgun, M. Uzunoglu, and B. Vural, "A fuzzy logic based supervisory controller for an FC/UC hybrid vehicular power system," *international journal of hydrogen energy*, vol. 34, no. 20, pp. 8681-8694, 2009.
- [105] N. D. F. Ramon, "Optimization of the sizing and the energy management for a hybrid fuel cell vehicle including fuel cell dynamics and durability constraints," INSA de Lyon, 2013.
- [106] Y. Ates, O. Erdinc, M. Uzunoglu, and B. Vural, "Energy management of an FC/UC hybrid vehicular power system using a combined neural network-wavelet transform based strategy," *International journal of hydrogen energy*, vol. 35, no. 2, pp. 774-783, 2010.

- [107] A. Askarzadeh and A. Rezazadeh, "Artificial neural network training using a new efficient optimization algorithm," *Applied Soft Computing*, vol. 13, no. 2, pp. 1206-1213, 2013.
- [108] D. V. Prokhorov, "Toyota Prius HEV neurocontrol and diagnostics," *Neural Networks*, vol. 21, no. 2-3, pp. 458-465, 2008.
- [109] P. VENET, "Stéphane BUTTERBACH Stockage d'énergie électrique par association de batteries au plomb et de supercondensateurs pour véhicule lourd," Université Bordeaux 1, 2012.
- [110] A. Hammani, R. Sadoun, N. Rizoug, P. Bartholomeüs, B. Barbedette, and P. Le Moigne, "Influence of the management strategies on the sizing of hybrid supply composed with battery and supercapacitor," in *2012 first international conference on renewable energies and vehicular technology*, 2012, pp. 1-7: IEEE.
- [111] Z. Song, H. Hofmann, J. Li, X. Han, X. Zhang, and M. Ouyang, "A comparison study of different semi-active hybrid energy storage system topologies for electric vehicles," *Journal of Power Sources*, vol. 274, pp. 400-411, 2015.
- [112] Y.-H. Hung and C.-H. Wu, "An integrated optimization approach for a hybrid energy system in electric vehicles," *Applied energy*, vol. 98, pp. 479-490, 2012.
- [113] J. Bernard, S. Delprat, F. Buechi, and T. M. Guerra, "Global Optimisation in the power management of a Fuel Cell Hybrid Vehicle (FCHV)," in *2006 IEEE Vehicle Power and Propulsion Conference*, 2006, pp. 1-6: IEEE.
- [114] E. Vinot, R. Trigui, and B. Jeanneret, "Optimal management of electric vehicles with a hybrid storage system," in *2010 IEEE Vehicle Power and Propulsion Conference*, 2010, pp. 1-6: IEEE.
- [115] A. Sciarretta, M. Back, and L. Guzzella, "Optimal control of parallel hybrid electric vehicles," *IEEE Transactions on control systems technology*, vol. 12, no. 3, pp. 352-363, 2004.
- [116] L. Tribioli, M. Barbieri, R. Capata, E. Sciubba, E. Jannelli, and G. Bella, "A real time energy management strategy for plug-in hybrid electric vehicles based on optimal control theory," *Energy Procedia*, vol. 45, pp. 949-958, 2014.
- [117] R. Xiong, X. Gong, C. C. Mi, and F. Sun, "A robust state-of-charge estimator for multiple types of lithium-ion batteries using adaptive extended Kalman filter," *Journal of Power Sources*, vol. 243, pp. 805-816, 2013.
- [118] Z. Song, H. Hofmann, J. Li, J. Hou, X. Han, and M. Ouyang, "Energy management strategies comparison for electric vehicles with hybrid energy storage system," *Applied Energy*, vol. 134, pp. 321-331, 2014.
- [119] L. Xu, M. Ouyang, J. Li, F. Yang, L. Lu, and J. Hua, "Application of Pontryagin's Minimal Principle to the energy management strategy of plugin fuel cell electric vehicles," *International Journal of Hydrogen Energy*, vol. 38, no. 24, pp. 10104-10115, 2013.
- [120] C.-K. Chau, K. Elbassioni, and C.-M. Tseng, "Drive mode optimization and path planning for plug-in hybrid electric vehicles," *IEEE Transactions on Intelligent Transportation Systems*, vol. 18, no. 12, pp. 3421-3432, 2017.

- [121] J. Han, Y. Park, and D. Kum, "Optimal adaptation of equivalent factor of equivalent consumption minimization strategy for fuel cell hybrid electric vehicles under active state inequality constraints," *Journal of Power Sources*, vol. 267, pp. 491-502, 2014.
- [122] R. S. Sutton and A. G. Barto, "Reinforcement learning: An introduction," ed: Cambridge, MA: MIT Press, 2011.
- [123] N. Lopes and B. Ribeiro, "Machine Learning for Adaptive Many-core Machines: A Practical Approach," 2015.
- [124] R. Schapire, "Theoretical machine learning," *Computer Science lecture, Princeton University, New Jersey, United States*, 2008.
- [125] M. Triki, A. C. Ammari, Y. Wang, and M. Pedram, "Reinforcement learning-based dynamic power management of a battery-powered system supplying multiple active modes," in *2013 European Modelling Symposium*, 2013, pp. 437-442: IEEE.
- [126] T. Liu, Y. Zou, D. Liu, and F. Sun, "Reinforcement learning-based energy management strategy for a hybrid electric tracked vehicle," *Energies*, vol. 8, no. 7, pp. 7243-7260, 2015.
- [127] T. Liu, X. Hu, S. E. Li, and D. Cao, "Reinforcement learning optimized look-ahead energy management of a parallel hybrid electric vehicle," *IEEE/ASME Transactions on Mechatronics*, vol. 22, no. 4, pp. 1497-1507, 2017.
- [128] X. Qi, G. Wu, K. Boriboonsomsin, and M. J. Barth, "Development and evaluation of an evolutionary algorithm-based online energy management system for plug-in hybrid electric vehicles," *IEEE Transactions on Intelligent Transportation Systems*, vol. 18, no. 8, pp. 2181-2191, 2016.
- [129] Y. L. Murphey *et al.*, "Intelligent hybrid vehicle power control—Part II: Online intelligent energy management," *IEEE Transactions on Vehicular Technology*, vol. 62, no. 1, pp. 69-79, 2012.
- [130] V. Agubra and J. Fergus, "Lithium ion battery anode aging mechanisms," *Materials*, vol. 6, no. 4, pp. 1310-1325, 2013.
- [131] R. Carter, A. Cruden, and P. J. Hall, "Optimizing for efficiency or battery life in a battery/supercapacitor electric vehicle," *IEEE Transactions on Vehicular Technology*, vol. 61, no. 4, pp. 1526-1533, 2012.
- [132] A.-L. Allègre, "Méthodologies de modélisation et de gestion de l'énergie de systèmes de stockage mixtes pour véhicules électriques et hybrides," Lille 1, 2010.
- [133] J. P. F. Trovao, V. D. Santos, C. H. Antunes, P. G. Pereirinha, and H. M. Jorge, "A real-time energy management architecture for multisource electric vehicles," *IEEE Transactions on Industrial Electronics*, vol. 62, no. 5, pp. 3223-3233, 2014.
- [134] J. P. Trovão, P. G. Pereirinha, H. M. Jorge, and C. H. Antunes, "A multi-level energy management system for multi-source electric vehicles—an integrated rule-based meta-heuristic approach," *Applied Energy*, vol. 105, pp. 304-318, 2013.
- [135] N. Hur, J. Jung, and K. Nam, "A fast dynamic DC-link power-balancing scheme for a PWM converter-inverter system," *IEEE Transactions on industrial electronics*, vol. 48, no. 4, pp. 794-803, 2001.

- [136] W. Jiang and B. Fahimi, "Active current sharing and source management in fuel cell–battery hybrid power system," *IEEE Transactions on Industrial Electronics*, vol. 57, no. 2, pp. 752-761, 2009.
- [137] É. Bouchard, "Analyse de la consommation énergétique de véhicules électriques," École Polytechnique de Montréal, 2018.
- [138] A. Eddahech, "Modélisation du vieillissement et détermination de l'état de santé de batteries lithium-ion pour application véhicule électrique et hybride," Université Sciences et Technologies-Bordeaux I, 2013.
- [139] S. Caux, W. Hankache, M. Fadel, and D. Hissel, "On-line fuzzy energy management for hybrid fuel cell systems," *International journal of hydrogen energy*, vol. 35, no. 5, pp. 2134-2143, 2010.

# **Chapter V: description of control approaches**

**I.**

## V.1. Introduction

Battery aging is one of the obstacles to the development of electric vehicles due to the limited number of charging cycles. The use of supercapacitors in addition to the battery makes it possible to significantly reduce the current requirements of the batteries and therefore to reduce their ageing. In this context, we have adopted an already existing solution to the problem of aging batteries, namely by associating them with supercapacitors [140].

Supercapacitors, which have recently appeared on the market, offer an alternative approach to the conversion of electrical energy and power systems. It is well known that driving cycles, particularly in urban areas, are characterized by a highly variable demand for loads due to unstable traffic. Thus, the electrical current required by the driving cycle varies randomly in real conditions depending on the acceleration, deceleration or the topology of the journey (inclined plane, etc.).

## V.2. Solving the energy management problem

As we have seen in the fourth chapter, the electrical vehicle being studied consists of two electrical sources (batteries and supercapacitors) and two reversible converters (Buck-boost converters) Figure IV.9. This topology is equipped with an energy management system to be referred to an EMS acronym (Energy Management System). This means that the Buck-boost converter between the battery and the DC bus ensures a stable DC bus voltage to gain of efficiency (Figure V.1).

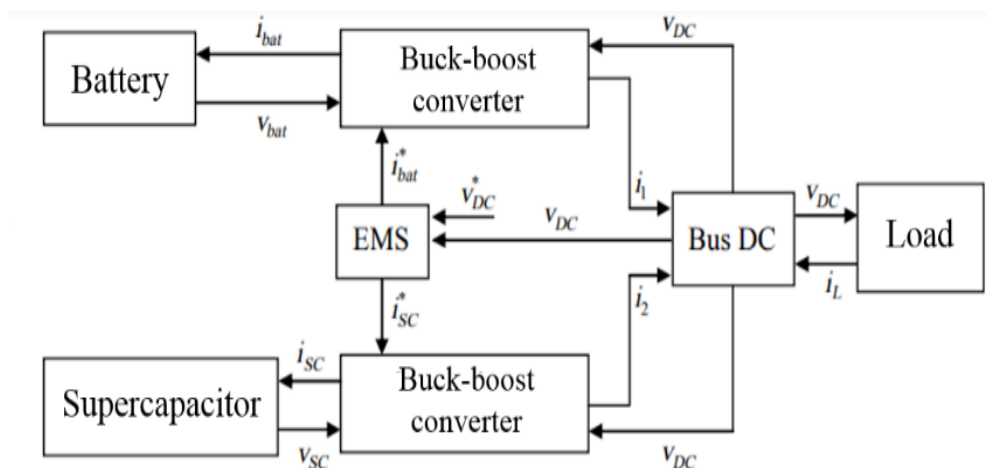


**Figure V.1.** The architecture of the studied electric vehicle

It should be remembered that the optimized energy management of the system consisting of the battery and the load-associated supercapacitors is designed to minimize the variation of the current supplied by the battery to the load during the driving cycle (speed/time).

### V.2.1. First order filter used for frequency separation

Limiting the variations of the instantaneous current in the battery is equivalent to making the current as close as possible to its average value. For this purpose, the current demand for the load is separated by filtering into two components. The low-frequency component becomes the reference current of the battery, which can be obtained by using a low-pass filter. Supercapacitors as well as those responding to high-frequency requests.

The notations used in Figure V.2 are:  $i_{bat}$  and  $v_{bat}$  the current and voltage of the battery,  $i_{sc}$  and  $v_{sc}$  the current and voltage of the supercapacitor,  $i_{bat}^*$  and  $i_{sc}^*$  the reference currents for the converter control loops,  $i_1$  and  $i_2$  the chopped output currents (converters),  $v_{DC}$  the DC bus voltage,  $v_{DC}^*$  the DC bus reference voltage and  $i_L$  the load current.

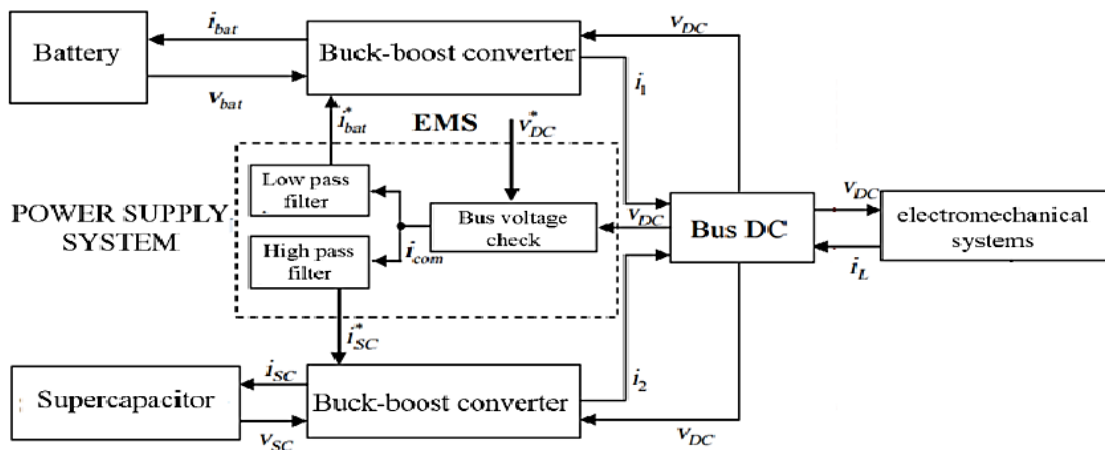


**Figure V.2.** Topology of the vehicle showing the interactions between its various subsystems.

Figure V.2 shows the main interactions between the different subsystems of the electric vehicle, where  $i_{com}$  is the total current considered to be the DC bus voltage control input,  $i_L$  is the image of the torque of the electromechanical systems, calculated from the rotational speed of the electromechanical systems (engine, wheels,). It depends on the driving cycle of the vehicle (the World Motor Test Cycle (WMTC), the Extra Urban Driving Cycle (EUDC), the American Federation Testing Cycle (FTP)).

The dynamics of the electric vehicle and its electromechanical systems are subject to external disturbances as a function of driving conditions and vehicle speed reference variations. The

exchange of electrical energy with the power supply system is carried out by a DC bus (DC bus). The traction control of the electric motor can be carried out in motor mode (by accelerating) or in generator mode (by slowing down). In the latter regime, DC busses are supplied with energy during braking and electrical energy sources are recharged via reversible converters. Breaking energy recovery increases the range of the vehicle. The connection between the electric motor and the DC bus is made by means of the inverter [141]. Indeed, the Energy Management System (see Figure V.2) must ensure a continuous supply of electrical energy while at the same time limiting voltage variations on the DC bus, regardless of driving conditions. Ideally, the constant value of this voltage ensures an optimum dimensioning of DC bus capacitors and a good dynamic performance of the electromechanical drive.

The energy management principle proposed in this chapter describes the sharing of power between the battery and the supercapacitor using a frequency approach [142,143].

### V.2.2. Design of the control structure

From the average circuit model, which is given in equation IV.10, the state vector of the system is  $[i_{bat} \ i_{SC} \ v_{DC}]$ , the control inputs are the two duty cycles corresponding to each power converter,  $[\alpha_{bat} \ \alpha_{SC}]$ , and the disturbance considered is the load current,  $i_L$ , which is, of course, reversible. It is also necessary to take into account the voltage of the supercapacitor,  $v_{SC}$ , as a state variable but, as the dynamic that emerges from it is quite slow compared to the other variables, in this case it was considered a variable parameter with bounded values.

The Figure V.3 shows the overall diagram of the proposed energy management system.

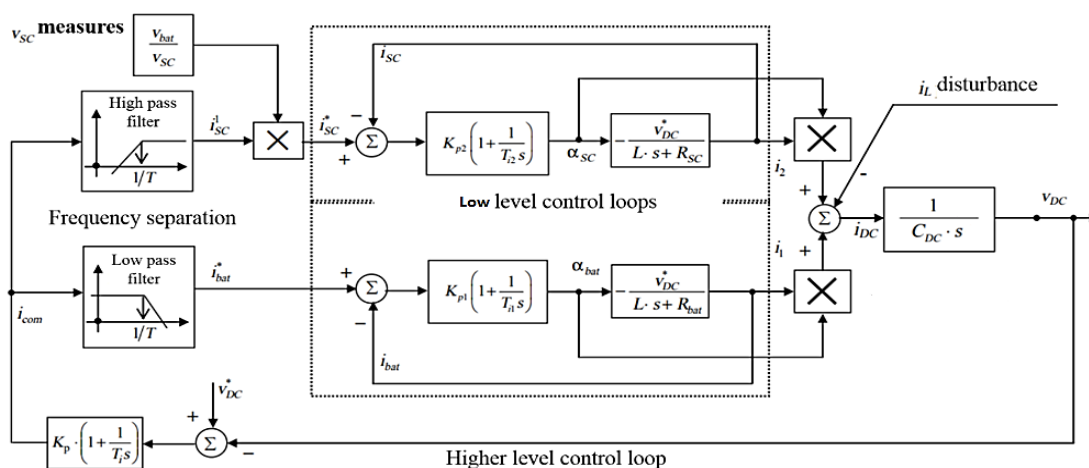


**Figure V.3.** Global diagram of the energy management system, organized at two hierarchical levels with nested loops [144].

The currents in the inductors and the dynamics of the DC bus voltage can be decoupled, therefore a classic two-level control structure is envisaged [145]. As can be seen, the order has been spread over two hierarchical levels:

- low level, the role of which is to regulate currents  $i_1$  and  $i_2$  in the two inductors, ( $L_{bat}$ ,  $L_{SC}$ ).
- the upper level, which enshrines the voltage across the  $C_{DC}$  capacitor and incorporates a frequency splitter consisting of a low-pass filter dedicated to energy management.

The external reference is the bus DC voltage,  $V_{DC}^*$ , required at the connection point.

The low-pass filter acts on the output of the proportional-integral (PI) corrector, reflecting the total demand for the load current, directing the low-frequency component, which becomes the reference for the battery current control loop, and the high-frequency component being the reference for the current control loop in the supercapacitor.

### V.2.3. Control of the supercapacitor and the battery current

According to the first two expressions of Equation (IV.10), the structures of the power converters are the same for the battery and supercapacitor circuits. If we consider that the permissible limits on the DC bus are reached, its voltage can be considered to have a constant value of  $V_{DC}^* = V_{DC}$  at this stage in the design of the correctors. Thus, the two low-level structures, either for the battery or the supercapacitor, are linear and invariant. The current supplied at the output of the supercapacitor is expressed by the transfer function in Equation (V.1) (similar modeling is done for the current of the battery, see Equation (V.2)):

$$H_{sc}(s) = \frac{i_{sc}}{\alpha_{sc}} = \frac{-V_{DC}^*}{L \cdot s + R_{SC}} \quad (V.1)$$

$$H_{bat}(s) = \frac{i_{bat}}{\alpha_{bat}} = \frac{-V_{DC}^*}{L \cdot s + R_{bat}} \quad (V.2)$$

Following this modeling, the classical regulation structure of the proportional-integral (PI) type (with anti-saturation loop) is used to follow the references of the currents of the battery and the supercapacitor [145] respectively.

The general transfer function of the PI correctors used in the low-level control structure has the following form:

$$H_{PI}(s) = K_p \cdot \left( 1 + \frac{1}{T_i s} \right) \quad (\text{V.3})$$

where  $K_p$  ( $k_{p1}$  or  $k_{p2}$ ) and  $T_i$  ( $T_{i1}$  and  $T_{i2}$ ) are the parameters of the PI correctors.

Using Equations (V.1) and (V.2) we can write the transfer function in the general case:

$$H(s) = \frac{- * V_{DC}}{L \cdot s + R} = \frac{\frac{-V_{DC}^*}{R}}{\frac{L}{R} \cdot s + 1} = \frac{-K}{T \cdot s + 1} \quad (\text{V.4})$$

where  $K = *V_{DC} / R$  and  $T = L/R$  with  $R = R_{bat}$  for the battery converter regulator or  $R = R_{SC}$  for the supercapacitor converter regulator.

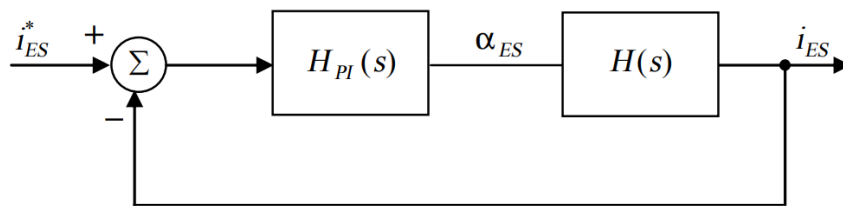


**Figure V.4:** Low level control architecture

From Figure V.7 and using the forms of the transfer functions  $H(s)$  and  $H_{PI}(s)$ , we find the equivalent closed-loop transfer function for the regulatory structure:

$$H_{FTBF}(s) = \frac{H_{PI}(s) \cdot H(s)}{1 + H_{PI}(s) \cdot H(s)} = \frac{\frac{K_p(T_i + 1)}{T_i s} \cdot \left( -\frac{K}{T_s + 1} \right)}{1 - \frac{K_p K (T_i s + 1)}{T_i s (T_s + 1)}} \quad (\text{V.5})$$

Finally, the  $H_{FTBF}(s)$  function is written in the form:

$$H_{FTBF}(s) = \frac{T_i \cdot s + 1}{-\frac{T_i \cdot T}{K_p \cdot K} \cdot s^2 + \left( -\frac{T_i}{K_p \cdot K} + T_i \right) \cdot s + 1} \quad (\text{V.6})$$

The regulator parameters,  $K_p$  and  $T_i$  are determined according to the form of the desired closed-loop response, for these two adjustment factors are available: the time constant corresponding to the cut-off frequency,  $T_0$ , and the damping coefficient,  $\xi$ .

In general, the transfer function of a second order system is expressed as:

$$H_{II}(s) = \frac{K}{T_0^2 \cdot s^2 + 2\xi T_0 \cdot s + 1} \quad (\text{V.7})$$

We would like a system response of order two for this regulator. Thus, by identification, the relationship (V.7) used to calculate the parameters is as follows:

$$\begin{cases} K_p = \frac{1}{K} \cdot \left( \frac{2\xi T}{T_0} - 1 \right) \\ T_i = 2\xi T_0 - \frac{T_0^2}{T} \end{cases} \quad (\text{V.8})$$

We imposed a closed-loop response dynamic five times faster than the main dynamic, i.e.  $T_0 = T / 5$  and damping coefficient  $\xi = 0.85$ . The values of the parameters of the regulators used are available in Appendix. E

#### V.2.4. Control of the DC bus voltage and the filters

High level control concerns the control of the voltage and the filters (low pass and high pass). Under the realistic assumption that the currents of the internal loops ( $i_{bat}$  and  $i_{SC}$  are much faster than the DC bus voltage. The power losses of the switching devices are assumed to be negligible. In this context, we can postulate the following:

$$\begin{cases} \alpha_{bat} = \frac{V_{bat}}{V_{DC}} \\ \alpha_{SC} = \frac{V_{SC}}{V_{DC}} \end{cases} \quad \text{and} \quad \begin{cases} i_1 = \alpha_{bat} \cdot i_{bat} \\ i_2 = \alpha_{SC} \cdot i_{SC} \end{cases} \quad (\text{V.9})$$

The second group of equations (V-10) implies that the two  $i_{bat}$  and  $i_{SC}$  currents can be used as control inputs for the DC bus structure with the output  $v_{DC}$  voltage. Hence, the total current injected into the DC bus by the two energy sources is written:

$$i_{DC} = i_1 + i_2 = \alpha_{bat} \cdot i_{bat}^* + \alpha_{SC} \cdot i_{SC}^* \quad (\text{V.10})$$

Note that, as stated in the first system of Equations (V.9), the two channels of influence have different benefits i.e. their duty cycles. It should also be remembered that, with regard to the difference in the voltage of the DC bus and of the battery, the gain of the battery, which is the duty cycle  $\alpha_{bat}$ , is almost constant. In order to equalize their effect, an additional gain for the supercapacitor must either be added or the reference current of the supercapacitor must be changed as follows (Figure V.3):

$$i_{SC}^* = i_{SC}^1 \cdot \frac{V_{bat}}{V_{SC}} \quad (V.11)$$

where  $i_{SC}^*$  is the output current of the high pass filter and the  $\frac{V_{bat}}{V_{SC}}$  ratio is the additional gain.

Thus, using Equations (V-9) and (V-11) in Equation (V-10) the current exchanged with the DC bus becomes:

$$i_{DC} = i_1 + i_2 = \alpha_{bat} \cdot (i_{bat}^* + i_{SC}^1) = \frac{V_{bat}}{V_{DC}} \cdot i_{com} \quad (V.12)$$

with  $i_{com}$  designating the total current considered as the control input within the DC bus voltage regulation loop. By equalizing the gains on the two current channels and replacing by Equation (V-12) the third expression of Equation (IV.15), the equation of the regulation structure of the DC bus is written as the following way:

$$C_{DC} \cdot \frac{dv_{DC}}{dt} = \frac{v_{bat}}{v_{DC}} \cdot i_{com} - i_L \quad (V.13)$$

**Note:** Sadly, this equation is not linear, which makes changing the corrector more complicated. An energy method allows the equation (V.13) to be linearized in an analogous way, that is, by multiplying the voltage of the DC bus on the left and on the right:

$$\frac{C_{DC}}{2} \cdot \frac{dv_{DC}^2}{dt} = v_{bat} \cdot i_{com} - i_L \cdot v_{DC} \quad (V.14)$$

Equation (V.14) integrates a non-linearity on the voltage of the DC bus with as control input  $i_{com}$  and the load current  $i_L$  as exogenous disturbance. In this case a linear regulator can be designed after linearization of this equation around a given operating point  $(v_{DC}^0, i_L^0)$ . Noting with  $\Delta(x)$  the variations around the given operating point, the linearized dynamics of the DC bus voltage is then written in the following form:

$$C_{DC} v_{DC}^0 \frac{d\Delta v_{DC}}{dt} = v_{bat} \Delta i_{com} - i_L^0 \Delta v_{DC} - v_{DC}^0 \Delta i_L \quad (V.15)$$

with  $v_{DC}^0, i_L^0$ , being the voltage of the DC bus and the load current in a given operating point,  $\Delta v_{DC}, \Delta i_{com}$  and  $\Delta i_L$  being respectively the variations around the same operating point.

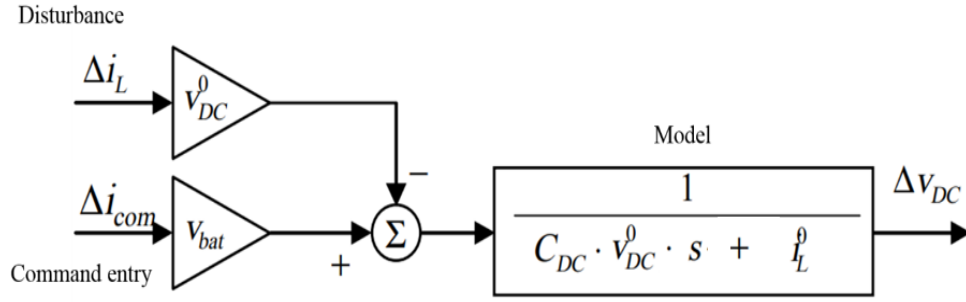


**Figure V.5:** The linearized dynamics of the DC bus voltage

From (V-15), the transfer function is written:

$$\frac{\Delta v_{DC}(s)}{\Delta i_{com}(s)} = \frac{K_{DC}}{T_{DC} \cdot s + 1} \quad (\text{V.16})$$

where the two gains  $K_{DC} = v_{bat}/i_L^0$  and the time constant  $T_{DC} = C_{DC}v_{DC}^0/i_L^0$  depend on the operating point, therefore mainly on the charge current  $i_L^0$ . The fact that  $\frac{K_{DC}}{T_{DC}} = v_{bat}/(C_{DC} \cdot v_{DC}^0)$  is invariant, can be used to design a PI regulator which is also nearly invariant, so that one can obtain the desired closed loop dynamics of the DC bus voltage.

With a PI corrector of the form  $C(s) = K_p (1 + (1 / T_i \cdot s))$  and using Equation (V-16), we find the closed loop transfer function:

$$H_{FTBF}(s) = \frac{T_i \cdot s + 1}{\frac{T_i \cdot T_{DC}}{K_p \cdot K_{DC}} \cdot s^2 + \left( \frac{T_i}{K_p \cdot K_{DC}} + T_i \right) \cdot s + 1} \quad (\text{V.17})$$

Finally, using Equations (V-17) and (V-7) by identification, we deduce the expressions of  $K_p$  and  $T_i$ .

$$\begin{cases} K_p = \frac{1}{K_{DC}} \cdot \left( \frac{2\xi T_{DC}}{T_0} - 1 \right) \\ T_i = 2\xi T_0 - \frac{T_0^2}{T_{DC}} \end{cases} \quad (\text{V.18})$$

The values of the time constants  $T_0$  and  $\xi$  are therefore chosen to ensure that the current loops provide an almost instantaneous response to the voltage loop. The values of the DC bus voltage corrector parameters are presented in Appendix. E

As regards the design of the system control, the delays introduced by the filters in the energy management strategy by filtering are negligible (Figure VI.3).

With regard to the choice of separation frequency,  $1/T$ , in order to solve the problem of energy management, it can be seen in Figure VI.2 that the smaller of separation frequency, the lower the current of the battery should vary. As a result, a small separation frequency provides better protection of the battery as well as improved service time.

### **V.3. Conclusion**

The introduction of energy management using the frequency separation between the super capacity and the battery has made it possible to use a simplified control structure that is easy to implement in a real vehicle while at the same time complying with the manufacturer's constraints.

#### V.4. References

- [140] J. M. Miller, T. Bohn, T. J. Dougherty, and U. Deshpande, "Why hybridization of energy storage is essential for future hybrid, plug-in and battery electric vehicles," in *2009 IEEE Energy Conversion Congress and Exposition*, 2009, pp. 2614-2620: IEEE.
- [141] B. K. Bose, "Power electronics and AC drives," *Englewood Cliffs*, 1986.
- [142] P. Chapoulie and S. Astier, "Modelling of an electric vehicle including ultracapacitors with SABER," *Proceedings of the EVS-15, AVERE, Brussels, Belgium*, 1998.
- [143] P. Chapoulie, "Modélisation systémique pour la conception de véhicules électriques multi-sources: application aux véhicules équipés de générateurs photovoltaïques ou de supercondensateurs," Toulouse, INPT, 1999.
- [144] A. Florescu, S. Bacha, I. Munteanu, and A. I. Bratcu, "Frequency-separation-based energy management control strategy of power flows within electric vehicles using ultracapacitors," in *IECON 2012-38th Annual Conference on IEEE Industrial Electronics Society*, 2012, pp. 2957-2964: IEEE.
- [145] K. J. Åström and T. Hägglund, *PID controllers: theory, design, and tuning*. Instrument society of America Research Triangle Park, NC, 1995.

**Chapter VI:**  
**Simulation Results and**  
**Discussion**

## VI.1. Introduction

The simulation results obtained during this analysis will be carried out using the models and control laws established in the previous chapters for the different elements of the electrical vehicle system. One of the objectives assigned to this work is the implementation of the energy management strategy described in Chapter 5 and also the stability of the DC bus, which is also analyzed from the point of view of voltage regulation.

## VI.2. Simulation results and discussion

In order to make a comparison in the same simulation setting, the results announced in this chapter are given as follows:

- ✓ Use the vehicle architecture chosen at the fourth chapter (Figure IV.9) and detailed in fifth chapter (Figure V.2).
- ✓ Considering the nominal vehicle output of 15 kW, the DC bus voltage is equivalent to 150 V and the converter power is equal to 20 kW.
- ✓ Using the model shown in Figure V.3; by selecting the real rolling cycle to have a wider range compared to the NEDC cycle (ECE15) [146] in the load current frequency domain (Figure.VI.1 et Figure.VI.2).
- ✓ Use a separation frequency value equivalent to  $T_f = 7.5$  s, depending on the frequency of analysis.

Figure VI.1 shows the varying driving conditions that require varying torque for the electric motor. It contains a typical variation of the load current,  $I_L$  taken from the DC bus [147]. It should be noted that its sign may change, especially in the event of a severe deceleration.

Figure VI.2 shows the frequency spectrum corresponding to the IFFT load current (Appendix. F). Its appearance suggests that the load current can be divided into two components in the frequency domain: a low-frequency component containing almost all the signal energy and a high-frequency component containing the dynamic residue.

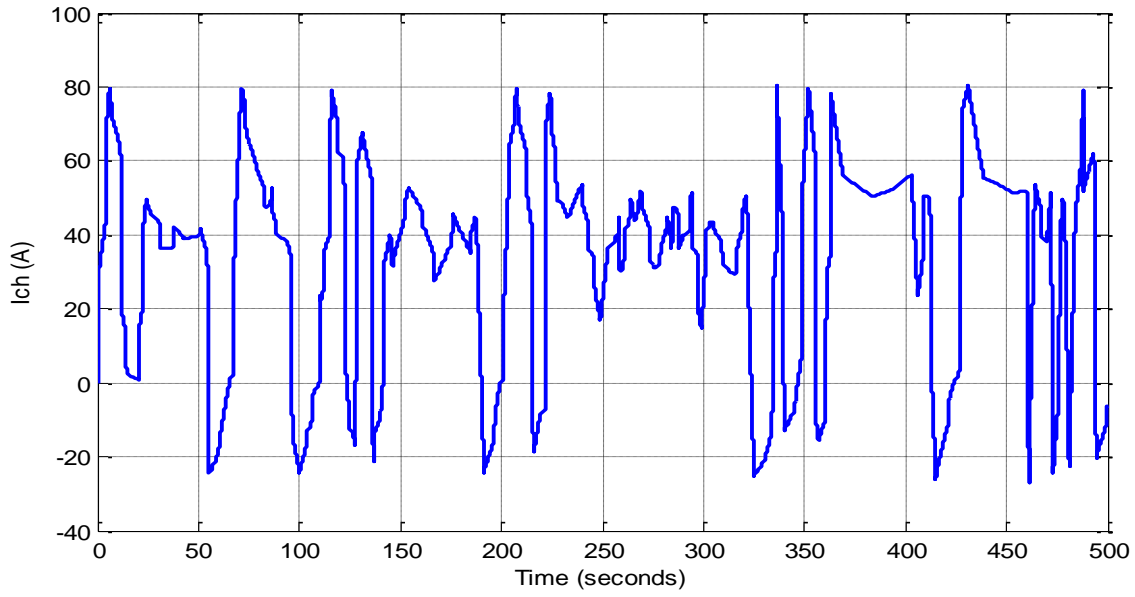


Figure.VI.1. Load Current

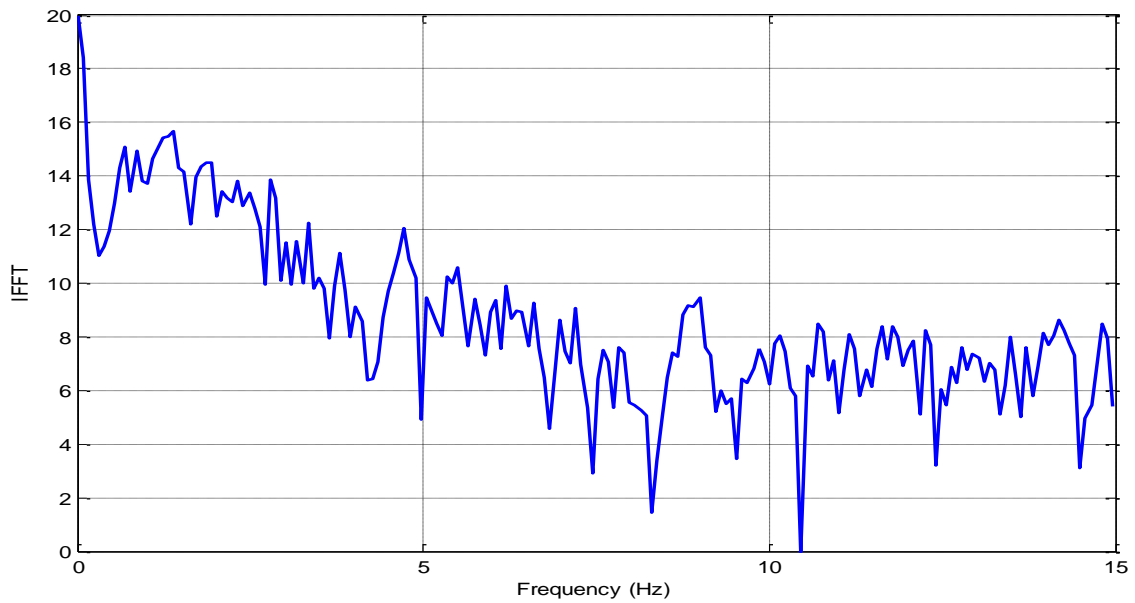


Figure.VI.2.  $I_{FF}$  of Load current

The Figure. VI.3. presents the current of the battery, supercapacitor and DC bus, we note that the current  $I_{bat}$ ,  $I_{sc}$  and  $I_{deref}$  varies depending on the current of the load.

In Figure VI.4 and VI.5, it is also noted that the current supplied by the battery varies depending on the frequency of separation and whether the supercapacitors supply or absorb the difference.

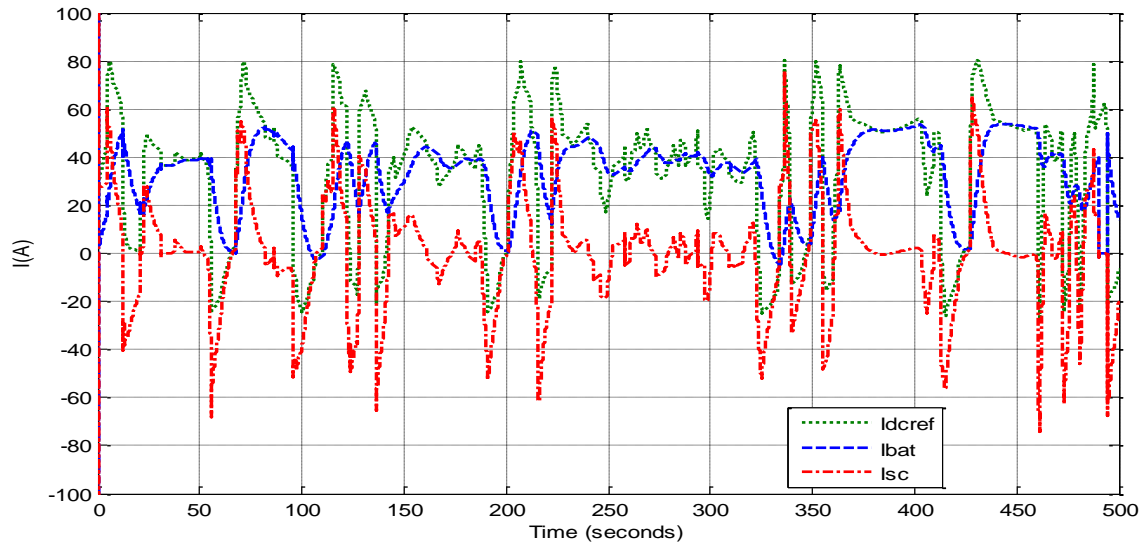


Figure. VI.3. Current of the battery, supercapacitor and DC bus

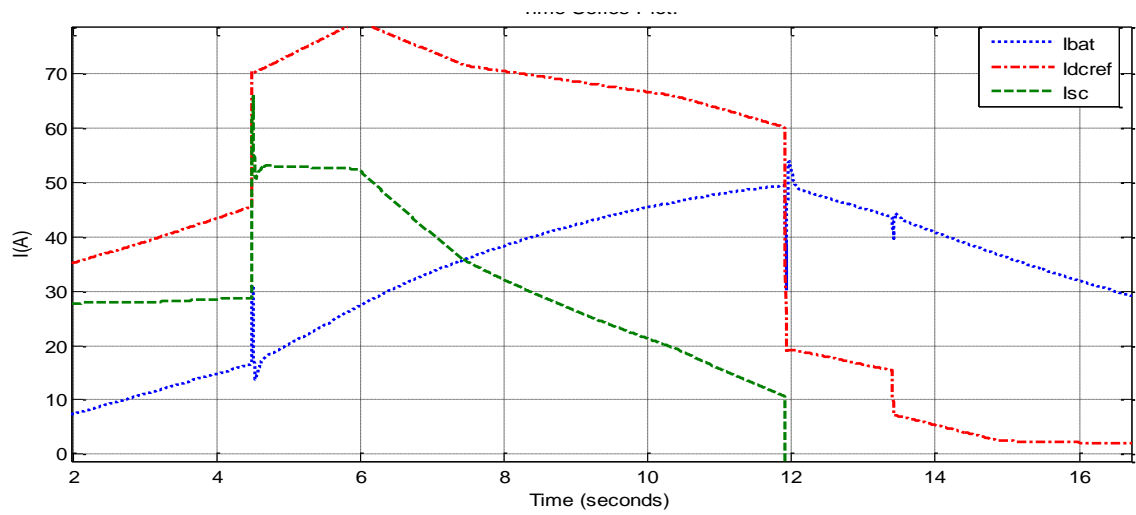


Figure. VI.4. Zoom.1 of Figure. VI.3

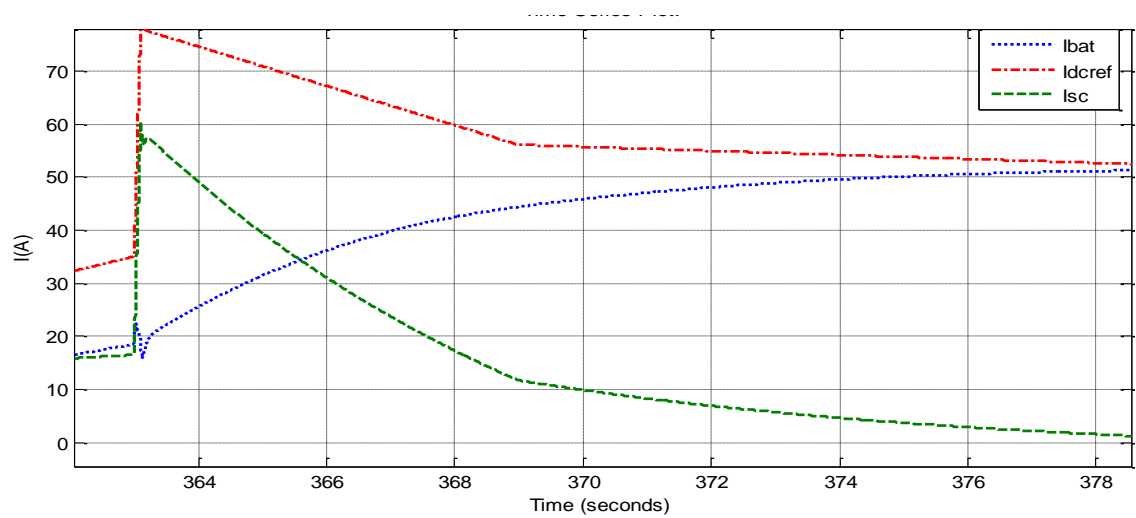


Figure. VI.5. Zoom.2 of Figure. VI.3

The Figure VI.6 is shown the DC bus voltage behavior during the operating cycle. As predicted, the voltage is maintained at its reference value ( $V_{DC}^* = 150 \text{ V}$ ) with fluctuations within the allowable limits ( $\pm 10 \text{ V}$ ).

Figure VI.7 and VI.8 indicate that the DC bus voltage is held within the allowable limits ( $\pm 10 \text{ V}$  V from the reference voltage,  $V_{DC}^*$ ). Note that the command coming from the DC bus regulator has a certain overshoot (less than 5%) but is still within its permissible limits. Device response time is less than 200 ms and completely meets the frequency range analysis.

Once we have the information on the output of the control system, we start with the effect of the separation frequency on the energy management of the vehicle,  $T = 7.5 \text{ s}$ . The current of the battery is smoothed, while the high frequency components are present in the current of the supercapacitor.

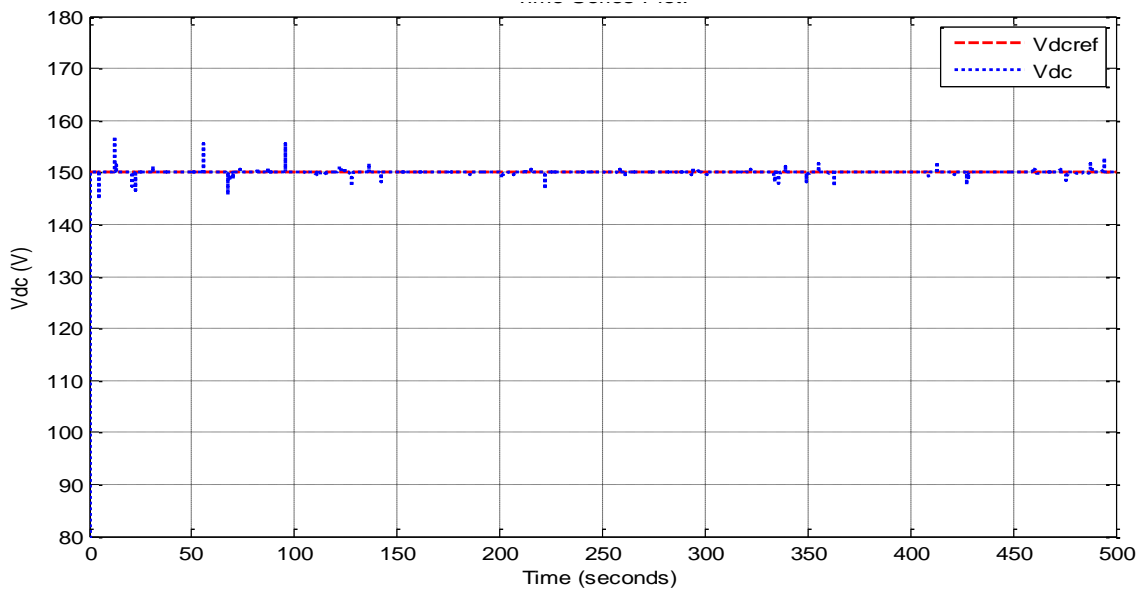


Figure. VI.6. the DC bus voltage and its reference

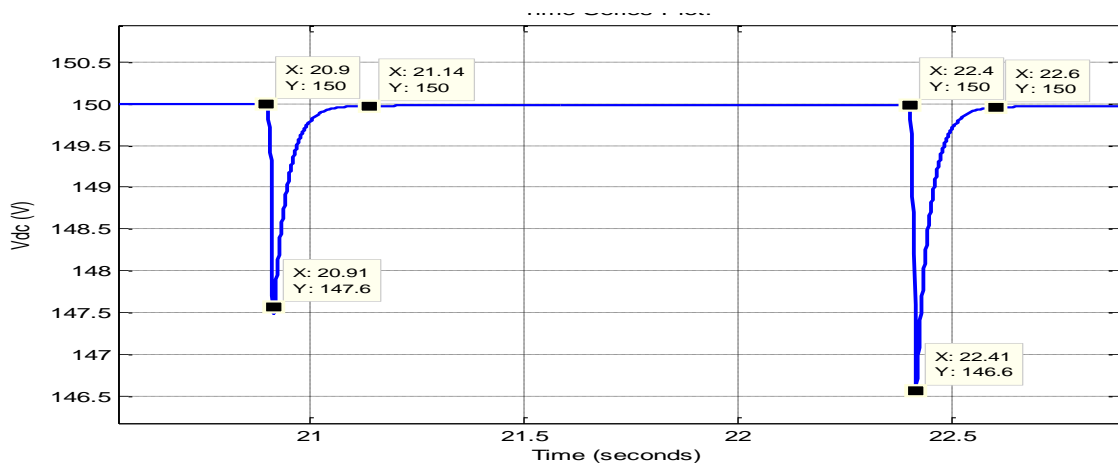


Figure. VI.7. Zoom.1 of Figure. VI.6

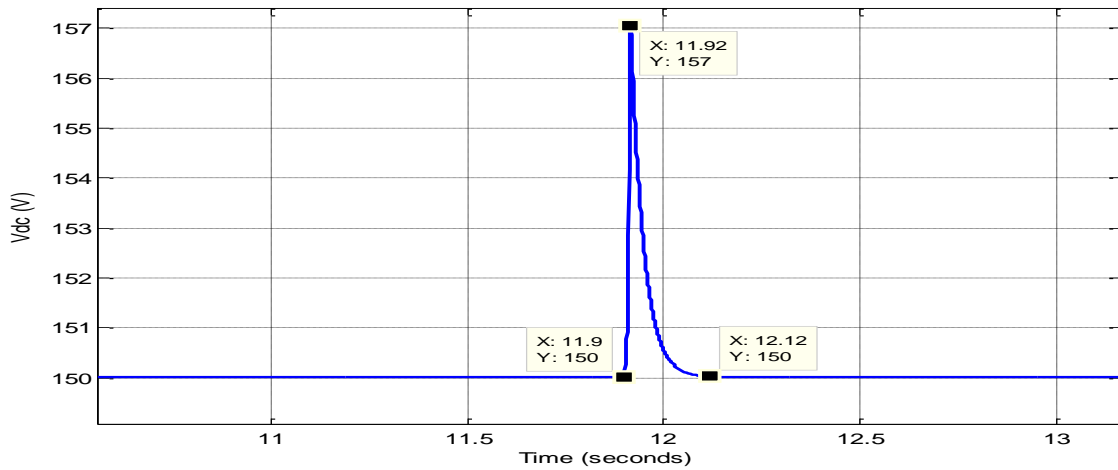


Figure. VI.8. Zoom.2 of Figure. VI.6

Figures VI.9 to VI.14 show the actions of the device as the load current differs depending on the actual task period (Figure VI.1) using the urban portion of the pipe used in real applications [147]. It should be noted that, with regard to the uniform cycle (EC15 [146] standard), the actual cycle is richer in high frequencies.

The negative values of  $I_L$  refer to the deceleration (electrical braking) during which the electric motor becomes a generator. As a result, the engine injects energy into the DC bus and the electrical energy sources are charged in this situation.

The Figure VI.9 and the Figure VI.10 respectively, indicate that the fluctuations of the battery current are low frequency, whereas the high frequency fluctuations of the load current ( $I_L$ ) is passed to the supercapacitor current.

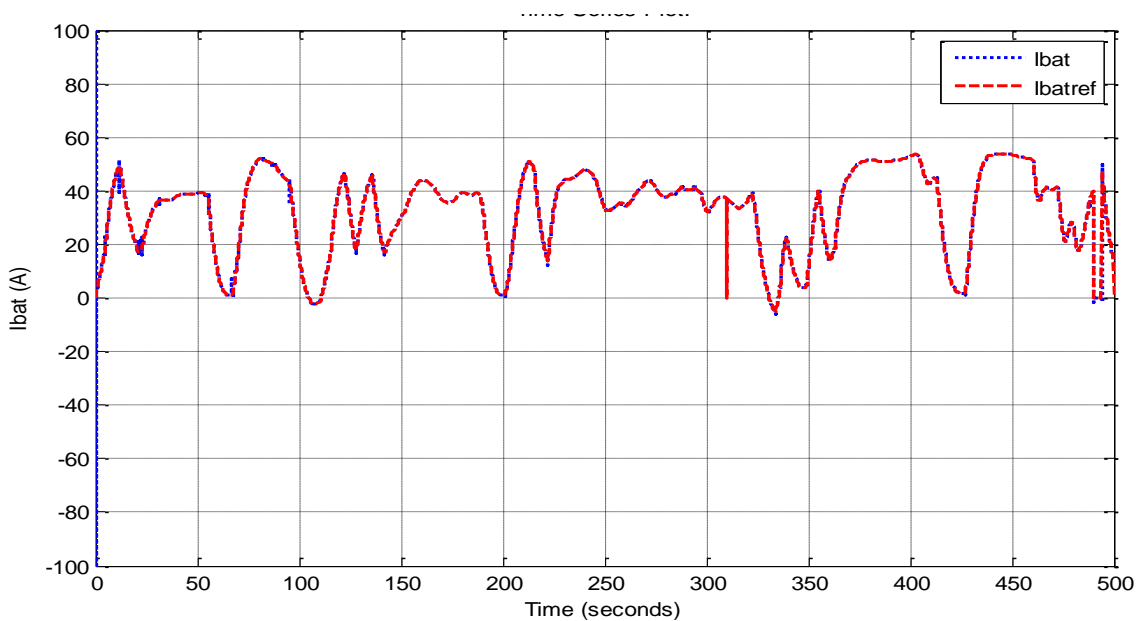


Figure.VI.9. The current of the battery and its reference

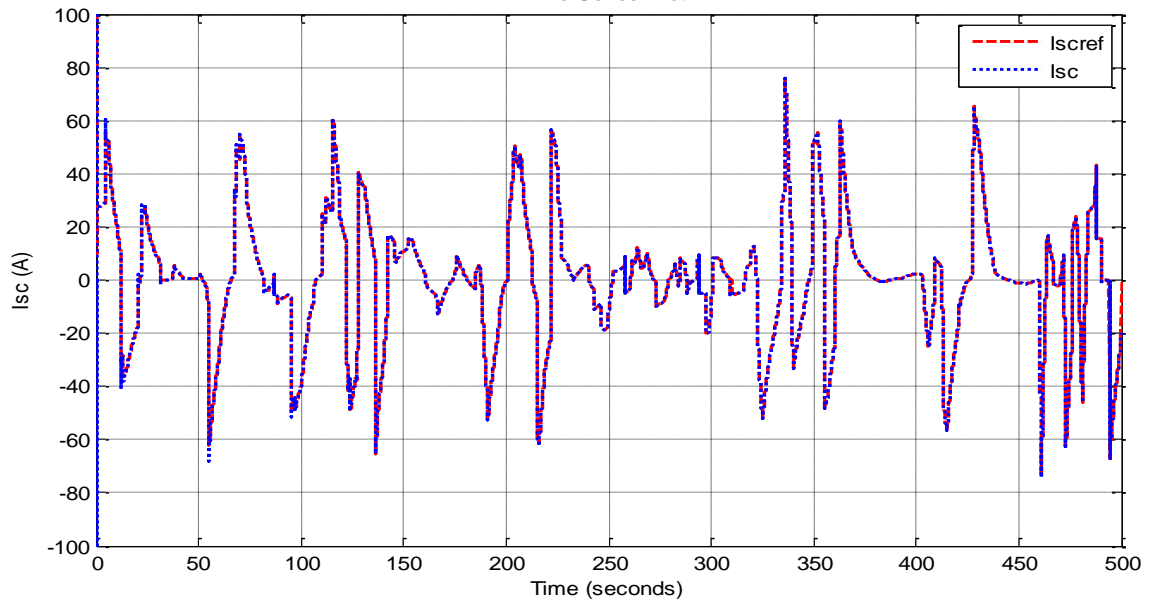


Figure. VI.10. The current of the supercapacitor and its reference

Battery voltage decreases slightly during acceleration (Figure VI.11). In addition, the voltage of the supercapacitor has broad variations (Figure VI.12) in response to the current being drawn/injected.

As can be shown, the values of both the battery voltage and the supercapacitor are different. Thus, according to the Equations scheme, the two duty cycles for the two power converters have different values (Figure VI.13 and Figure VI.14).

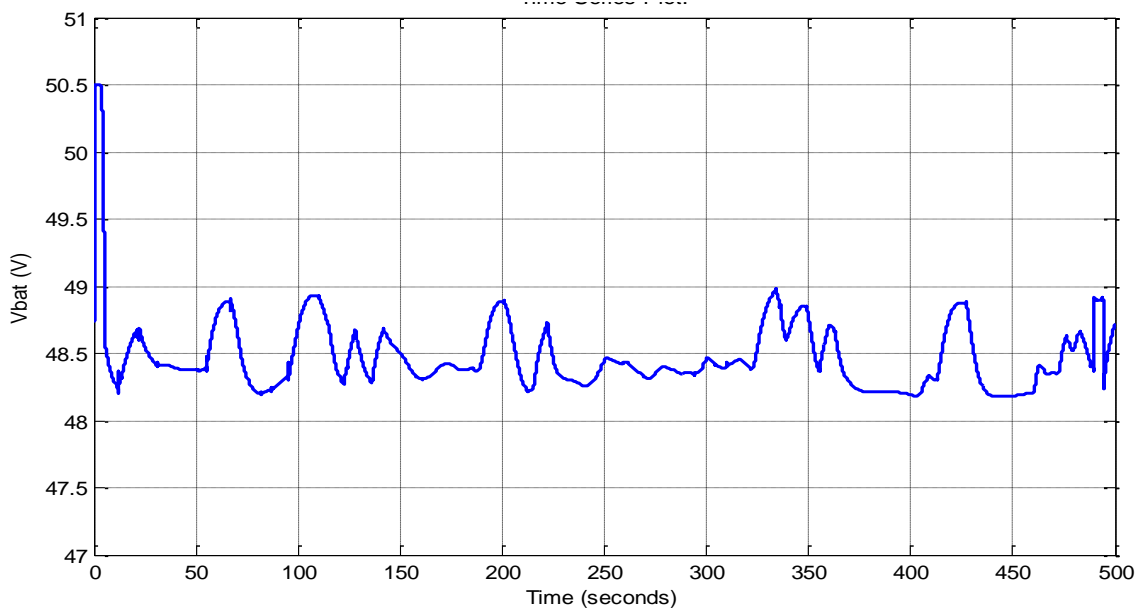


Figure. VI.11. Voltage of the battery

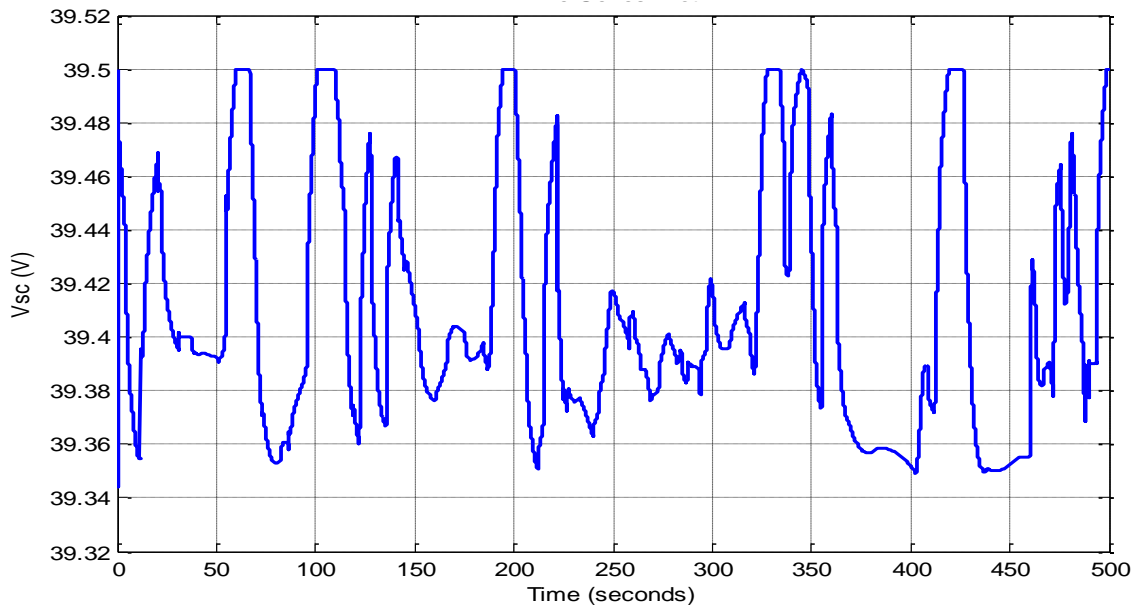


Figure. VI.12. Voltage of the supercapacitor

Analyzing Figure VI.13 and Figure VI.14 respectively indicate that the battery duty cycle varies about 0.66, while the supercapacitor duty cycle varies about 0.74 at the same time, this difference corresponds to the voltage variation of the supercapacitor (Figure VI.12) when the DC bus voltage is almost constant.

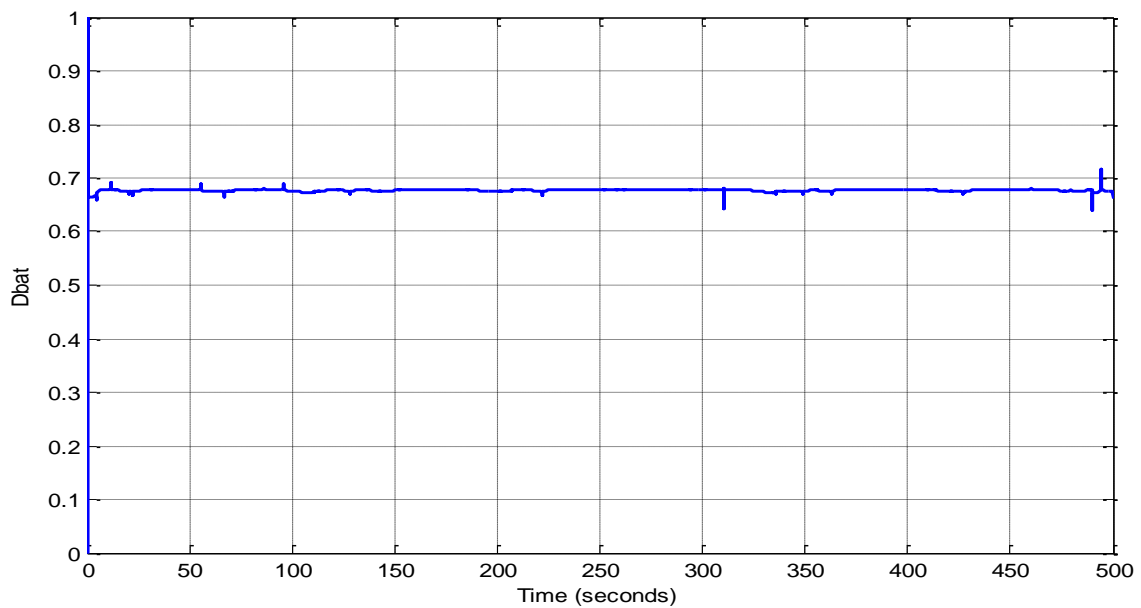


Figure. VI.13. Battery duty cycle

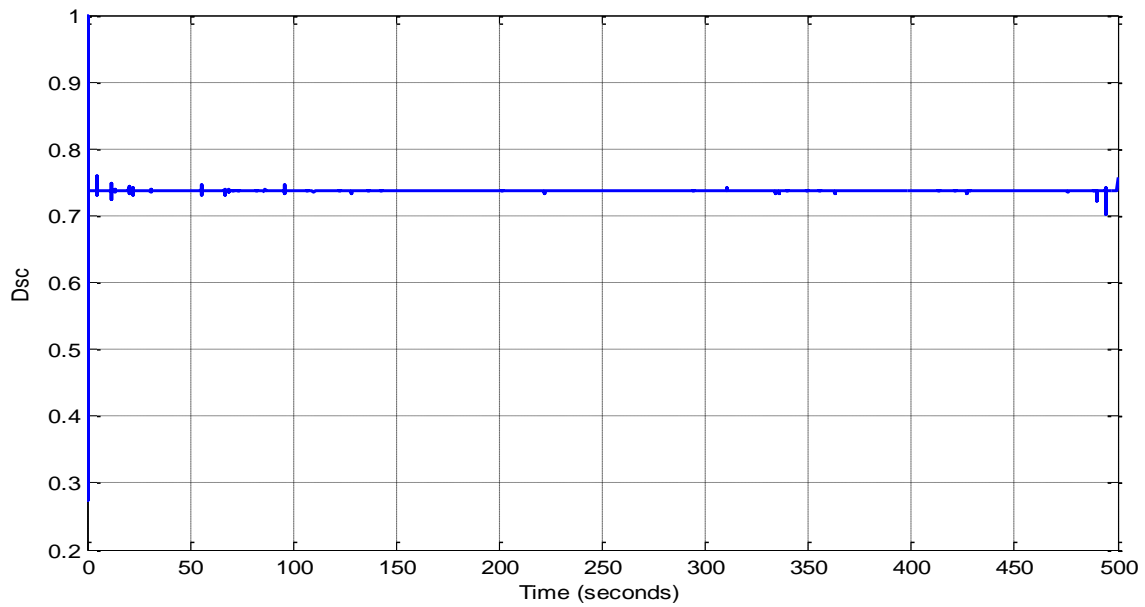


Figure. VI.14. Supercapacitor duty cycle

### VI.3. Choosing the frequency of separation

According to [148] the choice of the separation frequency depends on the rms value of the battery current, but taking into account the smallest value of the rms current of the battery according to the values of the separation frequency without neglecting the power sharing of the super capacity and, of course, its protection. According to the table above, the minimum value of the effective current of the battery corresponds to  $T_f = 15s$ , but at this value the voltage of the super capacitor varies greatly compared to  $T_f = 7.5s$  (see Figures VI.15 to VI.22) and the super capacity will be destroyed. In this case, the optimum value of the separation frequency is  $T_f = 7.5 s$ .

**Table.VI.1.** RMS value of the battery current corresponds to the different values of the separation frequency

$T_f$ (s)	0.4960	7.5	15
RMS(I <sub>bat</sub> ) (A)	42.5115	36.3606	34.3979

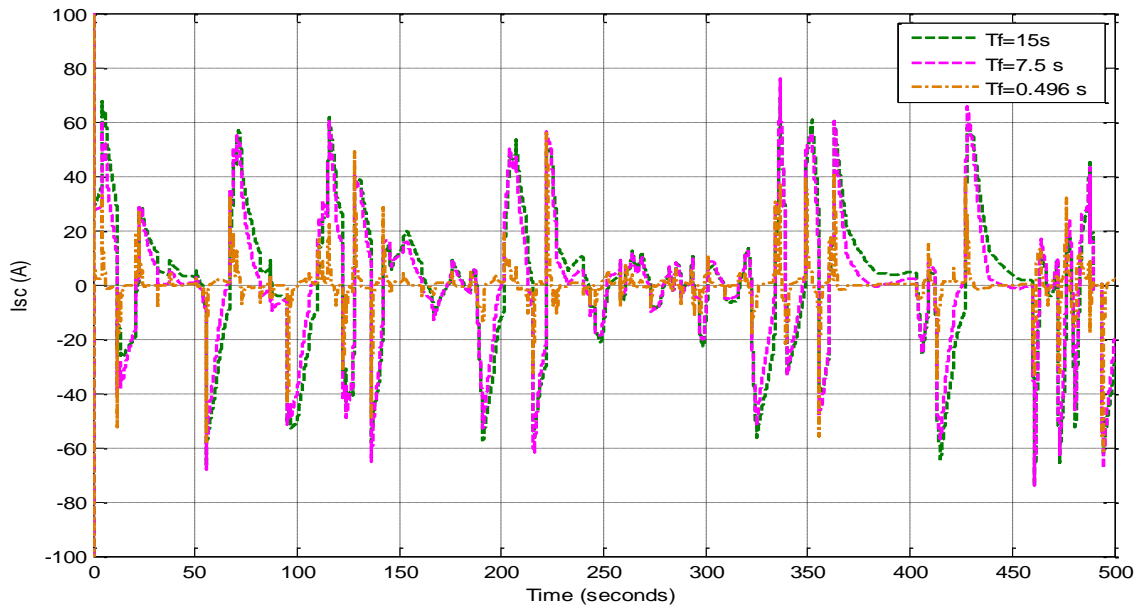


Figure. VI.15. The current of the supercapacitor

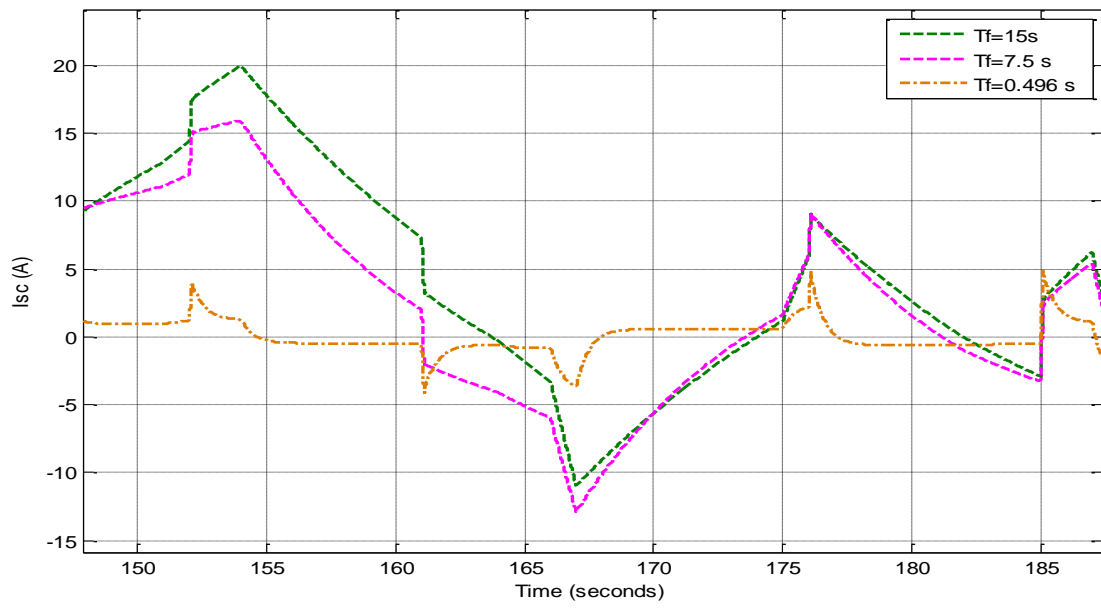


Figure. VI.16. Zoom of Figure. VI.15

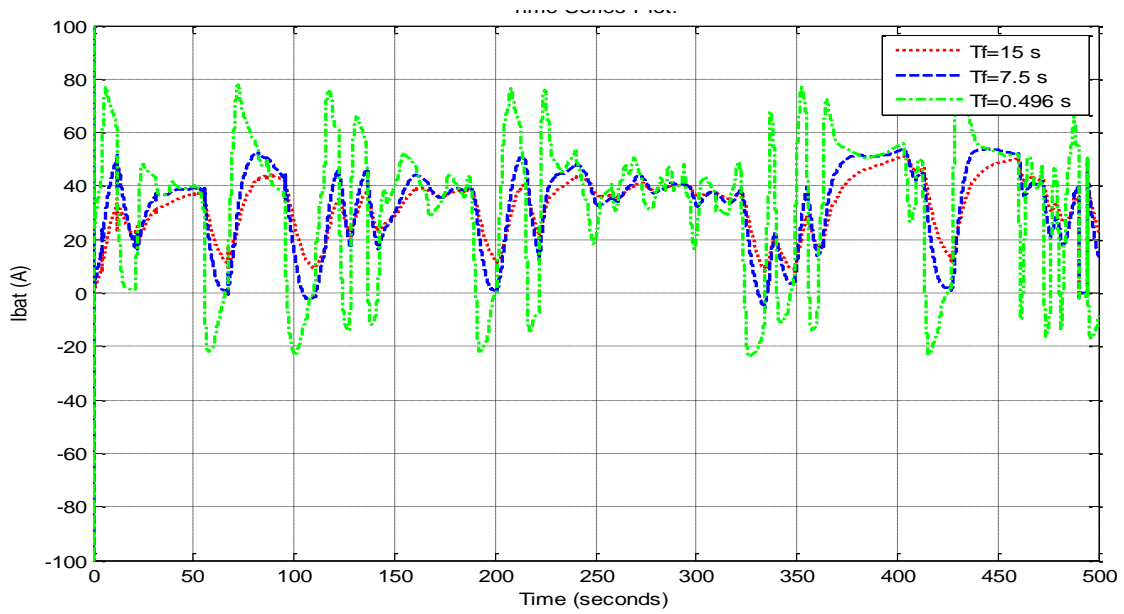


Figure. VI.17. The current of the battery

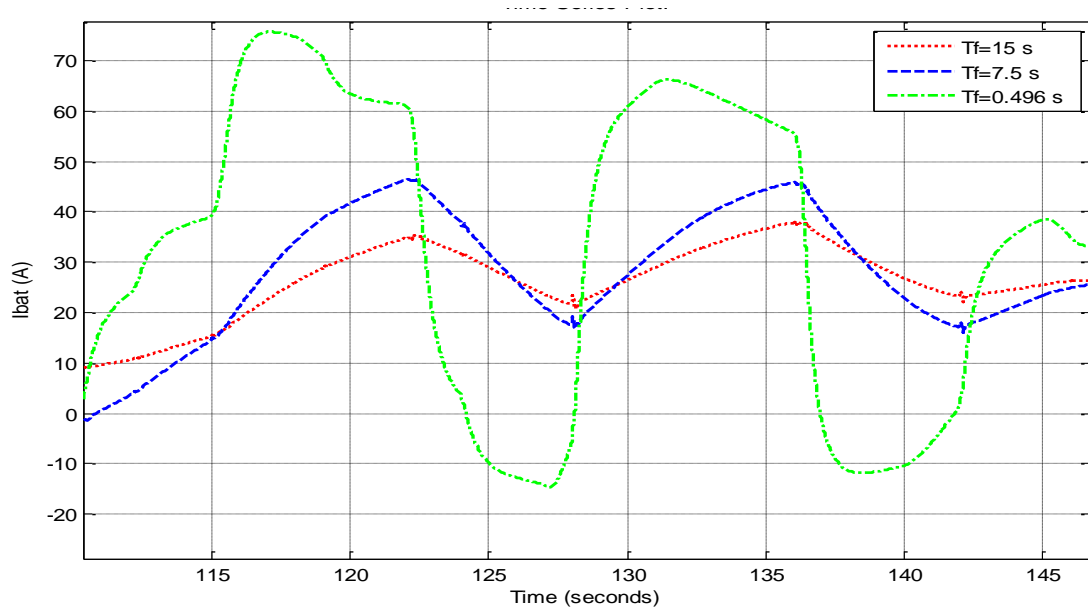


Figure. VI.18. Zoom of Figure. VI.17

Analyzing to Figure VI.15 and Figure VI.17 demonstrate the effect of the closed loop separation frequency of the device by presenting simulation results for different separation frequencies, i.e. corresponding to  $T = 0.496$  s, 7.5 s, and  $T = 15$  s respectively.

Note that for a separation frequency equal to  $F_{\max} = 1/T_{\min} = 1/0.496 = 2.016$  Hz, the batteries are often used, the supercapacitor being completely unused. The current of the battery comprises high-frequency elements. For a separation frequency of  $F_{\min} = 1/T_{\max} = 1/15 = 0.066$  Hz, the current in the supercapacitor is richer in high frequency and the stress in the battery decreases.

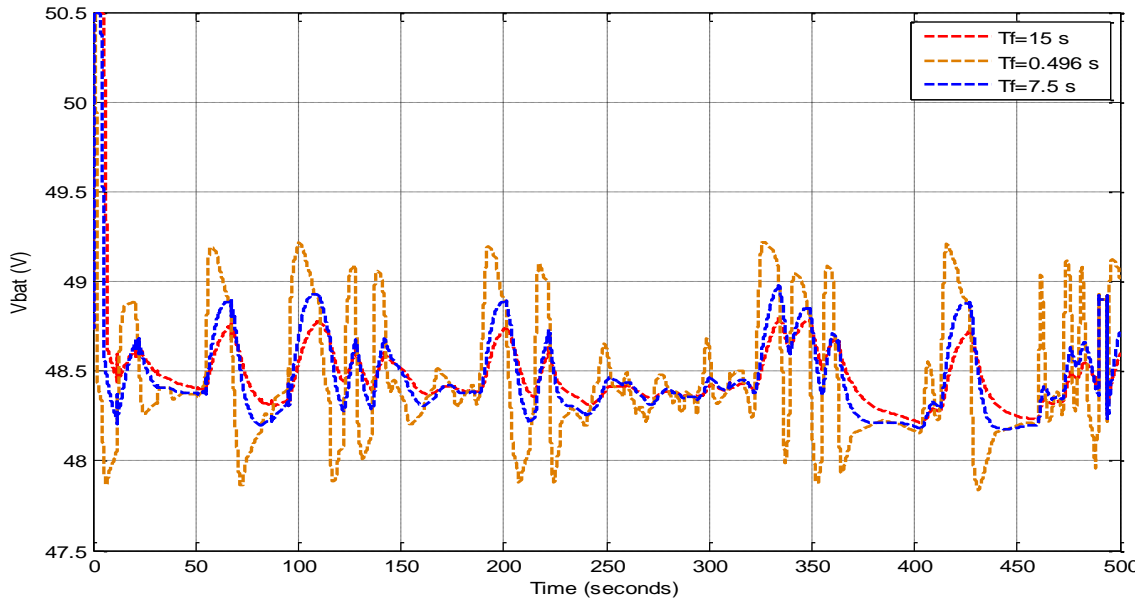


Figure. VI.19. The voltage of the battery

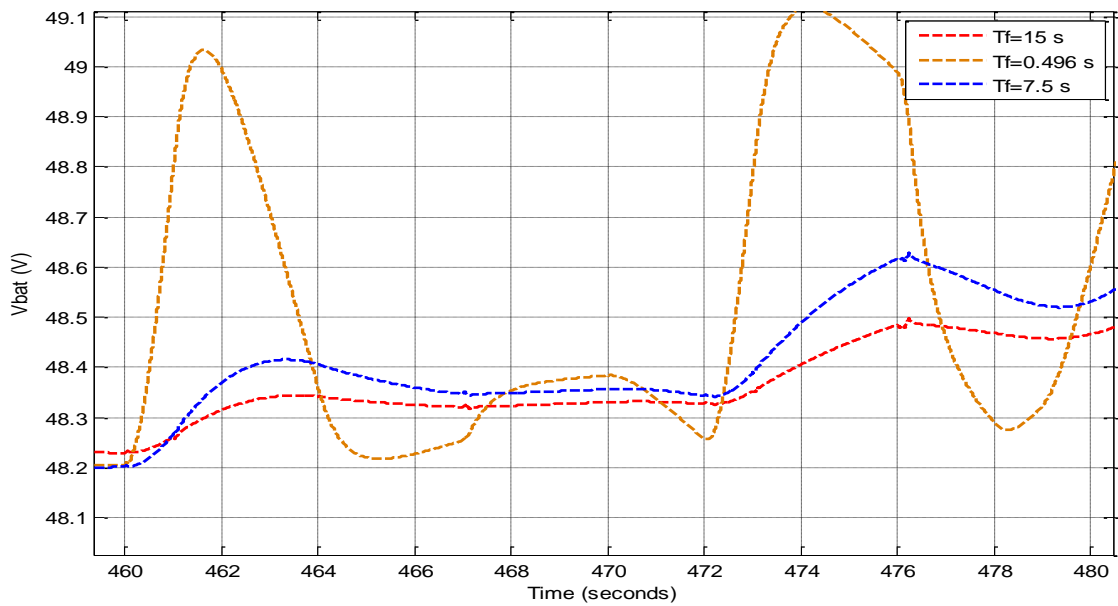


Figure. VI.20. Zoom of Figure. VI.19

Figures from VI.19 to VI.20 show that the range of variation of the battery voltage varies depending on the frequency of separation, so that the more the frequency of separation increases, the more this range increases, this shows that the long battery life is ensured at low frequency.

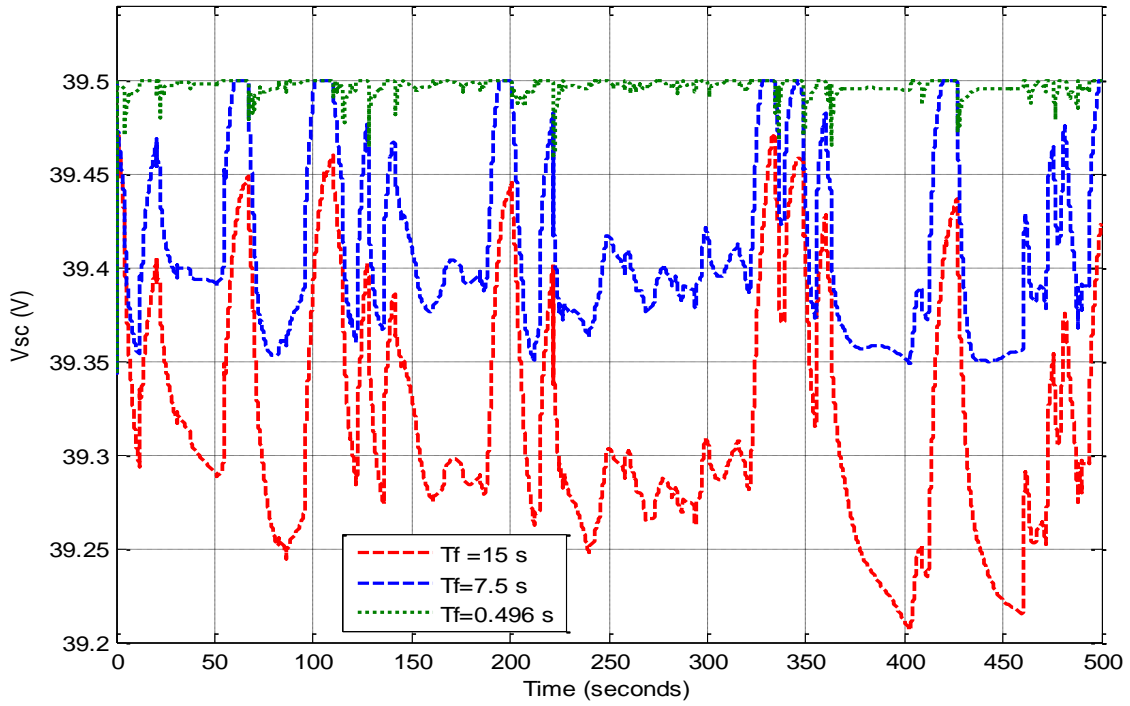


Figure. VI.21. The voltage of the supercapacitor

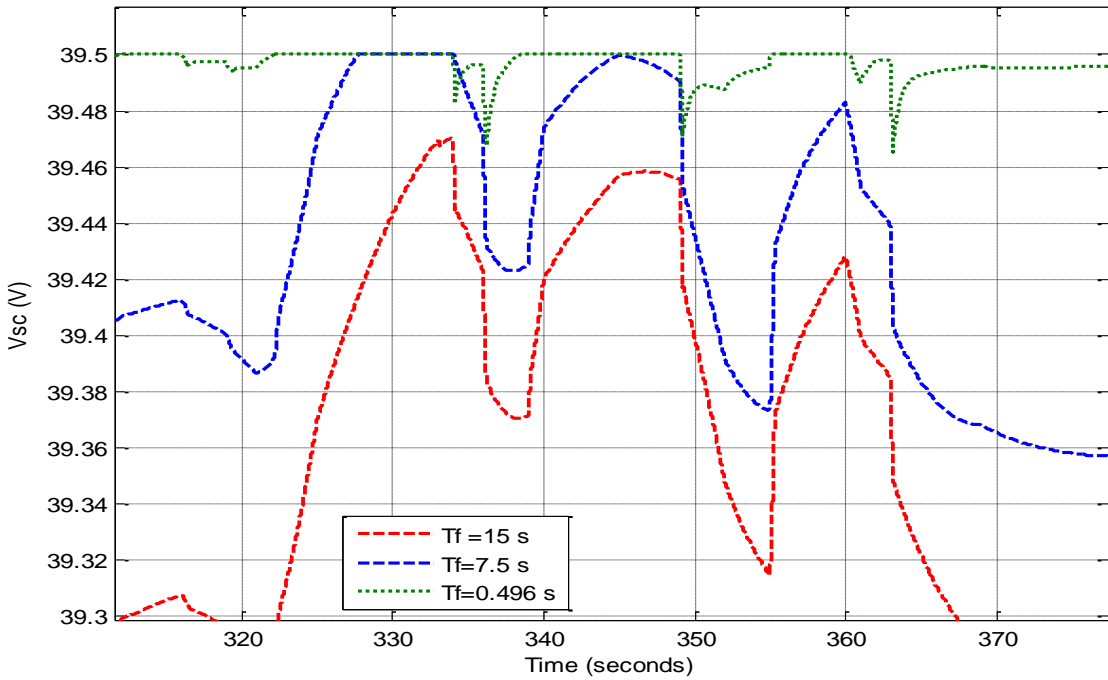


Figure. VI.22. Zoom of Figure. VI.21

Figures VI.21 and VI.22 shown that the super capacitor voltage range decreases when the frequency of separation increase, this is shows that the super capacitor is ensured at high frequency.

## VI.4. Conclusion

We addressed the energy management of an autonomous hybrid system in this chapter. The device consists of the lead acid battery pack considered to be the main source, and the supercapacitors used as auxiliary sources, not to mention the load modeled by the consumption profile. We conclude from the results obtained that:

- The hybrid source makes it possible to meet the power requirements of the load;
- The final stages of charging the batteries and the supercapacitors are acceptable for beginning other driving cycles. As a result, the life of the autonomous hybrid system will be improved.

The implementation of energy management using frequency separation has made it possible to use a simpler control structure that is easy to implement in a real vehicle while at the same time respecting to the constraints of the manufacturer.

## References

- [146] E.-L. Europa, "Communication de la Commission au Parlement européen, au Conseil, au Comité économique et social européen et au Comité des régions. Coopération renforcée contre les maladies à prévention vaccinale," ed, 2018.
- [147] M. Andre, "Real-world driving cycles for measuring cars pollutant emissions-Part A: The ARTEMIS European driving cycles," IFSTTAR-Institut Français des Sciences et Technologies des Transports, de l ..., 2009.
- [148] R. Abdelhedi, "Optimisation d'un système de stockage hybride de l'énergie électrique avec batterie et supercondensateurs pour véhicule électrique," Université de Lyon; Institut National des Sciences Appliquées et de ..., 2018.

# **General Conclusion**

## Conclusions and perspectives

The main objective of this thesis was to establish a battery charge estimator based on a series of charge / discharge tests in order to develop an accurate estimator. This estimate will depend on the battery technology, its electrical characteristics but also the ambient temperature. So, this information on the state of charge is used for energy management in an electric vehicle, in order to adapt the robust control of the motor converter.

A key element of the study was to set up a simulation project of the SOC estimation technique including coulomb counting with the use of the generic battery model. From the results we can conclude that:

- ✓ The model of the battery used in MATLAB Simulink is less accurate in charging mode. However, it is very accurate and has good behavior of the battery during the discharging mode at a constant current. This is why often found in the literature for this mode. Indeed, this mode is very important that the charge mode especially in hybrid/electric vehicles applications.
- ✓ The estimator of the state of charge of the battery by Coulomb Counting method is very accurate and is widely used in practice especially in embedded applications type hybrid/electric vehicles or renewable energy applications in the case of photovoltaic systems for example.
- ✓ The disadvantage of this technique is its inaccuracy and the difficulty to find the initial SOC. Also, it requires high-precision measurement instruments (voltage, current, and temperature sensor); therefore, we have to calibrate these devices periodically.
- ✓ Lead acid batteries are really suitable only for vehicles of short range. They remain the cheapest type of battery per unit of stored energy, and they are likely to continue to be widely used for those purposes. Very many useful EVs that don't need a long range can be made. So, by the simple calculation and simple hardware requirements, the proposed method can be easily implemented in all portable devices as well as electric vehicles.

Through this work, we addressed the energy management of an autonomous hybrid system. The device consists of the lead acid battery pack considered to be the main source, and the supercapacitors used as auxiliary sources, not to mention the load modeled by the consumption profile. We conclude from the results obtained that:

- ✚ The hybrid source makes it possible to meet the power requirements of the load;
- ✚ The final stages of charging the batteries and the supercapacitors are acceptable for beginning other driving cycles. As a result, the life of the autonomous hybrid system will be improved.

Simulations and application of the various energy conservation techniques applied to vehicle control systems have been carried out successfully. The implementation of energy management using frequency separation has made it possible to use a simpler control structure that is easy to implement in a real vehicle while at the same time respecting the constraints of the manufacturer.

In perspective, it would be interesting to:

- ✚ Work with batteries of other technologies (lithium)
- ✚ Test the technique used in real time
- ✚ Use other estimation techniques (Artificial Neural Network, Kalman Filter, ...)
- ✚ Use two combined techniques (Coulomb counting with OCV and Kalman Filter with OCV)
- ✚ Validate experimentally the simulation results of this energy management control approach with PI regulators.

# References

## The References

- [1] A. Devie, "Caractérisation de l'usage des batteries Lithium-ion dans les véhicules électriques et hybrides. Application à l'étude du vieillissement et de la fiabilité," 2012.
- [2] A. Lièvre, "Développement d'un système de gestion de batterie lithium-ion à destination de véhicules" mild hybrid": détermination des indicateurs d'état (SoC, SoH et SoF)," Université Claude Bernard-Lyon I, 2015.
- [3] A.-L. Allègre, A. Bouscayrol, and R. Trigui, "Flexible real-time control of a hybrid energy storage system for electric vehicles," IET Electrical Systems in Transportation, vol. 3, no. 3, pp. 79-85, 2013.
- [4] V. Pop, H. J. Bergveld, D. Danilov, P. P. Regtien, and P. H. Notten, Battery management systems: Accurate state-of-charge indication for battery-powered applications. Springer Science & Business Media, 2008.
- [5] H. Dreer, "Curtis wheelchair battery fuel gauge Product Test Report Marketing Services Dept., Curtis Instruments," ed: Inc, 1984.
- [6] J. Kauzlarich, "Electric wheelchair fuel gauge tests," Report N° UVA-REC-102-86. UVA Rehabilitation Engineering Center, 1986.
- [7] J. S. Martinez, D. Hissel, M.-C. Péra, and M. Amiet, "Practical control structure and energy management of a testbed hybrid electric vehicle," IEEE Transactions on Vehicular Technology, vol. 60, no. 9, pp. 4139-4152, 2011.
- [8] E. P. Finger and E. A. Sands, "Method and apparatus for measuring the state of charge of a battery by monitoring reductions in voltage," ed: Google Patents, 1980.
- [9] S. Lerner, H. Lennon, and H. Seiger, "Development of an alkaline battery state of charge indicator," Power Sources, vol. 3, pp. 135-7, 1970.
- [10] V. Pop, H. J. Bergveld, D. Danilov, P. P. Regtien, and P. H. Notten, "State-of-the-art of battery state-of-charge determination," Battery Management Systems: Accurate State-of-Charge Indication for Battery-Powered Applications, pp. 11-45, 2008.
- [11] R. Brandwein and M. L. Gupta, "Nickel-cadmium battery monitor," ed: Google Patents, 1976.
- [12] C. C. Christianson and R. F. Bourke, "Battery state of charge gauge," ed: Google Patents, 1976.
- [13] S. Rodrigues, N. Munichandraiah, and A. Shukla, "A review of state-of-charge indication of batteries by means of ac impedance measurements," Journal of power Sources, vol. 87, no. 1-2, pp. 12-20, 2000.
- [14] E. Peled, H. Yamin, I. Reshef, D. Kelrich, and S. Rozen, "Method and apparatus for determining the state-of-charge of batteries particularly lithium batteries," ed: Google Patents, 1988.
- [15] J. H. Aylor, A. Thieme, and B. Johnso, "A battery state-of-charge indicator for electric wheelchairs," IEEE transactions on industrial electronics, vol. 39, no. 5, pp. 398-409, 1992.

- [16] G. Richter and E. Meissner, "Method for determining the state of charge of storage batteries," ed: Google Patents, 2002.
- [17] O. Gérard, J.-N. Patillon, and F. d'Alché-Buc, "Neural network adaptive modeling of battery discharge behavior," in International Conference on Artificial Neural Networks, 1997, pp. 1095-1100: Springer.
- [18] J. Garche and A. Jossen, "Battery management systems (BMS) for increasing battery life time," in TELESCON 2000. Third International Telecommunications Energy Special Conference (IEEE Cat. No. 00EX424), 2000, pp. 81-88: IEEE.
- [19] H. Feil, H. J. Bergveld, and J. R. G. C. M. Van, "Method of predicting the state of charge as well as the use time left of a rechargeable battery," ed: Google Patents, 2003.
- [20] H. J. Bergveld, W. S. Kruijt, and P. H. Notten, "Battery management systems," in Battery Management Systems: Springer, 2002, pp. 9-30.
- [21] M. W. Verbrugge, E. D. Tate Jr, S. D. Sarbacker, and B. J. Koch, "Quasi-adaptive method for determining a battery's state of charge," ed: Google Patents, 2002.
- [22] B. A. Johnson and R. E. White, "Characterization of commercially available lithium-ion batteries," *Journal of power sources*, vol. 70, no. 1, pp. 48-54, 1998.
- [23] R. Xiong, J. Cao, Q. Yu, H. He, and F. Sun, "Critical review on the battery state of charge estimation methods for electric vehicles," *Ieee Access*, vol. 6, pp. 1832-1843, 2017.
- [24] D. Andre, M. Meiler, K. Steiner, H. Walz, T. Soczka-Guth, and D. Sauer, "Characterization of high-power lithium-ion batteries by electrochemical impedance spectroscopy. II: Modelling," *Journal of Power Sources*, vol. 196, no. 12, pp. 5349-5356, 2011.
- [25] H. He, R. Xiong, and H. Guo, "Online estimation of model parameters and state-of-charge of LiFePO<sub>4</sub> batteries in electric vehicles," *Applied Energy*, vol. 89, no. 1, pp. 413-420, 2012.
- [26] Y. Zhang, W. Song, S. Lin, and Z. Feng, "A novel model of the initial state of charge estimation for LiFePO<sub>4</sub> batteries," *Journal of Power Sources*, vol. 248, pp. 1028-1033, 2014.
- [27] G. L. Plett, "Sigma-point Kalman filtering for battery management systems of LiPB-based HEV battery packs: Part 1: Introduction and state estimation," *Journal of Power Sources*, vol. 161, no. 2, pp. 1356-1368, 2006.
- [28] R. Xiong, H. He, F. Sun, and K. Zhao, "Evaluation on state of charge estimation of batteries with adaptive extended Kalman filter by experiment approach," *IEEE Transactions on Vehicular Technology*, vol. 62, no. 1, pp. 108-117, 2012.
- [29] Y. Zhang, R. Xiong, H. He, and W. Shen, "Lithium-ion battery pack state of charge and state of energy estimation algorithms using a hardware-in-the-loop validation," *IEEE Transactions on Power Electronics*, vol. 32, no. 6, pp. 4421-4431, 2016.
- [30] L. Kang, X. Zhao, and J. Ma, "A new neural network model for the state-of-charge estimation in the battery degradation process," *Applied Energy*, vol. 121, pp. 20-27, 2014.

- [31] W. He, N. Williard, C. Chen, and M. Pecht, "State of charge estimation for Li-ion batteries using neural network modeling and unscented Kalman filter-based error cancellation," *International Journal of Electrical Power & Energy Systems*, vol. 62, pp. 783-791, 2014.
- [32] E. Chemali, P. J. Kollmeyer, M. Preindl, R. Ahmed, and A. Emadi, "Long short-term memory networks for accurate state-of-charge estimation of Li-ion batteries," *IEEE Transactions on Industrial Electronics*, vol. 65, no. 8, pp. 6730-6739, 2017.
- [33] C. Lin, H. Mu, R. Xiong, and W. Shen, "A novel multi-model probability battery state of charge estimation approach for electric vehicles using H-infinity algorithm," *Applied Energy*, vol. 166, pp. 76-83, 2016.
- [34] S. Boschert, *Plug-in hybrids: The cars that will recharge America*. New Society Publishers, 2006.
- [35] S. Al-Hallaj and J. R. Selman, "Thermal modeling of secondary lithium batteries for electric vehicle/hybrid electric vehicle applications," *Journal of power sources*, vol. 110, no. 2, pp. 341-348, 2002.
- [36] D. H. Doughty, P. C. Butler, A. A. Akhil, N. H. Clark, and J. D. Boyes, "Batteries for large-scale stationary electrical energy storage," *The Electrochemical Society Interface*, vol. 19, no. 3, pp. 49-53, 2010.
- [37] Y. Onoda, "Development of a large-sized, long-life, valve-regulated lead-acid battery," *Journal of power sources*, vol. 88, no. 1, pp. 101-107, 2000.
- [38] J. Jiang and C. Zhang, *Fundamentals and applications of lithium-ion batteries in electric drive vehicles*. John Wiley & Sons, 2015.
- [39] C. Glaize and S. Genies, *Lithium batteries and other electrochemical storage systems*. Wiley Online Library, 2013.
- [40] R. Korthauer, "Areas of activity on the fringe of lithium-ion battery development, production, and recycling," in *Lithium-Ion Batteries: Basics and Applications*: Springer, 2018, pp. 249-251.
- [41] M. E. Spahr et al., "Purely hexagonal graphite and the influence of surface modifications on its electrochemical lithium insertion properties," *Journal of The Electrochemical Society*, vol. 149, no. 8, pp. A960-A966, 2002.
- [42] J. Garche, C. K. Dyer, P. T. Moseley, Z. Ogumi, D. A. Rand, and B. Scrosati, *Encyclopedia of electrochemical power sources*. Newnes, 2013.
- [43] D. Pavlov, *Lead-acid batteries: science and technology*. Elsevier, 2011.
- [44] D. Linden, "Reddy TB handbook of batteries," ed: The McGraw-Hill Companies, Inc., New York, 2002.
- [45] T. Ikeya et al., "Multi-step constant-current charging method for an electric vehicle nickel/metal hydride battery with high-energy efficiency and long cycle life," *Journal of power sources*, vol. 105, no. 1, pp. 6-12, 2002.
- [46] C.-L. Liu, S.-C. Wang, Y.-H. Liu, and M.-C. Tsai, "An optimum fast charging pattern search for Li-ion batteries using particle swarm optimization," in *The 6th International Conference on Soft Computing and Intelligent Systems, and The 13th International Symposium on Advanced Intelligence Systems*, 2012, pp. 727-732: IEEE.

- [47] Y.-H. Liu, C.-H. Hsieh, and Y.-F. Luo, "Search for an optimal five-step charging pattern for Li-ion batteries using consecutive orthogonal arrays," *IEEE Transactions on Energy Conversion*, vol. 26, no. 2, pp. 654-661, 2011.
- [48] P. H. Notten, J. O. het Veld, and J. Van Beek, "Boostcharging Li-ion batteries: A challenging new charging concept," *Journal of Power Sources*, vol. 145, no. 1, pp. 89-94, 2005.
- [49] C.-H. Lin et al., "Fast charging technique for Li-Ion battery charger," in *2008 15th IEEE International Conference on Electronics, Circuits and Systems*, 2008, pp. 618-621: IEEE.
- [50] L.-R. Chen, "Design of duty-varied voltage pulse charger for improving Li-ion battery-charging response," *IEEE Transactions on Industrial Electronics*, vol. 56, no. 2, pp. 480-487, 2008.
- [51] T. T. Vo, X. Chen, W. Shen, and A. Kapoor, "New charging strategy for lithium-ion batteries based on the integration of Taguchi method and state of charge estimation," *Journal of Power Sources*, vol. 273, pp. 413-422, 2015.
- [52] L.-R. Chen, S.-L. Wu, T.-R. Chen, W.-R. Yang, C.-S. Wang, and P.-C. Chen, "Detecting of optimal Li-ion battery charging frequency by using AC impedance technique," in *2009 4th IEEE Conference on Industrial Electronics and Applications*, 2009, pp. 3378-3381: IEEE.
- [53] L.-R. Chen, S.-L. Wu, D.-T. Shieh, and T.-R. Chen, "Sinusoidal-ripple-current charging strategy and optimal charging frequency study for Li-ion batteries," *IEEE Transactions on Industrial Electronics*, vol. 60, no. 1, pp. 88-97, 2012.
- [54] Q. Gong, "Modeling study of a vehicle traction battery model," *Chinese LABAT Man*, vol. 42, no. 2, p. 76, 2005.
- [55] M. Ceraolo, "New dynamical models of lead-acid batteries," *IEEE transactions on Power Systems*, vol. 15, no. 4, pp. 1184-1190, 2000.
- [56] F. M. González-Longatt, "Circuit based battery models: A review," in *Congreso Iberoamericano de estudiantes De Ingenieria Electrica. Cibelec*, 2006.
- [57] H. Fakham, D. Lu, and B. Francois, "Power control design of a battery charger in a hybrid active PV generator for load-following applications," *IEEE Transactions on Industrial Electronics*, vol. 58, no. 1, pp. 85-94, 2010.
- [58] V. Johnson, "Battery performance models in ADVISOR," *Journal of power sources*, vol. 110, no. 2, pp. 321-329, 2002.
- [59] B. A. Manual, "Gates Energy Products," Inc., Gainesville, FL, 1989.
- [60] J. P. Christophersen et al., "DOE Advanced technology development program for lithium-ion batteries: INEEL Interim report for Gen 2 cycle-life testing," 9: INEEL/EXT-02-01055, 2002.
- [61] S. Wu, R. Xiong, H. Li, V. Nian, and S. Ma, "The state of the art on preheating lithium-ion batteries in cold weather," *Journal of Energy Storage*, vol. 27, p. 101059, 2020.
- [62] J. Huang, Z. Li, B. Y. Liaw, and J. Zhang, "Graphical analysis of electrochemical impedance spectroscopy data in Bode and Nyquist representations," *Journal of Power Sources*, vol. 309, pp. 82-98, 2016.

- [63] B. Wang, Z. Liu, S. E. Li, S. J. Moura, and H. Peng, "State-of-charge estimation for lithium-ion batteries based on a nonlinear fractional model," *IEEE Transactions on Control Systems Technology*, vol. 25, no. 1, pp. 3-11, 2016.
- [64] R. Yang, R. Xiong, H. He, and Z. Chen, "A fractional-order model-based battery external short circuit fault diagnosis approach for all-climate electric vehicles application," *Journal of cleaner production*, vol. 187, pp. 950-959, 2018.
- [65] I. Petráš, *Fractional-order nonlinear systems: modeling, analysis and simulation*. Springer Science & Business Media, 2011.
- [66] G. R. Dahlin and K. E. Strøm, *Lithium batteries: research, technology, and applications*. Nova Science Publishers, 2010.
- [67] M. Faizan, "Synthesis and Characterization of Lead based Anodic Electrode for Lead Acid Batteries," Department of Physics, COMSATS University Islamabad, Lahore campus, 2019.
- [68] D. Doerffel and S. A. Sharkh, "A critical review of using the Peukert equation for determining the remaining capacity of lead-acid and lithium-ion batteries," *Journal of power sources*, vol. 155, no. 2, pp. 395-400, 2006.
- [69] G. Albright, J. Edie, and S. Al-Hallaj, "A comparison of lead acid to lithium-ion in stationary storage applications," Published by AllCell Technologies LLC, 2012.
- [70] H. Chang and H. Wu, "Graphene-based nanocomposites: preparation, functionalization, and energy and environmental applications," *Energy & Environmental Science*, vol. 6, no. 12, pp. 3483-3507, 2013.
- [71] H. Keshan, J. Thornburg, and T. S. Ustun, "Comparison of lead-acid and lithium ion batteries for stationary storage in off-grid energy systems," 2016.
- [72] E. M. Krieger, J. Cannarella, and C. B. Arnold, "A comparison of lead-acid and lithium-based battery behavior and capacity fade in off-grid renewable charging applications," *Energy*, vol. 60, pp. 492-500, 2013.
- [73] B. Zine, K. Marouani, M. Becherif, and S. Yahmedi, "Estimation of battery SOC for hybrid electric vehicle using coulomb counting method," *International Journal of Emerging Electric Power Systems*, vol. 19, no. 2, 2018.
- [74] D. DinhVinh, "Lithium-Ion batteries diagnosis in embedded applications," ThesisforobtainingthedegreeofdoctorofCompiegneUniversityof TechnologyinInformationTechnologyandSystems, 2010.
- [75] X. Hu, F. Sun, and Y. Zou, "Estimation of state of charge of a lithium-ion battery pack for electric vehicles using an adaptive Luenberger observer," *Energies*, vol. 3, no. 9, pp. 1586-1603, 2010.
- [76] D. Lindner and F. Niedermayr, "Report for work package 6," ed: FRAUNHOFER-ITALIA, 2014.
- [77] K. S. Ng, C.-S. Moo, Y.-P. Chen, and Y.-C. Hsieh, "Enhanced coulomb counting method for estimating state-of-charge and state-of-health of lithium-ion batteries," *Applied energy*, vol. 86, no. 9, pp. 1506-1511, 2009.

- [78] F. Feng, R. Lu, and C. Zhu, "A combined state of charge estimation method for lithium-ion batteries used in a wide ambient temperature range," *Energies*, vol. 7, no. 5, pp. 3004-3032, 2014.
- [79] P. Vyroubal, J. Maxa, and T. Kazda, "Simulation of the behavior of the lithium ion battery," *Advances in Military Technology*, vol. 9, no. 1, pp. 107-115, 2014.
- [80] V. Pop, H. J. Bergveld, D. Danilov, P. P. Regtien, and P. H. Notten, *Battery management systems: Accurate state-of-charge indication for battery-powered applications*. Springer Science & Business Media, 2008.
- [81] O. Tremblay and L.-A. Dessaint, "Experimental validation of a battery dynamic model for EV applications," *World electric vehicle journal*, vol. 3, no. 2, pp. 289-298, 2009.
- [82] S. Wijewardana, "New Dynamic Battery Model for Hybrid Vehicles and Dynamic Model Analysis Using Simulink," *Engineer: Journal of the Institution of Engineers, Sri Lanka*, vol. 47, no. 4, 2014.
- [83] E. M. Allam, "Study vehicle battery simulation and monitoring system," *American Journal of Modeling and Optimization*, vol. 3, no. 2, pp. 40-49, 2015.
- [84] H. Alloui, M. Becherif, and K. Marouani, "Modelling and frequency separation energy management of fuel cell-battery hybrid sources system for hybrid electric vehicle," in *21st Mediterranean Conference on Control and Automation*, 2013, pp. 646-651: IEEE.
- [85] M. Becherif, F. Claude, T. Hervier, and L. Boulon, "Multi-stack fuel cells powering a vehicle," *Energy procedia*, vol. 74, pp. 308-319, 2015.
- [86] M. Becherif, M. Ayad, D. Hissel, and R. Mkahl, "Design and sizing of a stand-alone recharging point for battery electrical vehicles using photovoltaic energy," in *2011 IEEE Vehicle Power and Propulsion Conference*, 2011, pp. 1-6: IEEE.
- [87] S. Melentjev and D. Lebedev, "Overview of simplified mathematical models of batteries," in *13th International Symposium" Topical problems of education in the field of electrical and power engineering".-Doctoral school of energy and geotechnology: Parnu, Estonia*, 2013, pp. 231-235.
- [88] J. Labbé, "L'Hydrogène électrolytique comme moyen de stockage d'électricité pour systèmes photovoltaïques isolés," 2006.
- [89] P. Thounthong, "Conception d'une source hybride utilisant une pile à combustible et des supercondensateurs," 2005.
- [90] H. Maker, "Optimisation et gestion d'énergie pour un système hybride: association Pile à Combustible et Supercondensateurs," Besançon, 2008.
- [91] D. Paire, M. G. Simoes, J. Lagorse, and A. Miraoui, "A real-time sharing reference voltage for hybrid generation power system," in *2010 IEEE Industry Applications Society Annual Meeting*, 2010, pp. 1-8: IEEE.
- [92] Y. Riffonneau, "Gestion des flux énergétique dans un système photovoltaïque avec stockage connecter au réseau—Application à l'habitat," 2009.

- [93] O. Gergaud, "Modélisation énergétique et optimisation économique d'un système de production éolien et photovoltaïque couplé au réseau et associé à un accumulateur," 2002.
- [94] A. O. M. Yahya, A. O. Mahmoud, and I. Youm, "Modélisation d'un système de stockage intégré dans un système hybride (PV/Eolien/Diesel)," *Revue des énergies renouvelables*, vol. 10, no. 2, pp. 205-214, 2007.
- [95] H. A. Dang, C. Guyon, B. Delinchant, P. Béguery, and F. Wurtz, "Gestion de l'énergie électrique dans l'habitat, cas du stockage électrochimique," rapport de Schneider Electric, 2012.
- [96] R. Sadoun, "Intérêt d'une Source d'Energie Electrique Hybride pour véhicule électrique urbain—dimensionnement et tests de cyclage," 2020.
- [97] A. Merdassi, "Outil d'aide à la modélisation moyenne de convertisseurs statiques pour la simulation de systèmes mécatroniques," 2009.
- [98] M. Ayad, M. Becherif, D. Paire, A. Djerdir, and A. Miraoui, "Passivity-based control of hybrid power sources using fuel cell, supercapacitors, and batteries on the dc link for energy traction system," in *2007 IEEE International Electric Machines & Drives Conference*, 2007, vol. 1, pp. 453-458: IEEE.
- [99] K. Agbli, M. Péra, D. Hissel, O. Rallières, C. Turpin, and I. Doumbia, "Multiphysics simulation of a PEM electrolyser: Energetic Macroscopic Representation approach," *International journal of hydrogen energy*, vol. 36, no. 2, pp. 1382-1398, 2011.
- [100] A. Castaings, W. Lhomme, R. Trigui, and A. Bouscayrol, "Comparison of energy management strategies of a battery/supercapacitors system for electric vehicle under real-time constraints," *Applied Energy*, vol. 163, pp. 190-200, 2016.
- [101] T. Mesbahi, "Influence des stratégies de gestion d'une source hybride de véhicule électrique sur son dimensionnement et sa durée de vie par intégration d'un modèle multi-physique," *Ecole centrale de Lille*, 2016.
- [102] D. Gao, Z. Jin, and Q. Lu, "Energy management strategy based on fuzzy logic for a fuel cell hybrid bus," *Journal of Power Sources*, vol. 185, no. 1, pp. 311-317, 2008.
- [103] O. Erdinc, B. Vural, and M. Uzunoglu, "A wavelet-fuzzy logic based energy management strategy for a fuel cell/battery/ultra-capacitor hybrid vehicular power system," *Journal of Power sources*, vol. 194, no. 1, pp. 369-380, 2009.
- [104] Y. Eren, O. Erdinc, H. Gorgun, M. Uzunoglu, and B. Vural, "A fuzzy logic based supervisory controller for an FC/UC hybrid vehicular power system," *international journal of hydrogen energy*, vol. 34, no. 20, pp. 8681-8694, 2009.
- [105] N. D. F. Ramon, "Optimization of the sizing and the energy management for a hybrid fuel cell vehicle including fuel cell dynamics and durability constraints," *INSA de Lyon*, 2013.
- [106] Y. Ates, O. Erdinc, M. Uzunoglu, and B. Vural, "Energy management of an FC/UC hybrid vehicular power system using a combined neural network-wavelet transform based strategy," *International journal of hydrogen energy*, vol. 35, no. 2, pp. 774-783, 2010.

- [107] A. Askarzadeh and A. Reza zadeh, "Artificial neural network training using a new efficient optimization algorithm," *Applied Soft Computing*, vol. 13, no. 2, pp. 1206-1213, 2013.
- [108] D. V. Prokhorov, "Toyota Prius HEV neurocontrol and diagnostics," *Neural Networks*, vol. 21, no. 2-3, pp. 458-465, 2008.
- [109] P. VENET, "Stéphane BUTTERBACH Stockage d'énergie électrique par association de batteries au plomb et de supercondensateurs pour véhicule lourd," Université Bordeaux 1, 2012.
- [110] A. Hammani, R. Sadoun, N. Rizoug, P. Bartholomeüs, B. Barbedette, and P. Le Moigne, "Influence of the management strategies on the sizing of hybrid supply composed with battery and supercapacitor," in 2012 first international conference on renewable energies and vehicular technology, 2012, pp. 1-7: IEEE.
- [111] Z. Song, H. Hofmann, J. Li, X. Han, X. Zhang, and M. Ouyang, "A comparison study of different semi-active hybrid energy storage system topologies for electric vehicles," *Journal of Power Sources*, vol. 274, pp. 400-411, 2015.
- [112] Y.-H. Hung and C.-H. Wu, "An integrated optimization approach for a hybrid energy system in electric vehicles," *Applied energy*, vol. 98, pp. 479-490, 2012.
- [113] J. Bernard, S. Delprat, F. Buechi, and T. M. Guerra, "Global Optimisation in the power management of a Fuel Cell Hybrid Vehicle (FCHV)," in 2006 IEEE Vehicle Power and Propulsion Conference, 2006, pp. 1-6: IEEE.
- [114] E. Vinot, R. Trigui, and B. Jeanneret, "Optimal management of electric vehicles with a hybrid storage system," in 2010 IEEE Vehicle Power and Propulsion Conference, 2010, pp. 1-6: IEEE.
- [115] A. Sciarretta, M. Back, and L. Guzzella, "Optimal control of parallel hybrid electric vehicles," *IEEE Transactions on control systems technology*, vol. 12, no. 3, pp. 352-363, 2004.
- [116] L. Tribioli, M. Barbieri, R. Capata, E. Sciubba, E. Jannelli, and G. Bella, "A real time energy management strategy for plug-in hybrid electric vehicles based on optimal control theory," *Energy Procedia*, vol. 45, pp. 949-958, 2014.
- [117] R. Xiong, X. Gong, C. C. Mi, and F. Sun, "A robust state-of-charge estimator for multiple types of lithium-ion batteries using adaptive extended Kalman filter," *Journal of Power Sources*, vol. 243, pp. 805-816, 2013.
- [118] Z. Song, H. Hofmann, J. Li, J. Hou, X. Han, and M. Ouyang, "Energy management strategies comparison for electric vehicles with hybrid energy storage system," *Applied Energy*, vol. 134, pp. 321-331, 2014.
- [119] L. Xu, M. Ouyang, J. Li, F. Yang, L. Lu, and J. Hua, "Application of Pontryagin's Minimal Principle to the energy management strategy of plugin fuel cell electric vehicles," *International Journal of Hydrogen Energy*, vol. 38, no. 24, pp. 10104-10115, 2013.
- [120] C.-K. Chau, K. Elbassioni, and C.-M. Tseng, "Drive mode optimization and path planning for plug-in hybrid electric vehicles," *IEEE Transactions on Intelligent Transportation Systems*, vol. 18, no. 12, pp. 3421-3432, 2017.

- [121] J. Han, Y. Park, and D. Kum, "Optimal adaptation of equivalent factor of equivalent consumption minimization strategy for fuel cell hybrid electric vehicles under active state inequality constraints," *Journal of Power Sources*, vol. 267, pp. 491-502, 2014.
- [122] R. S. Sutton and A. G. Barto, "Reinforcement learning: An introduction," ed: Cambridge, MA: MIT Press, 2011.
- [123] N. Lopes and B. Ribeiro, "Machine Learning for Adaptive Many-core Machines: A Practical Approach," 2015.
- [124] R. Schapire, "Theoretical machine learning," Computer Science lecture, Princeton University, New Jersey, United States, 2008.
- [125] M. Triki, A. C. Ammari, Y. Wang, and M. Pedram, "Reinforcement learning-based dynamic power management of a battery-powered system supplying multiple active modes," in 2013 European Modelling Symposium, 2013, pp. 437-442: IEEE.
- [126] T. Liu, Y. Zou, D. Liu, and F. Sun, "Reinforcement learning-based energy management strategy for a hybrid electric tracked vehicle," *Energies*, vol. 8, no. 7, pp. 7243-7260, 2015.
- [127] T. Liu, X. Hu, S. E. Li, and D. Cao, "Reinforcement learning optimized look-ahead energy management of a parallel hybrid electric vehicle," *IEEE/ASME Transactions on Mechatronics*, vol. 22, no. 4, pp. 1497-1507, 2017.
- [128] X. Qi, G. Wu, K. Boriboonsomsin, and M. J. Barth, "Development and evaluation of an evolutionary algorithm-based online energy management system for plug-in hybrid electric vehicles," *IEEE Transactions on Intelligent Transportation Systems*, vol. 18, no. 8, pp. 2181-2191, 2016.
- [129] Y. L. Murphey et al., "Intelligent hybrid vehicle power control—Part II: Online intelligent energy management," *IEEE Transactions on Vehicular Technology*, vol. 62, no. 1, pp. 69-79, 2012.
- [130] V. Agubra and J. Fergus, "Lithium ion battery anode aging mechanisms," *Materials*, vol. 6, no. 4, pp. 1310-1325, 2013.
- [131] R. Carter, A. Cruden, and P. J. Hall, "Optimizing for efficiency or battery life in a battery/supercapacitor electric vehicle," *IEEE Transactions on Vehicular Technology*, vol. 61, no. 4, pp. 1526-1533, 2012.
- [132] A.-L. Allègre, "Méthodologies de modélisation et de gestion de l'énergie de systèmes de stockage mixtes pour véhicules électriques et hybrides," Lille 1, 2010.
- [133] J. P. F. Trovao, V. D. Santos, C. H. Antunes, P. G. Pereirinha, and H. M. Jorge, "A real-time energy management architecture for multisource electric vehicles," *IEEE Transactions on Industrial Electronics*, vol. 62, no. 5, pp. 3223-3233, 2014.
- [134] J. P. Trovão, P. G. Pereirinha, H. M. Jorge, and C. H. Antunes, "A multi-level energy management system for multi-source electric vehicles—an integrated rule-based meta-heuristic approach," *Applied Energy*, vol. 105, pp. 304-318, 2013.
- [135] N. Hur, J. Jung, and K. Nam, "A fast dynamic DC-link power-balancing scheme for a PWM converter-inverter system," *IEEE Transactions on industrial electronics*, vol. 48, no. 4, pp. 794-803, 2001.

- [136] W. Jiang and B. Fahimi, "Active current sharing and source management in fuel cell–battery hybrid power system," *IEEE Transactions on Industrial Electronics*, vol. 57, no. 2, pp. 752-761, 2009.
- [137] É. Bouchard, "Analyse de la consommation énergétique de véhicules électriques," École Polytechnique de Montréal, 2018.
- [138] A. Eddahech, "Modélisation du vieillissement et détermination de l'état de santé de batteries lithium-ion pour application véhicule électrique et hybride," Université Sciences et Technologies-Bordeaux I, 2013.
- [139] S. Caux, W. Hankache, M. Fadel, and D. Hissel, "On-line fuzzy energy management for hybrid fuel cell systems," *International journal of hydrogen energy*, vol. 35, no. 5, pp. 2134-2143, 2010.
- [140] J. M. Miller, T. Bohn, T. J. Dougherty, and U. Deshpande, "Why hybridization of energy storage is essential for future hybrid, plug-in and battery electric vehicles," in *2009 IEEE Energy Conversion Congress and Exposition*, 2009, pp. 2614-2620: IEEE.
- [141] B. K. Bose, "Power electronics and AC drives," Englewood Cliffs, 1986.
- [142] P. Chapoulie and S. Astier, "Modelling of an electric vehicle including ultracapacitors with SABER," *Proceedings of the EVS-15, AVERE*, Brussels, Belgium, 1998.
- [143] P. Chapoulie, "Modélisation systémique pour la conception de véhicules électriques multi-sources: application aux véhicules équipés de générateurs photovoltaïques ou de supercondensateurs," Toulouse, INPT, 1999.
- [144] A. Florescu, S. Bacha, I. Munteanu, and A. I. Bratcu, "Frequency-separation-based energy management control strategy of power flows within electric vehicles using ultracapacitors," in *IECON 2012-38th Annual Conference on IEEE Industrial Electronics Society*, 2012, pp. 2957-2964: IEEE.
- [145] K. J. Åström and T. Hägglund, *PID controllers: theory, design, and tuning*. Instrument society of America Research Triangle Park, NC, 1995.
- [146] E.-L. Europa, "Communication de la Commission au Parlement européen, au Conseil, au Comité économique et social européen et au Comité des régions. Coopération renforcée contre les maladies à prévention vaccinale," ed, 2018.
- [147] M. Andre, "Real-world driving cycles for measuring cars pollutant emissions-Part A: The ARTEMIS European driving cycles," *IFSTTAR-Institut Français des Sciences et Technologies des Transports*, de l ..., 2009.
- [148] R. Abdelhedi, "Optimisation d'un système de stockage hybride de l'énergie électrique avec batterie et supercondensateurs pour véhicule électrique," Université de Lyon; Institut National des Sciences Appliquées et de ..., 2018.

# APPENDICES

## APPENDIX A: The program developed

### Calculation of experimental SOC by the coulomb counting method

```
x=fopen('C:\Users\bachir\Desktop\partie experimentale\test decharge de la
batterie 6FM100E-X\essai decharge 10 05 2016\Idech10A.txt','r');
a=fscanf(x,'%g %g',[2 inf]);
i=a(1,:);
t=60*a(2,:);
integ=cumtrapz(t,i);
SOC=(100-2.9e-4*integ)/100;
plot(t,SOC)
```

## APPENDIX. B: The battery «Valve regulated rechargeable lead acid battery»

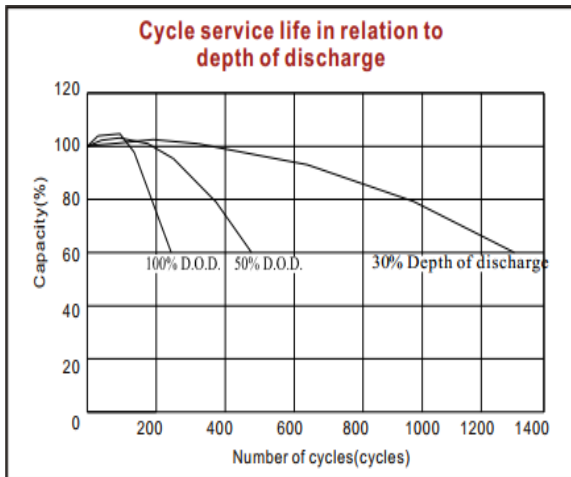
The battery used in our project is of type: **6FM100EX 12V 100AH:**



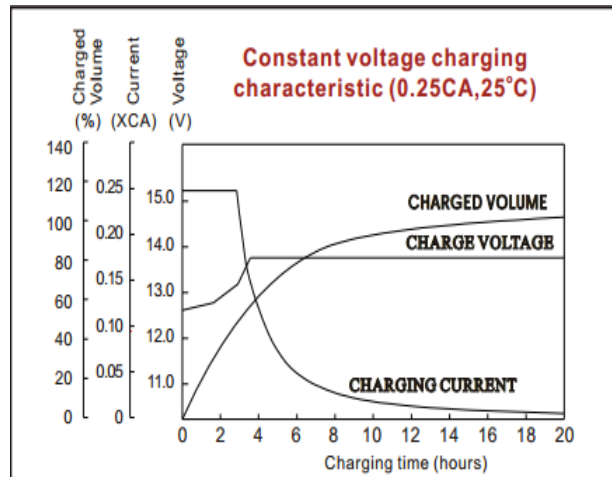
**Figure B.1:** battery photograph 6FM100EX 12V 100AH

This battery has the following characteristics:

- ✓ A nominal voltage is 12 V;
- ✓ The number of cells is 6;
- ✓ Storage capacity is 100Ah ;
- ✓ Internal resistance is 5.2  $m\Omega$  ;
- ✓ The maximum discharge current is 900A (5s);
- ✓ The maximum charging current is 30A;
- ✓ The short circuit current is 2100A.

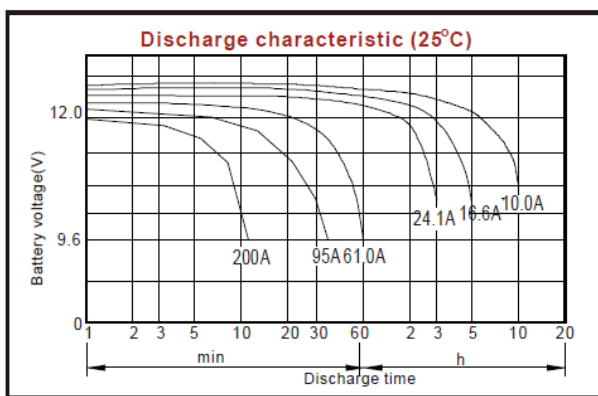


(a)

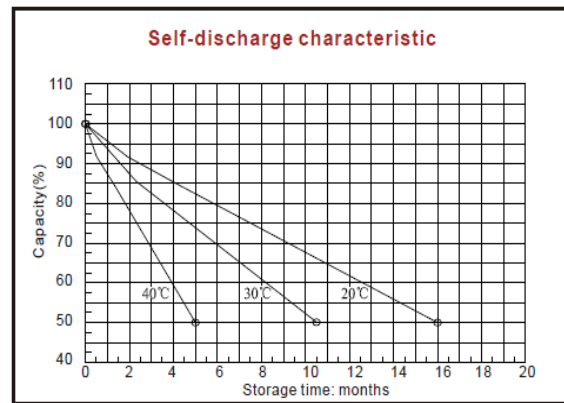


(b)

**Figure B.2:** the depth of discharge as a function of the number of cycles (a), V; I; SOC as a function of time (b)



(a)



(b)

**Figure B.3:** the discharge voltage as a function of time (a), the self-discharge of the battery as a function of time (b)

**B.1. Effect of the temperature on capacity**

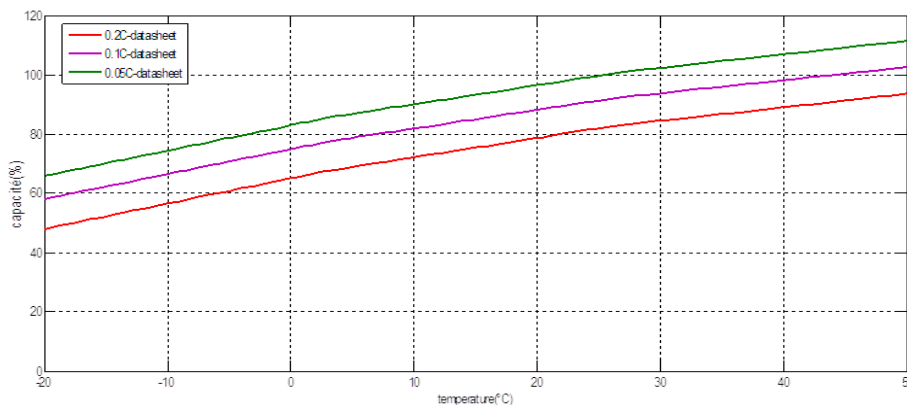


**Figure.B.4:** effect of the temperature on discharge capacity with different rate of discharge current (datasheet).

The discharge process is done in a thermal chamber, first the battery is charged and then it discharged with a discharge current rate of 0.05C and vary the temperature of the chamber from 20 ° C up to 50 ° C at the same time the discharge process is in progress until the battery is completely discharged (cut of voltage). and then repeat the same operation twice with the discharge current rate of 0.1C and 0.2C. In the temperature of -20 ° C the following remarks are made:

- the maximum drop in capacity
- the different percentages of the decrease in capacity with different rates of discharge current; 0.05C, 0.1C, 0.2C respectively as the following: 66%, 58%, 48%. Then when the temperature increases the capacity increases with different percentage in different rate of discharge current, this phenomenon calls the Peukert effect:  $C = T * I_k$

C: battery capacity.

I: discharge current.

T: the discharge time.

K: Peukert constant, practically calculate.

The variations in capacitance with the temperature and the intensity of the discharge current are usually modeled by empirical laws, because the phenomena then occurring are not well known. The formulas most often used are Peukert's law with regard to the capacitance / current relationship and a formula determined by the IEC (International Electrotechnical Commission) for the capacitance / temperature dependence [90]:

Peukert's law:  $C = I^n * t$

Formula IEC 254-1:  $C_T = 30 * (1 + 0.008 * (T-30))$

In Peukert's law, C is the capacity in Ah, I is the current in Ampere and t is the time in hours. The coefficients n and C are determined experimentally for the battery examined, the value of n is close to 1 for low currents and can reach the value 2 for large currents. For the IEC formula, we start from the capacity  $C_T = 30$  measured at 30 ° C. for a fixed discharge current and we deduce the capacity  $C_T$  at another temperature T for the same current. [90]

## B.2. Relationship between charging voltage and temperature

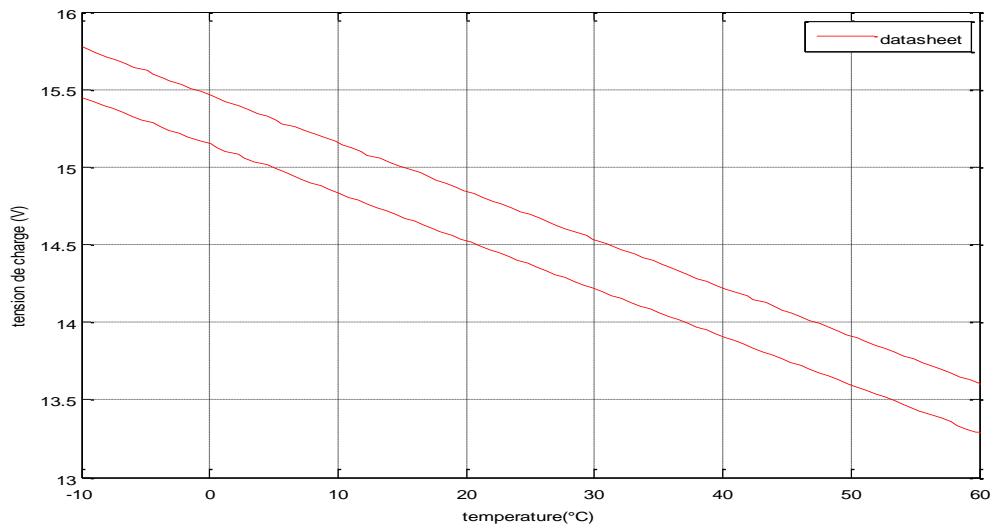


**Figure.B.5:** the charge voltage margin as a function of temperature.

According to the datasheet, if the temperature rises above 25 ° C the charging voltage will decrease by a factor of 30mV / ° C. Such as:

$$\left( \begin{array}{l} 14.4\text{V à } 25^{\circ}\text{C} \\ 13.8\text{V à } 45^{\circ}\text{C} \end{array} \right) \longrightarrow \left( \begin{array}{l} \Delta T = 45 - 25 = 20^{\circ}\text{C} \\ \Delta V = 14.4 - 13.8 = 0.6\text{V} \end{array} \right)$$

That is, the temperature increases by 20 ° C compared to 25 ° C.

Therefore;  $\Delta V = \Delta T * 30\text{mV} = 20 * 30 = 0.6\text{V}$ . Then the voltage decreases by 0.6V;  $14.4 - 0.6 = 13.8\text{V}$ . On the other hand, if the temperature below 25 ° C, the charging voltage increases by 30mV / ° C.

$$\left( \begin{array}{l} 14.4\text{V à } 25^{\circ}\text{C} \\ 15.0\text{V à } 5^{\circ}\text{C} \end{array} \right) \longrightarrow \left( \begin{array}{l} \Delta T = 25 - 5 = 20^{\circ}\text{C} \\ \Delta V = 15.0 - 14.4 = 0.6\text{V} \end{array} \right)$$

Therefore;  $\Delta V = \Delta T * 30\text{mV} = 20 * 30 = 0.6\text{V}$ . Then the voltage increases by 0.6V;  $14.4 + 0.6 = 15\text{V}$ .

## APPENDIX. C: Realized Cards

### C.1. Current sensor (LA 55-P)

The LA 55-P current sensor is a Hall effect current sensor, used for measuring alternating, direct, pulsed or mixed currents, with galvanic isolation between the primary (high power) and secondary (low power) circuits, its synoptic diagram is shown in Figure C.1:

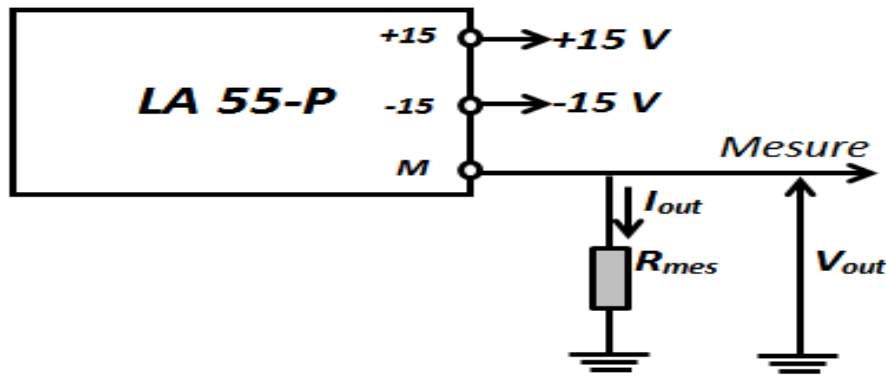


**Figure C.1:** Block diagram of the sensor LA 55-P

The sensor supplies a secondary current  $I_{out}$  proportional to the primary current  $I_{in}$  with a ratio of 1000, so to fix the gain of the sensor, all you have to do is choose the resistor  $R_{mes}$  connected to the secondary.

We have:  $V_{out} = R_{mes} \cdot I_{out}$ ,  $I_{out} = 1000I_{in}$

We take:  $(I_{in})_{max} = 30$ ,  $V_{out} (max) = 3$  V

The calculation of  $R_{mes}$  is done as follows:  $(I_{out})_{max} = (I_{in})_{max} / 1000 = 30\text{mA}$

Then:  $R_{mes} = (V_{out})_{max} / I_{out} = 100\Omega$

## C.2. Voltage sensor (LV 25-P)

The LV25-P sensor is a voltage sensor that can reach 500 Volts with galvanic isolation between the primary (high voltage  $V_p$ ) and the secondary (electronic circuit). Its synoptic diagram is shown in Figure C.2.

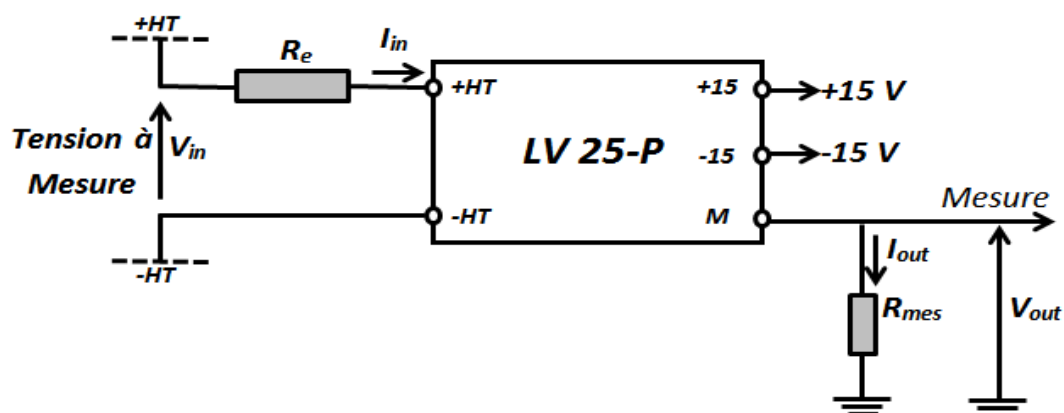


**Figure C.2:** Block diagram of the sensor LV25-P

Among the advantages of the LV25-P sensor are:

- Good precision.
- Good linearity.
- Low temperature sensitivity.

- Large bandwidth.
- High immunity against external interference.
- A weak disturbance by the common mode.

The sensor supplies a secondary current  $I_{out}$  proportional to the primary current  $I_{in}$  with a ratio of 2.5, so to fix the gain of the sensor, it suffices to choose the resistor  $R_{mes}$  connected to the secondary and the power resistor  $R_e$  in series with the primary.

We have:  $V_{in} = R_e * I_{in} * V_{out} = R_{mes} * I_{out}$

$I_{out} = 2.5 * I_{in}$  Such that:  $(max) \leq 10mA$

We take:  $R_e = 47$ ,  $V_{in} (max) = 94V$  and  $V_{out} (max) = 3 V$

The calculation of  $R_{mes}$  is done as follows:

$(max) = (max) / R_e = 0.42mA$ ,  $I_{out} = 2.5 * I_{in} = 1.06mA$

Then:  $R_{mes} = V_{out} (max) / I_{out} = 2.8 k\Omega$

### C.3. Printed circuit board

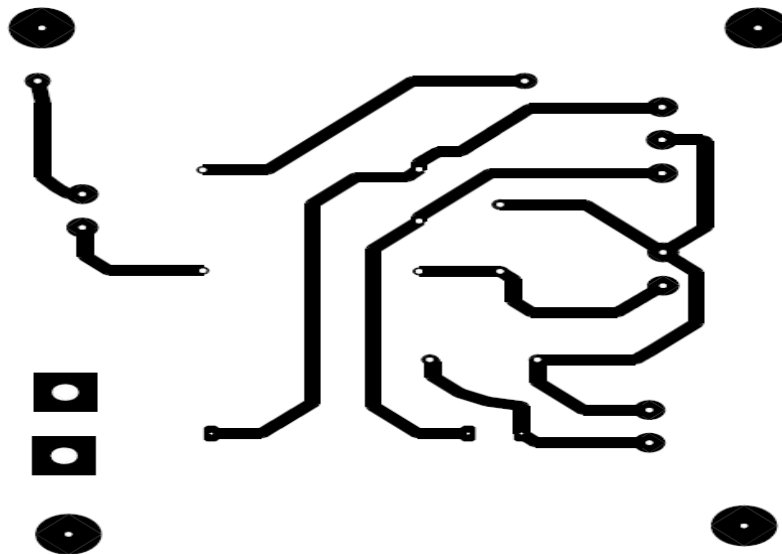


Figure C.3: Sensor card (Current and voltage).

## APPENDIX. D. The battery and the supercapacitor parameters

### D.1. The battery parameters

$R_{bat} = 13.4 m\Omega$ ,  $n = 24$  cells,  $V_{cell} = 2.15V$ ,  $V_n = 48V$

### D.2. The supercapacitor parameters

$R_{sc} = 0.8 m\Omega$ ,  $C_{sc} = 2600F$ ,  $V_{sc} = 40V$

### D.3. The DC/DC converter parameters

$$L_{sc} = L_{bat} = 0.5 \text{ mH}$$

#### D.4. The DC bus voltage parameters

$$C_{DC} = 2200 \mu\text{F}, V_{DC}^* = 150\text{V}$$

### APPENDIX. E. PI regulators parameters

#### E.1. The battery regulators parameters

$$K_P = -0.05, T_i = 20 \text{ ms}$$

#### E.2. The supercapacitor regulators parameters

$$K_P = -0.05, T_i = 20 \text{ ms}$$

#### E.4. The DC bus voltage regulators parameters

$$K_P = 2.5, T_i = 33 \text{ ms}$$

### APPENDIX. F. Frequency analyzes of loud current

```
load ich
%tracé de FFt et son enveloppe%
L=length(ich);
Fs=30;
[B,F,T]=specgram(ich,L,Fs,hanning(L),1)
ab1=-abs(B)
abn=ab1/(max(max(ab1)))
abl=6*log10(abn)
plot(F,abl)
```